

Homogeneous Velocity-Distance Data for Peculiar Velocity Analysis.

III. The Mark III Catalog of Galaxy Peculiar Velocities

Jeffrey A. Willick^a, Stéphane Courteau^b, S.M. Faber^c,
David Burstein^d, Avishai Dekel^e, and Michael A. Strauss^{f,g}

^a Dept. of Physics, Stanford University, Stanford, CA 94305-4060 (jeffw@perseus.stanford.edu)

^b NOAO/KPNO, 950 N. Cherry Ave., Tucson, AZ 85726 (courteau@noao.edu)

^c UCO/Lick Observatory, University of California, Santa Cruz, CA 95064 (faber@ucolick.org)

^d Arizona State University, Dept. of Physics and Astronomy, Box 871504, Tempe, AZ 85287 (burstein@samuri.la.asu.edu)

^e Racah Institute of Physics, The Hebrew University of Jerusalem, Jerusalem 91904, Israel (dekel@astro.huji.ac.il)

^f Dept. Astrophysical Sciences, Princeton University, Princeton, NJ 08544 (strauss@astro.princeton.edu)

^g Alfred P. Sloan Foundation Fellow

ABSTRACT

This is the third in a series of papers in which we assemble and analyze a homogeneous catalog of peculiar velocity data. In Papers I and II, we described the Tully-Fisher (TF) redshift-distance samples that constitute the bulk of the catalog, and our methodology for obtaining mutually consistent TF calibrations for these samples. In this paper, we supply further technical details of the treatment of the data, and present a subset of the catalog in tabular form. The full catalog, known as the *Mark III Catalog of Galaxy Peculiar Velocities*, is available in accessible on-line databases, as described herein. The electronic catalog incorporates not only the TF samples discussed in Papers I and II, but also elliptical galaxy D_n - σ samples originally presented elsewhere. The relative zeropointing of the elliptical and spiral data sets is discussed here.

The basic elements of the Mark III Catalog are the observables for each object (redshift, magnitude, velocity width, etc.) and inferred distances derived from the TF or D_n - σ relations. Distances obtained from both the forward and inverse TF relations are tabulated for the spirals. Malmquist bias-corrected distances are computed for each catalog object using density fields obtained from the *IRAS* 1.2 Jy redshift survey. Distances for both individual objects and groups are provided. A variety of auxiliary data, including distances and local densities predicted from the *IRAS* redshift survey reconstruction method, are tabulated as well. We study the distributions of TF residuals for three of our samples and conclude that they are well-approximated as Gaussian. However, for the Mathewson *et al.* sample we demonstrate a significant decrease in TF scatter with increasing velocity width. We test for, but find no evidence of, a correlation between TF residuals and galaxy morphology. Finally, we derive transformations that map the apparent magnitude and velocity width data for each spiral sample onto a common system. This permits the application of analysis methods which assume that a unique TF relation describes the entire sample.

Subject headings: galaxies: distances and redshifts—cosmology: large-scale structure

1. Introduction

Analyses of the peculiar velocity field in the local universe can provide strong constraints on cosmological models [cf. the reviews by Dekel (1994) and Strauss & Willick (1995)]. Among other things, they hold the promise of testing the gravitational instability mechanism as the origin of large-scale structure, clarifying the relative distribution of luminous and dark matter, and, when analyzed jointly with full-sky redshift surveys, constraining the value of the density parameter Ω_0 . Detailed peculiar velocity analyses require large samples of galaxies with both redshifts and redshift-independent distance estimates. The latter are notoriously difficult to obtain free of serious systematic errors. It has been apparent for some time that a full realization of the promise of peculiar velocity studies requires redshift-distance catalogs sufficiently large ($\gtrsim 10^3$ objects) as to minimize purely statistical errors, and prepared with great attention to uniformity so as to minimize systematics.

In this paper, the third in a series, we present the first velocity-distance catalog to substantially meet these criteria. In Papers I (Willick *et al.* 1995) and II (Willick *et al.* 1996), we described the principles behind the catalog assembly and construction, and calibrated the Tully-Fisher (TF) relations (Tully & Fisher 1977) for the individual spiral samples. Here we address several issues that were not dealt with in Papers I and II, and present representative subsections of the final data set, known as the *Mark III Catalog of Galaxy Peculiar Velocities*. Because of its large size, the Mark III catalog is not presented here in full, but has been made available electronically via on-line astronomical databases as described below (§ 6.4). In later papers in this series (Faber *et al.* 1996, Paper IV; Dekel *et al.* 1996, Paper V) we analyze the velocity field in the local universe derived from the catalog. It is not our intention that the Mark III catalog remain the private domain of the present authors. We hope, rather, that it will be widely exploited by members of the community.

The outline of this paper is as follows. In § 2, we give a broad overview of the principles behind the catalog’s construction, and clarify the nature of the redshift-independent distances it contains. In § 3 we provide details of the various corrections to which the TF observables (velocity widths and apparent magnitudes) were subjected prior to use in the TF relation. In § 4 we tabulate the data used in the “overlap comparison” used to derive relative TF zero points between samples (Paper II, § 6). Our method for computing Malmquist bias corrections to sample galaxies is described in § 5, along with a discussion of further subtleties of bias correction. In § 6, we first rederive inverse TF relation zero points (superseding the inverse TF zero points derived in Paper II, § 6), and present the final forward and inverse TF relations for the Mark III spiral samples. We then present representative parts of the spirals catalog and provide instructions for accessing the full catalog electronically. The incorporation of the elliptical galaxy sample of Faber *et al.* (1989) into the spiral database is discussed in § 7, with special attention paid to the normalization of the elliptical and spiral distance scales. In § 8 we carry out a simple analysis of the TF residuals, and test the

usual assumption that they are Gaussian. The motivation behind and procedure for putting the TF observables for all samples on a common system characterized by a single TF relation is presented in § 9. We conclude the paper in § 10 by briefly summarizing our procedures and discussing various possible systematic errors which might yet lurk in the catalog.

2. Overview of the Mark III Catalog

Before giving the details of the data in the Mark III catalog, we provide a brief overview of what the catalog contains—and what it does not. Our ultimate goal is to construct a homogeneous database of redshift-independent distance estimates for use in velocity field analyses such as POTENT (Dekel 1994). This pursuit is in keeping with the approach of Burstein in his electronic distribution of the Mark I (1987) and Mark II (1989) catalogs. The challenge is how to construct such a database from separate samples of galaxies selected and observed in different ways by different observers. We have brought together a disparate set of six spiral galaxy samples for which distance estimates are obtained using the TF relation. The main properties of these six spiral samples are summarized in Table 1; full details of their selection criteria may be found in Papers I and II. Some of these samples (HMCL, MAT) are based on *I*-band CCD photometry, some (W91CL, W91PP, CF) on *r*-band CCD photometry¹, and one (A82) on *H*-band photoelectric photometry. Most are based on H I velocity widths, while one (CF) uses exclusively optical rotation curves and one (MAT) a mixture of both H I and optical widths. Furthermore, the various samples typically probe different regions of the sky (maps of the spatial distribution of these samples are presented by Kolatt *et al.* 1996). To this already disparate group of spiral samples, we are adding a sample of elliptical galaxies (Faber 1989; distributed electronically by Burstein 1989 as the part of the Mark II Catalog) whose distances are estimated using the D_n - σ relation.

Because of this diversity of input data, our chief concern has been to ensure that the estimated galaxy distances are on a uniform system. Papers I and II described how we sought to achieve this goal for the spiral samples, but the overall approach bears repeating here. We began with the assumption that the HMCL sample consisted of a uniformly measured set of *I*-band apparent magnitudes m and velocity width parameters η (see equation 2 below). We further assumed that the HMCL clusters had vanishing radial peculiar velocities in the mean, which we justified on the grounds of the sample’s wide sky coverage and depth. This last assumption enabled us to take the HMCL cluster radial velocities as being, in the mean, fair measures of their cosmological distances. Taken together, our assumptions enabled us to fit a single TF relation (zero point A , slope b , and scatter σ) to the entire HMCL sample. The zero point is such that the TF relation yields distances in units of km s^{-1} . Such a distance is defined as the part of the observed radial velocity due to

¹Although we treat W91CL and W91PP as distinct samples (cf. Paper II, § 3.1.2, for further explanation), photometrically they are identical (Willick 1991). We will thus lump them together at times when commenting on purely photometric aspects of the data set, referring to them collectively as “W91”.

the Hubble expansion alone. From this it follows that the difference between the observed radial velocity and the TF distance is a fair measure of the radial peculiar velocity (neglecting various bias effects; see below).

Our next step was to carry out analogous TF calibrations for the remaining spiral samples, except that we did not initially assign final TF zero points. Because these samples are either not full-sky (W91CL, W91PP, CF, MAT) or very shallow (A82), we argued that it was not safe to assume that their radial peculiar velocities vanished on average (i.e., that redshift equals distance in the mean) and thus assign TF zero points as we had with HMCL. Instead, we relied on an “overlap procedure” to establish the remaining zero points: We identified, first, objects in common between HMCL and W91CL and required that their TF distances were the same on average, which determined the W91CL TF zero point. We then did the same for W91PP, CF, MAT, and A82, in each case adjusting the TF zero point to obtain consistent distances for objects in common with all already-calibrated samples (cf. Paper II, § 6). In this way, we argued, the distances derived from the various samples were guaranteed to be on a uniform system.

Several other aspects of the approach developed in Papers I and II bear reemphasis as well. First, we adopt the raw measurements (apparent magnitudes and velocity widths) reported by the original authors, but subject these quantities to our own, uniform correction procedures (detailed below in § 2). By doing this we ensure that spurious differences between samples are not introduced as a result of the distinct approaches to raw data correction present in the original papers. Second, the TF relations of the various samples are calibrated with careful attention paid to the role of *selection bias* (Willick 1994), specifically, the effects of magnitude, diameter, and other limits that define the data sets. In order to make the selection bias corrections, we have devoted considerable effort to characterizing sample selection criteria as quantitatively as possible. Selection bias is especially strong when the *forward* form of the TF relation—absolute magnitude considered as a function of velocity width—is employed. Such bias is weak or negligible, however, when the *inverse* form of the relation—velocity width considered as a function of absolute magnitude—is used. In Papers I and II, we calibrated both forward and inverse TF relations for each sample. The latter form of the relation is characterized by an inverse slope e and inverse zero point D , which are not trivially related to their forward counterparts (i.e. $e \neq b^{-1}$, $D \neq A$; cf. Appendix C for further discussion). Relative distances for groups or clusters resulted from both the forward and inverse TF calibrations. The large corrections for forward TF selection bias were validated by demonstrating good agreement between the forward and (nearly unbiased) inverse distance moduli of these groups or clusters (cf. Paper I, § 5 and Paper II, § 2.2.7, § 3.1.5, § 5.2.6).²

²In view of the nearly unbiased nature of the inverse relation one can ask why it is worthwhile working with the forward relation at all. The answer is that in Method I velocity field analyses (cf. § 2.1) such as POTENT, the forward relation yields distances with relatively straightforward Malmquist bias corrections that are independent of sample selection. Inverse TF distances used in a Method I analysis require Malmquist corrections that depend on both sample selection criteria and the luminosity function. See Strauss & Willick (1995), § 6.5, for further details.

We have recently recognized, however, that our assignment of final inverse TF zero points in Paper II did not lead to consistent forward and inverse group distances within each sample. We describe this problem in greater detail in § 6.1, and discuss the method we have adopted for rederiving final inverse TF zero points. The new zero points differ from the old (cf. Paper II, Table 12) at the level of ~ 0.05 mag. Final forward and inverse TF parameters for all the Mark III spiral samples are presented in § 6.1. None of the important conclusions of Papers I and II are affected in any way by this revision in our procedure. In particular, the validation of the forward bias corrections by comparison of forward and inverse distance moduli did not depend on final TF zero points.

2.1. TF Distances in the Mark III Catalog

The procedures just described yield fully corrected TF observables (m, η) for each object, as well as forward and inverse TF parameters (zero point, slope, and scatter) for each sample (cf. Table 3). From these data we may derive any number of redshift-independent distance estimates for individual galaxies. The ones we actually tabulate in the Mark III spiral singles catalog are the following:

1. A *raw forward TF distance*, $d_{\text{TF}} = 10^{0.2[m-(A-b\eta)]}$. These are the distances which were used (Paper II, § 6) to bring the spiral samples onto a uniform TF distance scale. Such distances are not, however, suitable as input directly into velocity analysis methods: they are strongly affected by Malmquist bias or selection bias, depending on whether a *Method I* (TF-distance taken as the *a priori* distance indicator) or *Method II* (redshift taken as the *a priori* distance indicator) approach is taken (cf. Strauss & Willick 1995, § 6.4.1, for further explanation).
2. A *raw inverse TF distance*, $d_{\text{TF}}^{\text{inv}} = 10^{0.2[m-(D-\eta/e)]}$. Such distances are not suitable for a straightforward Method I analysis, but are relatively unbiased in a Method II analysis. For reasons described in § 6.1, the raw inverse distances do not necessarily agree in the mean with their forward counterparts.
3. A *Malmquist-corrected forward TF distance*, $d_{\text{TF}}^{\text{mc}}$. Computation of this quantity is discussed in § 5. In general, this is the distance that should be used in a Method I velocity analysis, and is the quantity used in POTENT, subject to the caveats discussed in § 5.1.

In the spiral groups catalog we provide two measures of distance for the clusters of Paper I and the field galaxy groups of Paper II: selection-bias corrected forward and inverse TF distances. In contrast to the forward and inverse TF distances to individual galaxies, the group distances agree, by construction, in the mean (§ 6.1). These group distances may be used as they stand in a Method II analysis. They will be subject to a subtle though diminished Malmquist bias in a Method I approach, as we discuss further below.

2.2. Further Discussion

It is important for users of the catalog to bear in mind three caveats about the TF distances contained therein. First, *which of the various measures of TF distance to use depends on the method of velocity field analysis employed*. For example, while a Malmquist-corrected forward distance is generally appropriate for a Method I analysis, it is incorrect to use such a distance in a Method II analysis, in which redshift-space information is used as the *a priori* distance indicator. Second, *we have not included all possible measures of TF distance in the catalog*. For example, we do not calculate a Malmquist-corrected inverse TF distance, which has properties quite distinct from its forward counterpart; we will address this issue in a future paper (Eldar, Dekel, & Willick 1997; see Strauss & Willick 1995, § 6.5.5 for further discussion). Third, *the refined distance estimates we do tabulate are based on certain model-dependent assumptions and are not necessarily correct in an absolute sense*. As we discuss more fully in § 5, our Malmquist bias corrections are based on an assumed model of the underlying galaxy density field. The selection-bias corrected group distances depend on the validity of our quantitative model of sample selection criteria (although for the inverse TF relation the dependence is small). One should critically examine all such model dependencies when interpreting velocity field analyses based on the Mark III—or, indeed, any other redshift-distance—catalog.

Two issues implicit in these caveats merit further comment. First, we have neglected a potentially significant effect in computing the Malmquist-corrected forward TF distances that appear in the catalog: the role of a redshift limit in the definition of a velocity distance sample. If sample objects are required to lie within some maximum redshift, then in the vicinity of that limit the proper Malmquist correction can differ considerably from the usual expression (e.g., equation 13 below), which assumes that objects may lie at any distance along the line of sight. In § 5.1, we discuss this problem in some detail, and indicate how the effect may be accounted for in a given analysis (and how, in fact, it is done in recent implementations of POTENT). However, as discussed in § 5.1, the redshift limit effect is unimportant for most Mark III galaxies. Moreover, accounting for its effect is quite model-dependent (§ 5.1). Consequently, we neglect redshift limits in computing the Malmquist corrected distances in the catalog, but provide sufficient information for the user to take them into account if desired.

The second issue concerns the Malmquist corrections that should be applied to groups. As already noted, we tabulate selection-bias corrected group distances in the catalog. These distances are the correct ones to use in Method II analyses. However, one may also use such groups in Method I analyses such as POTENT. In that case, the selection-bias corrected group distances play a role roughly analogous to the raw individual galaxy distances in an ungrouped analysis, but with smaller distance errors. One might infer from this that the corresponding Malmquist correction is a straightforward adaptation of the singles formula. However, this is not the case; now, in addition to the standard Malmquist effects (density and volume) that affect the probability of selection as a function of distance along the line of sight, there is also the effect of the relative likelihood that an object is in a group, or is single, as a function of distance. We have recognized

this effect for several years and incorporated a correction for it into preliminary POTENT analyses (e.g., Dekel 1994; Hudson *et al.* 1995). However, our understanding and treatment of this effect are still being refined; recent work with the simulated catalogs of Kolatt *et al.* (1996) has suggested that our initial approach to the problem may require modification. Because this subject is in flux, we have elected to present only selection-bias corrected group and cluster distances. We hope to present more definitive conclusions on this subject in the future.

In summary, we have chosen to present only raw (forward and inverse) TF distances, and those processed measures of TF distance (forward Malmquist corrected for singles, forward and inverse selection-bias corrected for groups) whose computation is straightforward and based on reasonably well-founded assumptions. We have neglected several effects (redshift limit, grouped versus ungrouped fraction) whose proper correction may be ambiguous or model-dependent. We have attempted in this discussion to clarify these points. What must be borne in mind above all, however, is that all refinements of the redshift-independent distances will be to no avail, or even lead to spurious results, if the user of the catalog does not keep in mind a fundamental tenet: *the proper measure of TF distance depends on the type of analysis adopted*. Indeed, for some analytic approaches one takes the TF observables (m, η) as the basic input quantities and bypasses the distances altogether. A detailed discussion of these issues is provided by Strauss & Willick (1995, § 6.5) and references therein.

To the discussion above we add an important if perhaps obvious remark. The scientific analysis of any catalog is only as good as the data it contains. We believe that our procedures for producing the catalog are valid and that the results are reliable. We cannot exclude the possibility, however, that we have erred in some of the basic assumptions that underlie the catalog construction. We have already emphasized in Papers I and II that the global TF zero point could be in error were the HMCL clusters to possess a net radial peculiar velocity. A more serious possibility is that the HMCL sample could be less uniform with respect to its Northern and Southern hemisphere components than we have assumed. Because HMCL is the glue that holds the Mark III spirals together, any such nonuniformity would propagate throughout the data set. The best way to test for such possibilities is to continue to subject the Mark III catalog to cross-checks with new data as it comes in. Plans are presently underway for such checks, and, as we reiterate in this paper’s conclusion, we will seek to keep the community apprised of the outcome of this program.

3. Corrections to the Observables

The TF relation is applied to *corrected*, rather than raw, values of the input data, namely apparent magnitudes and linewidths. The corrections are for effects such as extinction and inclination which affect the values of the observables but are of no fundamental relevance to the scientific analysis. Because these corrections can be sizable, they must be considered as hidden but nonetheless integral parts of the TF calibration. A change in the details of the corrections would entail changes in the TF relations themselves. Before we describe the corrections in detail, some

general remarks concerning our approach are in order.

We have adopted a uniform set of rules for the corrections to the observables, as this contributes to the homogeneity of the samples. These rules are, in general, not the same as those adopted by the original authors of each Mark III sample. Consequently, the values of the TF observables found in the Mark III catalog differ from those originally published. At the same time, though, we have attempted to minimize these changes by departing to the smallest degree possible from the approach of the original authors, consistent with the requirement of uniformity. For example, MAT used a different algorithm for computing HI velocity widths than did the other samples based on 21 cm linewidths. The MAT widths are thus quite different from those in other samples for the same objects. We do not attempt to force the MAT widths onto the system used by the other samples; instead, the difference is accounted for by the distinctly different TF slope found for MAT as compared with, say, HMCL³. Another feature of our approach is that we forgo corrections to the observables that depend specifically on morphological type, for two reasons. First, we have not found that morphological information correlates in any way with residuals from the Tully-Fisher relation, as we demonstrate below (§ 8). Second, in many cases the existing imaging data not allow us to assign a reliable morphological type. This is particularly true of the many sample objects which are relatively distant ($\gtrsim 5000 \text{ km s}^{-1}$), as well as objects viewed at high inclination angles.

3.1. Details of the Corrections

There are four important corrections which we make to the observables: an inclination correction applied to velocity widths, Galactic and internal extinction corrections applied to the apparent magnitudes, and a cosmological correction applied to the magnitudes.

3.1.1. Inclination correction

Velocity widths must be corrected for projection. If we begin with a velocity width Δv corrected only for redshift (*i.e.*, the raw width divided by $(1 + z)$), the width corrected for projection is

$$\Delta v^{(c)} = \frac{\Delta v}{\sin i}, \quad (1)$$

where i is the inclination of the galaxy to the line of sight. We remind the reader that the TF relation is expressed not directly in terms of $\Delta v^{(c)}$, but rather in terms of the *velocity width parameter*

$$\eta \equiv \log \Delta v^{(c)} - 2.5, \quad (2)$$

with $\Delta v^{(c)}$ expressed in km s^{-1} .

³The exception to this procedure is when we place the observable data onto a common system in § 8.

We calculate the inclination angle i in all cases according to the formula

$$\cos^2 i = \begin{cases} \frac{(1-\varepsilon)^2 - (1-\varepsilon_{max})^2}{1 - (1-\varepsilon_{max})^2}, & \varepsilon < \varepsilon_{max}; \\ 0, & \varepsilon \geq \varepsilon_{max}. \end{cases} \quad (3)$$

In the above equation, ε is the ellipticity of the image of the galaxy disk, and ε_{max} is the ellipticity above which the galaxy is automatically assigned an inclination of 90° , i.e., the typical ellipticity of a galaxy seen edge-on. While the inclination formula (3) is a standard one (e.g., Bothun *et al.* 1985), some workers (e.g., Aaronson, Huchra, & Mould 1979) have adopted modifications of it in TF work, while others have taken ε_{max} to have a morphological type dependence. We apply equation (3) in all cases without modification. For three of our samples (A82, MAT, and HMCL) we use the value $\varepsilon_{max} = 0.80$. However, for the r -band samples (W91 and CF), we use $\varepsilon_{max} = 0.82$. This difference is trivial, and is made only for consistency with the original authors. For the samples (HMCL, W91, CF, and MAT) based on CCD photometry, we use the ellipticities determined by the original authors from the CCD images. For the one sample based on H -band aperture photometry (A82), we compute ellipticities from the blue axial ratios given in the RC3 Catalog (de Vaucouleurs *et al.* 1991), following Tormen & Burstein (1995).

3.1.2. Galactic Extinction Correction

The Galactic extinction correction is taken to be proportional to the Burstein-Heiles (Burstein & Heiles 1978, 1984; BH) reddening estimate in the direction of each galaxy. If we write the BH reddening estimate as $E(B - V)$, then Galactic extinction correction for bandpass j is given by

$$A_G(j) = f_B(j)A_B = f_B(j) \times 4E(B - V), \quad (4)$$

where $f_B(j)$ is the ratio of extinction in bandpass j to that in B , and we assume that the B -band extinction is four times the $(B - V)$ reddening.⁴ We have adopted the following values for f_B for the various samples: $f_B = 0.10$ for the H bandpass (A82); $f_B = 0.42$ for the I bandpass (HMCL and MAT); and $f_B = 0.56$ for the r bandpass (W91, CF). The derivation of this last value, for a somewhat nonstandard bandpass, is discussed by Courteau (1992).

3.1.3. Internal Extinction Corrections

A number of possible internal extinction formulae exist, as summarized by Willick (1991). However, it is difficult to distinguish between the quality of the various formulae; most can adequately describe the data provided the right parameters are chosen. As discussed in Paper I, § 2,

⁴This assumption is not made universally; in particular, the RC3 catalog assumes that $A_B = 4.3E(B - V)$.

we adopt one of the simpler forms. We write the logarithm of the (major to minor) axial ratio by \mathcal{R} , *i.e.*,

$$\mathcal{R} = -\log(1 - \varepsilon) \quad (5)$$

where ε is, as before, the apparent ellipticity of the galaxy disk. We then compute the internal extinction correction in bandpass j as

$$A_{\text{int}}^j(\mathcal{R}) = C_{\text{int}}^j \times \begin{cases} \mathcal{R}_{\text{min}} - \mathcal{R}_0^j, & \mathcal{R} < \mathcal{R}_{\text{min}}; \\ \mathcal{R} - \mathcal{R}_0^j, & \mathcal{R}_{\text{min}} \leq \mathcal{R} \leq \mathcal{R}_{\text{max}}; \\ \mathcal{R}_{\text{max}} - \mathcal{R}_0^j, & \mathcal{R} > \mathcal{R}_{\text{max}}. \end{cases} \quad (6)$$

C_{int}^j is the bandpass-dependent internal extinction coefficient. As discussed at length in Papers I and II, we determined its value for the various bandpasses by minimizing TF scatter. We found, in particular, $C_{\text{int}}^r = C_{\text{int}}^I = 0.95$, and $C_{\text{int}}^H = -0.30$ (see next paragraph for further discussion).⁵ The quantity \mathcal{R}_0^j that appears in equation (6) is the value of the logarithmic axial ratio to which the internal extinction correction is referenced. We have used $\mathcal{R}_0 = 0$ (correction to face-on orientation) for the H -band (A82) and I -band (HMCL, MAT) samples, and $\mathcal{R}_0 = 0.418$ (correction to $\sim 70^\circ$ inclination) for the r -band (W91, CF) samples. The latter value is adopted for consistency with the original authors, who preferred to keep the absolute size of the correction small. It should be clear that a non-zero value of \mathcal{R}_0 has no physical significance whatsoever, as it is ultimately absorbed into the TF zero point. The quantities \mathcal{R}_{min} and \mathcal{R}_{max} in equation (6) reflect the “saturation” of the internal extinction effect at low and high inclination. We have adopted the values $\mathcal{R}_{\text{min}} = 0.27$ and $\mathcal{R}_{\text{max}} = 0.70$ for all the spiral samples. These values were arrived at by adjusting them until TF residuals at high and low axial ratios exhibited no trends. In Paper II, we considered the possibility that internal extinction is luminosity-dependent, as has recently been suggested by Giovanelli (1995). We carried out careful tests for such an effect but found no evidence for it (Paper II, § 2.3.1 and § 3.2.1).

Two aspects of the derived internal extinction coefficients warrant further comment. First, we have recognized a significant (though harmless) error in our estimates of the uncertainties in these coefficients in Papers I (§ 3.2.3, § 4.2.1) and II (§ 2.3, § 3.2, § 5.2.7). Specifically, we based those estimates on an erroneous statement (Paper I, 3.2.3) of the relationship between a χ^2 statistic for the TF calibration fit and the TF σ . The correct statement is $\chi^2(C_{\text{int}}) \simeq N_{\text{eff}} \sigma^2(C_{\text{int}}) / \sigma_{\text{min}}^2$, where $\sigma^2(C_{\text{int}})$ is the TF scatter for an arbitrary value of C_{int} , and σ_{min}^2 is the TF scatter for the value of C_{int} that minimizes scatter. With this corrected expression for $\chi^2(C_{\text{int}})$, one can once again go through our basic argument that a 65% confidence interval on C_{int} is obtained by asking, for what values of C_{int} does χ^2 change by 1 unit from its minimum value of N_{eff} . The result is that our confidence intervals on C_{int} for all three bandpasses (I , r , and H) were too wide. In particular, our

⁵Bottinelli *et al.* (1995) have also addressed the issue of internal extinction using minimization of TF residuals. They worked with B -band photometric data and found $C_{\text{int}}^B = 1.67 \pm 0.23$. This is larger than what we find for the r and I bandpasses, as is expected for shorter wavelength photometry. While these results are reasonably consistent, quantitative agreement is difficult to establish in the absence of a satisfactory theory of internal extinction in galaxies.

final estimate of C_{int}^I is uncertain by $\lesssim 0.1$, and of C_{int}^r and C_{int}^H by $\lesssim 0.15$, roughly half as large as the uncertainty estimates given in Paper II, § 8. (The reduction is comparatively modest, despite the fact that our χ^2 s were badly off, because of the flat behavior of χ^2 near its minimum.)

Second, we emphasize that the negative coefficient of H -band internal extinction does not represent an important physical distinction between 1.6μ and far-red optical galaxian light. It reflects, rather, the fact that the original aperture photometry from which the H -band magnitudes were derived has been scaled to standard *diameter* measurements. These diameters were not corrected for inclination (Tormen & Burstein 1995). Thus, any systematic dependence of diameter on inclination would manifest itself as an inclination dependence of the apparent magnitudes as well. (The CCD-measured magnitudes of HMCL, W91, CF, and MAT are, in contrast, *total* magnitudes and thus unaffected by diameter measurements.) In particular, if galaxies actually get systematically larger with increasing inclination, as is certainly possible, then the corresponding H -band magnitudes would get systematically brighter. This is the sense of the effect we have detected, and is the most likely explanation of the negative value of C_{int}^H .

3.1.4. Cosmological Correction

The final correction we apply to the apparent magnitudes is for cosmological effects (by which we mean all effects associated with redshift; see below). It is closely related but not identical to the standard K-correction (*e.g.*, Oke & Sandage 1968; Pence 1976). In many previous studies (*e.g.*, Mathewson *et al.* 1992), this K-correction has been applied to CCD total magnitudes used for TF purposes. However, such a procedure is not rigorously correct. In what follows, we will discuss why this is, and derive a cosmological correction appropriate for CCD magnitudes used as input to the TF relation in peculiar velocity analyses. Although the practical differences from earlier work are small in the present application, our modification may be significant in studies that apply the TF relation to galaxies at redshifts $\gtrsim 0.1$.

Before proceeding, a clarification is desirable. We use the term “cosmological correction” in the same sense that Oke & Sandage (1968) use “K-correction”: to signify correction for the effects of both the shift of the spectrum relative to the observational bandpass and the change in spacetime geometry with increasing redshift. Our cosmological correction differs from the K-correction for two reasons, the first quite straightforward and the second considerably more subtle. First, standard K-corrections (*e.g.*, Oke and Sandage 1968; Pence 1976) are derived under the assumption that it is the *energy* detected from the source that determines apparent magnitude. However, with CCD photometry it is instead the number of photons detected (as recognized by Schneider, Gunn, & Hoessel 1983). This difference must be accounted for both in the way the spectral shape is characterized (as we do in this section) and in the mathematical derivation of the correction (as we do in Appendix A). Second, the “distance” one wishes to obtain from comparison of observed apparent magnitudes and inferred absolute magnitudes in a velocity field analysis is not one of the standard measures of cosmological distance (*e.g.*, the angular diameter or luminosity distances).

Instead, it is the quantity cz_c , where z_c is the redshift the object would possess if its peculiar velocity were zero. It is this particular measure of cosmological distance which, when compared with the observed redshift cz , yields the radial component of peculiar velocity.

The K-correction $K(z)$ (e.g., Oke & Sandage 1968) is defined so that

$$m - K(z) - M = 5 \log d_L, \quad (7)$$

where m is the observed apparent magnitude, M is the absolute magnitude of the standard candle, and the *luminosity distance* is given by (cf. Weinberg 1972)

$$d_L(z) = \frac{c}{q_0^2} \left[zq_0 + (q_0 - 1)(-1 + \sqrt{2q_0z + 1}) \right]. \quad (8)$$

(In equations 7 and 8 we have conformed to our usual practice of defining distance in km s^{-1} units and taken 1 km s^{-1} as the fiducial distance at which absolute magnitude is defined.) By contrast, for the purposes of peculiar velocity analysis, the corrected distance modulus should correspond to the distance $r = cz_c$, where z_c is the “cosmological redshift” defined in the previous paragraph. Thus, the relevant cosmological correction for our purposes, K_{TF} , is defined by the relation⁶

$$m - K_{\text{TF}}(z, z_c) - M(\eta) = 5 \log cz_c. \quad (9)$$

Because $d_L \neq cz_c$, as we show in Appendix A, the K-correction defined by equation (7) is not equal to $K_{\text{TF}}(z, z_c)$ as defined by equation (9). In particular, while $K(z)$ is independent of q_0 —for which d_L may be used as a diagnostic— $K_{\text{TF}}(z, z_c)$ is not. The distinction between the classical K-correction and the cosmological correction suitable for peculiar velocity work was first recognized by Lynden-Bell *et al.* (1988), who considered peculiar velocities estimated from the D_n - σ relation. The corresponding expression that applies for the TF case is different. The full derivation of K_{TF} is outside our main line of argument, and is presented in Appendix A. The result (to first order in z and z_c) is

$$K_{\text{TF}}(z, z_c) = 1.086 [(\epsilon + 2)z - (1 + q_0)z_c], \quad (10)$$

where ϵ is the power-law index (which we model as depending on the velocity width parameter η , as discussed below) of the photon number distribution $N(\lambda)$ (see Appendix A). It is the photon number, rather than the energy flux, distribution that is relevant for CCD magnitudes, as discussed above.

In applying equation (10) to the Mark III TF samples, we take z to be the heliocentric redshift, and estimate z_c by the cosmic microwave background frame (CMB) redshift. While peculiar velocities might invalidate this estimate in any given instance, we expect that on average the CMB

⁶In equation (9), K_{TF} is written as a function of both z (the observed, or heliocentric, redshift) and z_c , as it is the former that determines the amount by which the spectrum is shifted, while it is the latter that determines specifically cosmological effects (see Appendix A for further details). The distinction is of course very small, but we preserve it in our analysis procedure, as discussed further in the text.

redshift is a good estimator of the cosmological redshift. As discussed above, equation (10) also contains the deceleration parameter q_0 , for which we must thus adopt a value. We take $q_0 = 0.25$, halfway between an open and flat universe. It is important to bear in mind that although we are obliged to make these uncertain assumptions ($z_c \simeq z_{\text{CMB}}$ and $q_0 = 0.25$), the effect on our data analysis by adopting plausible alternatives would be inconsequential, given that the mean redshift of the sample is $\lesssim 4000 \text{ km s}^{-1}$.

The power-law exponent ϵ in equation (10) must be properly modeled in order to avoid systematic errors. In previous work (*e.g.*, Han 1991; Mathewson *et al.* 1992), this effect has been approximated by assuming spectrum shape to be a function of morphological type. As noted above, we consider morphological information to be of limited accuracy for objects distant enough that the cosmological correction is meaningful. We thus adopt the following alternative criterion of spectral shape. As shown by Willick (1991), the $r - I$ colors of spiral galaxies correlate well with their velocity widths. The colors are in turn a measure of the spectrum shape; Willick (1991) calibrated the latter effect by fitting the photon number power law indices of spectrophotometric standard stars to their $(r - I)$ colors. Combining the color-velocity width and spectrum shape-color correlations, Willick (1991) derived the $\epsilon - \eta$ relation for spiral galaxies shown in Figure 1; the explicit formula for $\epsilon(\eta)$ is given in the plot. The sense of the relation is that relatively faint ($\eta < 0$) spirals tend to be blue ($\epsilon < 0$), while luminous spirals tend to be red. The trend saturates for the most luminous galaxies, however. The variation in ϵ over the range of observed width parameters is such that the cosmological correction at $z \gtrsim 0.02$ can differ by several hundredths of a magnitude for bright as compared with faint galaxies. This corresponds to distance differences of $\sim 100 \text{ km s}^{-1}$, and is not negligible.

Finally, then, we apply the following η -dependent redshift correction to apparent magnitudes in the samples based on r - and I -band CCD photometry (HMCL, W91, CF, MAT):

$$K_{\text{TF}}(z_{\odot}, z_{\text{CMB}}, \eta) = 1.086 [(\epsilon(\eta) + 2)z_{\odot} - 1.25z_{\text{CMB}}], \quad (11)$$

where $\epsilon(\eta)$ is given in Figure 1. This correction is *not* applied to the one sample (A82) which uses H -band aperture magnitudes, for two reasons. First, the $\epsilon(\eta)$ relation derived by Willick (1991) does not apply at H . Second and more importantly, the H -band magnitudes are tied to photographic diameters (Tormen & Burstein 1995), which display a rather different behavior with increasing redshift. As mentioned in Paper II, for A82, we instead apply the simple redshift correction $K(z) = 1.9z_{\odot}$ derived by Aaronson *et al.* (1980). As A82 objects lie mainly at redshifts $\lesssim 2000 \text{ km s}^{-1}$, their cosmological corrections are very small in any case.

3.1.5. Summary

We have standardized the corrections to the raw observables for the six spiral samples. A single formula, equation (3), is used to compute inclinations and thus deprojected velocity widths. The raw apparent magnitudes undergo corrections for Galactic and internal extinction, and for

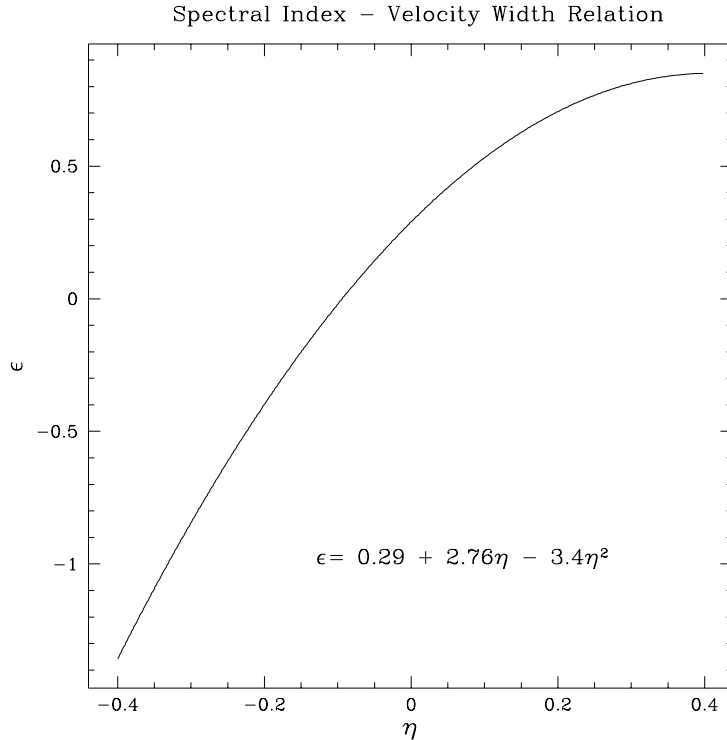


Fig. 1.— The relation between the photon number spectrum power law index ϵ , and the velocity width parameter η , adopted for the cosmological correction applied to apparent magnitudes for the r and I band Mark III spiral samples.

cosmological effects. If we denote by m the corrected apparent magnitude, and by m_j the raw apparent magnitude (where $j = r$ or I), then our full correction procedure is described by

$$m = m_j - A_G(j) - A_{\text{int}}(j, \mathcal{R}) - K_{\text{TF}}(z_{\odot}, z_{\text{CMB}}, \eta), \quad (12)$$

where A_G is given by equation (4), A_{int} by equation (6), and $K_{\text{TF}}(z_{\odot}, z_{\text{CMB}}, \eta)$ by equation (11). For the H -bandpass, the equation is the same, except that the cosmological correction is replaced by the simple expression $1.9z_{\odot}$, as discussed above.

4. Presentation of the Overlap-Comparison Data

The reliability of the Mark III data for probing large-scale peculiar motions depends on our ability to tie together the various samples in a uniform way. As discussed in Paper II, § 6, we have done this by first identifying galaxies present in two or more of the Mark III samples (“overlap” objects), and then determining relative TF zero points by minimizing TF distance modulus differences (Paper II, § 6). The global TF zero point was set by the HMCL sample (cf. Paper I,

§ 3.2.2).⁷

Because the sample-to-sample matching is such an important part of our procedure, we present in Table 2 the complete list of the 403 individual galaxies which participate in the overlap comparison. The objects are listed in order of ascending heliocentric redshift. Column 1 lists the Principal Galaxy Catalog (Paturel *et al.* 1985; PGC) number of the object. This number provides a unique way of identifying the galaxy. (Its common name or names may be found by cross-referencing the PGC number with Table 3, which lists all Mark III galaxies.) Columns 2 and 3 list the Galactic longitude (l) and latitude (b) in degrees. Column 4 lists the heliocentric redshift of the object in km s^{-1} , averaged over the two or more samples in which the object appears. In the great majority of cases, the individual redshift measurements agree to within $< 100 \text{ km s}^{-1}$. Redshift differences greater than this were found for only six of the overlap objects. In these instances, we used the value deemed most reliable for all samples.

Columns 5–22 list the TF observables (m, η), and the raw forward TF distance d_{TF} , for each of the Mark III samples in which the object is found. This TF distance is not corrected for Malmquist or selection bias and is expressed in km s^{-1} units. Columns 5–7 list the data for HMCL; columns 8–10 for W91CL; columns 11–13 for W91PP; columns 14–16 for CF; columns 17–19 for MAT; and columns 20–22 for A82. If the object in question does not appear in a particular sample, all three values (η , m , and d_{TF}) are simply listed as zero.

Twenty HMCL galaxies listed in Table 2, indicated by a superscript a , are found in the HMPP subset of HMCL, but not in the restricted HMCL sample used in the analyses presented in Papers I and II, which excluded the HMPP subset. However, these 20 objects are used in the common system definition presented in § 8. There are, in addition, six objects which appear in both the HMPP subset and in the restricted HMCL sample of Papers I and II. The HMPP data for these galaxies do not appear in Table 2, but may be found in Table 3. These objects are NGC 444 (PGC 4561); NGC 452 (PGC 4596); UGC 841 (PGC 4735); UGC 987 (PGC 5284); NGC 536 (PGC 5344); and UGC 1066 (PGC 5563).

5. Malmquist Bias Corrections

When TF or D_n - σ distances are used in a *forward, Method I* analysis (cf. Strauss & Willick 1995, § 6.4), they must be corrected for Malmquist bias in order to yield unbiased peculiar velocities. Malmquist bias arises because objects with a given TF-inferred distance lie in reality at a range of true distances because of TF errors. The average true distance of a set of objects with a given TF-inferred distance depends on the underlying galaxy density field as well as on the TF magnitude scatter σ . A variety of approaches to Malmquist correction are possible (Lynden-Bell *et al.* 1988;

⁷The elliptical data cannot of course be normalized to the spirals via this procedure. In § 7 we discuss our method for establishing the elliptical distance scale.

Willick 1991; Landy & Szalay 1992; Dekel 1994; Hudson 1994; Hudson *et al.* 1995; Freudling *et al.* 1996). Our technique will follow that outlined by Strauss & Willick (1995).

The main complication is that the Malmquist bias correction to a given galaxy depends non-locally on the underlying galaxy density field. In particular, if $d = 10^{0.2(m-M(\eta))}$ is the raw forward TF distance, then the expected true distance r is given by (Strauss & Willick, § 6.5.2).

$$E(r|d) = \frac{\int_0^\infty r^3 n(r) \exp\left(-\frac{[\ln r/d]^2}{2\Delta^2}\right) dr}{\int_0^\infty r^2 n(r) \exp\left(-\frac{[\ln r/d]^2}{2\Delta^2}\right) dr}, \quad (13)$$

where $n(r)$ is the (real-space) galaxy number density along the line of sight, and

$$\Delta \equiv \left(\frac{\ln 10}{5}\right) \sigma \simeq 0.46 \sigma \quad (14)$$

is the fractional distance estimation error due to the TF magnitude scatter σ . If $n(r)$ were effectively constant on the scale ($\sim \Delta d$) of TF distance errors, the above expression would reduce to the familiar expression for uniform-density Malmquist bias, $E(r|d) = de^{7\Delta^2/2}$ (e.g., Lynden-Bell *et al.* 1988); basically, objects are more likely to be farther away than d because there is more volume at larger distances. However, for realistic samples this is not always a good approximation, as the density can vary rapidly along the line of sight. The overall Malmquist bias arising from both the volume effect and density variations is known as *inhomogeneous Malmquist bias*, or IHM. In order to correct properly for IHM, it is important that a realistic model of the density field be substituted into equation (13).

There is no perfect way to do this. One might use, for example, redshift-space density $n(cz)$ as a substitute for $n(r)$, but this would ignore the distorting effects of peculiar velocity. Alternatively, one could estimate the real-space density from the number density in inferred-distance space, $n(d)$. The latter approach is closely related to the Landy-Szalay (1992) method of Malmquist-bias correction, which we will implement elsewhere (Eldar, Dekel, & Willick 1996). However, for our present purposes the preferred technique for the spiral samples is to use a model of $n(r)$ derived from the *IRAS* 1.2 Jy redshift survey (Fisher *et al.* 1995), with the effects of peculiar velocities corrected for using linear theory (Yahil *et al.* 1991; Strauss & Willick 1995, § 5.9). The advantage of this approach is that *IRAS* galaxies are expected to be good tracers of the general spiral density field. The disadvantage is that the reconstruction of $n(r)$ from redshift data is necessarily model-dependent: it assumes that gravitational instability is valid, and moreover requires that a smoothing scale and a value of $\beta \equiv \Omega_0^{0.6}/b$, where Ω_0 is the density parameter and b is the linear bias factor be chosen for the reconstruction.

While we recognize the objections that can be raised to this procedure, we do not consider it to be a serious issue in practice. The effects of density variations on the overall Malmquist bias correction are typically smaller than the uniform-density bias. The relatively small differences in the size of the correction between the various possible reconstructions of $n(r)$ from *IRAS* are smaller still. We have chosen a reconstruction model in which $\beta = 0.6$, the velocity reconstruction

assumes pure linear theory, and a Gaussian smoothing scale of 300 km s^{-1} was used. The value of $\beta = 0.6$ was adopted based on a maximum likelihood comparison of a subset of Mark III spirals with the *IRAS* density and velocity fields (Strauss & Willick 1995, § 8.1.3; Willick *et al.* 1997). The smallest smoothing scale possible is optimal for Malmquist bias correction, and 300 km s^{-1} is the smallest that can effectively be used in the reconstruction. Further details of the *IRAS* reconstruction method are given by Yahil *et al.* (1996).

In practice, equation (13) is not especially robust for numerical calculation of Malmquist corrections owing to the log-normal factor in the integrands. Instead, we use the following, completely equivalent, expression for $E(r|d)$ (Willick 1997):

$$E(r|d) = de^{\frac{7}{2}\Delta^2} \frac{1 + \frac{1}{\sqrt{\pi}} \int_{-\infty}^{\infty} \delta \left(de^{4\Delta^2} e^{\sqrt{2}\Delta x} \right) e^{-x^2} dx}{1 + \frac{1}{\sqrt{\pi}} \int_{-\infty}^{\infty} \delta \left(de^{3\Delta^2} e^{\sqrt{2}\Delta x} \right) e^{-x^2} dx}, \quad (15)$$

where $\delta(r) = n(r)/n_0 - 1$ is the fractional galaxy overdensity. Equation 15 is simple to integrate because of the strict Gaussian factor and the use of δ rather than density itself. Furthermore, in this form one clearly sees that the IHM correction implicitly contains the standard homogeneous Malmquist term. All Malmquist corrected distances in Table 3, to be discussed in the next section, are obtained by numerical evaluation of equation (15).

5.1. The Effect of Redshift Limits on Malmquist Bias Corrections

The Malmquist bias corrections discussed above assume that sample objects can lie at any distance along the line of sight. This is reflected in the limits of integration—zero to infinity—in equation (13). Many current TF samples, however, do not have this property, because in addition to magnitude or diameter limits, sample selection may depend on redshift as well. Restrictions on redshift may be imposed either by observational constraints (e.g., HI receivers are limited in frequency range) or sample definition (e.g., observers make TF measurements only for objects with known redshifts less than a chosen value). In this section we discuss a modification to the IHM correction in the presence of a redshift limit, and comment on how such considerations apply to the Mark III spiral samples.

The fact that a redshift limit modifies the nature of Malmquist bias has been recognized by other workers. Freudling *et al.* (1995), for example, modeled the effect of redshift limits using a Monte Carlo procedure, and da Costa *et al.* (1996) used these models in constructing peculiar velocity maps from their *I*-band TF sample. In contrast, we have taken an analytic approach to bias corrections. Such an approach has the advantage that the assumptions and model parameters that go into it are more evident, and their effect on the final corrections more easily assessed, than in a Monte Carlo scheme. We present the outlines of our approach below. However, for reasons described in § 5.1.2, we have not actually made redshift limit corrections in the Mark III database. The discussion to follow is designed to enable users to do so should they deem it necessary for their

particular analysis.

5.1.1. Analytic Approach to the Redshift Limit Correction

To modify the IHM correction for a redshift limit, one must first model the redshift-distance relation in the vicinity of the limit. This entails making assumptions about the peculiar velocity field, as did the IHM correction itself (see above). In the discussion to follow we assume the redshift-distance relation near a limit is at most a bulk departure from uniform Hubble flow. It is also necessary to adopt a value for the small-scale velocity “noise,” σ_v , about the mean flow. A reasonable value is $\sigma_v = 200 \text{ km s}^{-1}$ (cf. Davis, Nusser, & Willick 1996 for further discussion).

Suppose that a particular subsample is subject to a limit $cz \leq cz_{\text{lim}}$. Suppose furthermore that the bulk flow of galaxies near cz_{lim} (and in the part of the sky under consideration) is given by \mathbf{v}_p . Then the first-order effect of the redshift limit is to exclude all objects at *distances* greater than $cz_\ell \equiv cz_{\text{lim}} - \mathbf{v}_p \cdot \hat{\mathbf{n}}$, where $\hat{\mathbf{n}}$ is a unit vector along the line of sight. Note that the distance limit for a given redshift limit is direction-dependent. However, the presence of velocity noise means that objects whose observed radial velocities place them at the redshift limit actually lie within a range ($\sim cz_\ell \pm \sigma_v$) of distances. Thus, rather than an abrupt distance limit at cz_ℓ , there is a fuzzy limit, and we cannot simply replace the upper limit of integration by cz_ℓ . Instead, we multiply the integrands in both numerator and denominator of equation (13) by the probability, $P(r|cz_{\text{lim}}, \mathbf{v}_p, \hat{\mathbf{n}})$, that an object at distance r along line of sight $\hat{\mathbf{n}}$ satisfies the redshift limit criterion. This probability is given by (Willick 1997)

$$P(r|cz_{\text{lim}}, \mathbf{v}_p, \hat{\mathbf{n}}) = \frac{1}{2} \left[1 - \text{erf} \left(\frac{r - cz_\ell}{\sqrt{2}\sigma_v} \right) \right], \quad (16)$$

where “erf” is the error function. In the limit $\sigma_v \rightarrow 0$, $P(r|cz_{\text{lim}}, \mathbf{v}_p, \hat{\mathbf{n}}) \rightarrow \Theta(cz_\ell - r)$. In other words, when σ_v is very small in comparison with other relevant scales (in this case, the TF distance error Δd) the effect of multiplying by $P(r|cz_{\text{lim}}, \mathbf{v}_p, \hat{\mathbf{n}})$ differs little from replacing the upper limit of integration by cz_ℓ . Similarly, it is clear that when $cz_\ell - r \gg \sigma_v$, $P(r|cz_{\text{lim}}, \mathbf{v}_p, \hat{\mathbf{n}}) \simeq 1$, i.e., far from the redshift limit (relative to the velocity noise) the standard Malmquist formula is recovered.

5.1.2. Redshift Limit Effects in the Mark III Spiral Samples

As noted above, we have not taken account of redshift limit effects in computing the IHM-corrected distances tabulated in the Mark III catalog (§ 6.2). We have, in effect, taken $cz_{\text{lim}} \rightarrow \infty$ for all of the Mark III objects. This is not to say that redshift limit effects are entirely absent in the selection of the Mark III samples. Rather, as noted in § 2, these limits are in most cases⁸ so

⁸The exceptions are the cluster samples, HMCL and W91CL, as discussed below.

ill-defined as to preclude a well-defined correction without making explicit, *a posteriori* cuts on the samples. This is in fact what we do in POTENT (Hudson *et al.* 1995; Dekel *et al.* 1996): we identify a redshift beyond which redshift-selection effects appear to become important in each sample (see below), and then eliminate from the analysis all galaxies at higher redshifts. Equation (16) then strictly applies to the reduced samples. Since the distributed catalog includes *all* galaxies in the original samples, however, we believe it would be misleading to adopt such hard redshift cuts in computing IHM corrections for the catalog. The discussion above should enable potential users of the catalog to account for redshift-limit effects if they so choose. To allow such calculations to be made, we include at the Mark III distribution sites (cf. § 6.4) the density grid, $n(r)$, toward each Mark III spiral.

We now discuss the redshift selection criteria that affect the makeup of the Mark III spiral samples. There is one spiral sample for which we know that no redshift limit effects are present: the CF sample, which was selected strictly on the basis of magnitude and diameter limits (Courteau 1992, 1996). For the remaining field samples, redshift selection effects of a more or less pronounced character apply, as follows:

1. A82 exhibits an abrupt reduction in number of objects per unit redshift at $cz_{\odot} = 3000 \text{ km s}^{-1}$ (Paper II, § 6). In the POTENT analysis, only A82 galaxies with $cz_{\odot} \leq 3000 \text{ km s}^{-1}$ are used. The POTENT IHM correction accounts for this effect according to the prescription outlined above (see Paper V for further details). There are 59 A82 galaxies at heliocentric redshifts $> 3000 \text{ km s}^{-1}$ presented in the on-line Mark III catalog. Users should be aware that the IHM corrections presented for these objects are thus indicative only, as the sample is strongly incomplete at $cz_{\odot} > 3000 \text{ km s}^{-1}$.
2. Any redshift limits affecting MAT are very weak. Mathewson *et al.* (1992) indicate that their sample is confined “in general” to radial velocities $< 7000 \text{ km s}^{-1}$, but this appears to be a consequence of the sample diameter limit (cf. Paper II, § 2.1) rather than a redshift limit *per se*. Mathewson *et al.* further indicate that in the GA region, a number of fainter galaxies at higher redshifts were included. Again, however, these more distant objects appear to have been selected by relaxing the diameter limit rather than by explicitly selecting on redshift. Thus, to a good approximation the MAT Mark III sample is not redshift limited. However, users are advised that this statement is probably rigorously true only if the diameter limited nature of the sample is respected, i.e., if small ($D_{\text{ESO}} < 1.6'$) MAT galaxies are excluded from the analysis.
3. The W91PP sample was not subjected to a redshift limit by Willick (1991). However, it is an HI-selected sample based on the Arecibo observations of Giovanelli *et al.* (1985, 1986). The observations were implicitly limited by the prevailing restrictions on the Arecibo receivers at the time. W91PP is thus effectively redshift-limited at $\sim 12,000 \text{ km s}^{-1}$. This limit is applied in the POTENT IHM correction for W91PP.

For the cluster Mark III samples, of course, the situation is quite different. HMCL and W91CL are composed of galaxies that were *expressly selected to lie with a narrow ($\sim 1500 \text{ km s}^{-1}$) range of redshifts centered on the mean cluster redshift*. The effect on the IHM correction of such redshift cuts is extremely strong. As a result, the Malmquist-corrected forward TF distances for individual HMCL and W91CL galaxies presented in the Mark III catalog are not applicable in a Method I analysis of these samples. We have included them for purposes of completeness only. Cluster galaxies should not, in any case, be treated individually in Method I analyses, but should be grouped together and corrected for selection bias, as we have done in the spiral groups catalog (§ 6.3).

6. Final TF Relations and Partial Presentation of the Spirals Catalog

In this section we present illustrative portions of the Mark III Catalog. Because of its large size, the full catalog will be made available electronically only, as we describe below. We present data for both individual spiral galaxies (the singles catalog, § 6.2) and groups of spiral galaxies (the groups catalog, § 6.3). In § 6.4 we describe how to access the complete, on-line versions of the catalog. First, however, we revisit our Paper II determination of inverse TF zero points, and present a corrected, final tabulation of the TF relations for the Mark III spiral samples.

6.1. Corrected Inverse TF Zero Points and Final TF Relations

We have modified slightly the inverse TF zero points presented in Paper II, after recognizing a problem with our earlier approach. In Paper II, § 6, we applied the same reasoning to the forward and inverse relations, minimizing individual galaxy distance modulus differences to determine final zero points. However, while this approach ensures consistency of raw inverse TF distances *between* samples, it does not guarantee consistency of forward and inverse distances *within* samples. There is no need for forward and inverse *individual* galaxy distances to agree within a sample, because forward and inverse distances are subject to substantially different Malmquist bias corrections (e.g., Strauss & Willick 1995, § 6.6.5). However, once corrected for selection bias, forward and inverse *group* distances should agree within a sample. Each is, in principle, an unbiased measure of the distance to the group, to which no further correction is necessary in a Method II analysis.

However, we found in preparing the catalog that there were systematic offsets between forward and inverse group distances within each Mark III sample (except HMCL; see below). For example, the inverse TF distances to the W91CL clusters were 0.04 mag larger, in the mean, than the corresponding forward TF distances, when the inverse zero point obtained in Paper II was used. The origin of these differences is not entirely clear. While they are small in an absolute sense, they are typically twice as large as the relative zero point errors we estimated in Paper II, Table 12, and thus significant. Their existence requires us to decide which criterion of homogeneity we value more: agreement of individual galaxy inverse distances between samples, or of forward and inverse

group distances within samples.

Our view is that the latter criterion is more basic, and we used it to redetermine the inverse TF zero points for each sample except HMCL. Specifically, we adopted the inverse zero point that minimized a χ^2 statistic formed from forward minus inverse TF distance moduli and errors assumed to scale as $n^{-\frac{1}{2}}$, where n was the number of objects in the group or cluster. For HMCL, however, the original inverse zero point was determined in the same way as the forward zero point—zero net cluster motion, cf. Paper I, § 3.2.2—and thus required, in principle, no further adjustment. Application of the χ^2 minimization procedure to the HMCL forward and inverse cluster distances confirmed that this was indeed the case. In redetermining the inverse zero points we did *not* change the inverse slopes or scatters from their Paper II values. The new procedure resulted in a small ($\lesssim 0.05$ mag) changes in the inverse zero points. In most cases, the sense of this adjustment was to make the inverse TF distances slightly ($\sim 2\%$) smaller. We emphasize that while the new inverse zero points have not been determined *directly* by the overlap method, ultimately the overlap principle governs their values: the overlap method was used to determine forward TF zero points, and inverse distances are now normalized by forward ones.

The one exception to the procedure just described was the CF sample, for which we formed no independent groups. In this case, we simply assumed that the difference between the forward TF zero point A and the inverse TF zero point D for CF was the same as for the W91CL sample. This assumption is justified on the grounds that W91CL and CF exhibit very similar TF relations (Paper II, § 4).

Having corrected the inverse TF zero points as just described, we list the parameters of the final TF relations for the Mark III spiral samples in Table 3. Note that, with the exception of the modified inverse zero points, this table is identical to Table 12 of Paper II.

6.2. The Spiral Galaxy Singles Catalog

In Table 4 we present data for 45 galaxies in the MAT sample. The format of this printed table is the same as that of the complete electronic tables. In the on-line version of the catalog, there is a separate file for each sample. Each has an identical format, however, so the portion of the MAT table presented here will provide sufficient guidance.

The galaxies are listed in order of ascending heliocentric redshift in Table 4. Column 1 lists the *Mark III Catalog internal identification number* for the object. These numbers reflect the order in which the original authors listed their objects, typically in order of increasing Right Ascension. For example, the first and second entries in Table 4 were the 1322nd and sixth entries, respectively, in the data table presented by Mathewson *et al.* (1992). The number presented in Column 1 is unique within each sample. Thus, specifying the Mark III sample (e.g., MAT, HMCL, etc.) and the internal identification number uniquely specify a Mark III object. The internal identification number also facilitates cross-referencing between the singles catalog itself, and the files of auxiliary

data for the catalog objects that are also to be found in the electronic data base. The remaining columns in Table 4 are as follows:

Column 2: PGC Number.

Column 3: Name of the galaxy as listed by the original authors. In the on-line A82 catalog, the names of the 22 Virgo Cluster galaxies whose heliocentric radial velocities were set to 1153 km s^{-1} (the mean Virgo value) in the application of the grouping algorithm (cf. Paper II, § 5.2.2) are followed by “[V]”.

Column 4: Group number of the galaxy. This number corresponds to the groups listed in Table 4 (see below). For the cluster samples (HMCL and W91CL), all objects have a group number unless they were explicitly excluded from the TF calibration procedure (cf. Paper I). The latter objects have group number -1 . For the field samples (W91PP, CF, MAT, A82), objects that were placed into groups by the grouping algorithm of Paper II have group numbers ≥ 1 . Group number zero signifies that the algorithm attempted to group the object but could not because it did not have neighbors sufficiently close in redshift space. Group number -1 signifies that the object was excluded *a priori* from the grouping procedure. For example, as explained in Paper II, § 2, the grouping algorithm was not applied to objects with ESO diameters smaller than $1.6'$, with $\eta < -0.42$, and with inclinations less than 35° . In addition, a small number of objects was excluded *a priori* for what were judged to be unreliable axial ratios, even if they were nominally large enough that the derived inclination was $> 35^\circ$. Although the CF sample was not grouped in Paper II, CF objects that lie in the Perseus-Pisces region, and which are not present in the W91PP sample, were consolidated with W91PP for the purpose of forming maximal groups for later velocity analysis. The resulting grouped sample is known as “WCF.” CF and W91PP sample group numbers correspond to the WCF grouped sample.

Column 5: Galactic longitude (degrees).

Column 6: Galactic latitude (degrees).

Column 7: Circular velocity parameter η (equation 2).

Column 8: Apparent magnitude m (mag), fully corrected for extinction and redshift (cf. § 2.1).

Column 9: ESO blue angular diameter (arcminutes), in the case of the MAT sample, which is illustrated here. However, more generally this column contains the variable upon which sample selection was based: UGC blue diameters in the case of CF and W91PP; UGC blue diameters or Zwicky apparent magnitudes for HMCL North, ESO blue diameters for HMCL South; RC3 B magnitudes for A82.

Column 10: Total correction from raw to corrected apparent magnitude Δm (mag), as described in § 2.1. The quantity Δm is > 0 when the corrected apparent magnitude is smaller (brighter) than the raw magnitude (the usual case). The case $\Delta m < 0$ can occur because we correct to a fiducial axial ratio (rather than face-on) for W91 and CF (cf. § 2.1.3), and also because we derived

a negative internal extinction coefficient for A82 (cf. Paper II, § 5.2.7).

Column 11: B -band Galactic extinction (mag; § 2.1.2).

Column 12: Logarithm of the (major-to-minor) axial ratio \mathcal{R} (§ 2.1.3).

Column 13: For all samples except A82, this column lists the Burstein Numerical Morphological Type (BNMT). This index is a numerical encoding of the RC3 morphological type, developed by one of us (DB). A detailed description of the BNMT is given in Appendix B. For the A82 sample, the BNMT was not available, and the RC2 numerical morphological type is listed instead.

Columns 14–16: Three measures of the TF distance to the object, all given in km s^{-1} . Column 14 gives the raw forward TF distance. Column 15 gives the forward TF distance corrected for IHM, as described in § 5. Column 16 gives the raw inverse TF distance. For reasons described in Strauss & Willick 1995 (§ 6.5.5), the inverse distances have a more complicated Malmquist bias correction, which we consider elsewhere (Eldar, Dekel, & Willick 1996).

Columns 17–19: Radial velocities in km s^{-1} , as measured in the heliocentric (v_{\odot}), Local Group (v_{LG}), and Microwave Background (v_{CMB}) frames of reference, respectively. The heliocentric velocities are those measured by the original authors except for a few cases, discussed in § 3, where the overlap comparison revealed a deviant value, in which case the deviant values are replaced by the valid ones. We transform from heliocentric to Local Group velocities according to the transformation of Yahil *et al.* (1979). CMB-frame velocities are obtained using the motion of the sun with respect to the CMB determined by the COBE dipole anisotropy (Kogut *et al.* 1993).

Column 20: The expected distance in km s^{-1} , d_{IRAS} , derived from the same *IRAS* reconstruction as was used in the Malmquist correction procedure (§ 5). This distance was computed as the expectation value of true distance, given the observed radial velocity and the *IRAS*-predicted peculiar velocity and density fields. A small-scale velocity dispersion of 150 km s^{-1} was assumed in the calculation. See Strauss & Willick (1995, § 8.1.3) for further explanation.

Column 21: The local galaxy overdensity δ , defined as $(n_g - n_0)/n_0$, where n_g is the local number density and n_0 is the mean number density, again obtained from the *IRAS* reconstruction. The *IRAS* density was evaluated at the IHM-corrected forward TF distance when $v_{\text{LG}} < 750 \text{ km s}^{-1}$, and at the *IRAS*-expected distance otherwise.

Column 22: The forward TF residual, δm_{TF} , in mag. This residual was computed with respect to the TF fits to the groups formed by the grouping algorithm of Paper II (W91PP, CF, MAT, A82) or the cluster TF fits of Paper I (HMCL, W91CL). As noted above, W91PP and nonoverlapping CF galaxies in Perseus-Pisces were grouped together for the purposes of this compilation. When an object either was not included in the grouping algorithm or cluster fits (e.g., MAT objects with $D_{\text{ESO}} < 1.6'$ or CF objects away from PP), or was not placed in a group by the algorithm because of a lack of redshift-space neighbors, there is no TF residual for the object; the value in column 22 is then given as -9.999 .

6.3. The Spiral Groups Catalog

In Table 5, we present representative data from the grouped portion of the Mark III catalog spirals. For consistency with Table 4, we present here groups formed from the MAT sample. In the on-line version of the catalog, grouped data are also presented for HMCL, W91CL, A82, and W91PP plus Perseus-Pisces CF galaxies (WCF). HMCL and W91CL galaxies were grouped *a priori* based on assumed cluster membership (Paper I). The field samples (MAT, A82, WCF) were grouped by the grouping algorithm (cf. Paper II, § 2.2.2).

The groups in Table 5, and in the on-line catalog, are listed approximately in order of ascending heliocentric redshift⁹ for the field samples. For the cluster samples the order reflects the convention originally adopted for HMCL (cf. Paper I, Table 1; the HMPP clusters are listed at the end of the HMCL list). Column 1 is the group number, which uniquely identifies a group within each sample. This number corresponds to that listed in column 4 of Table 4; it is thus straightforward to identify the individual members of the group by cross-referencing the two tables. Column 2 lists the number of galaxies in the group, N_g . Columns 3 and 4 list the mean Galactic longitude (l) and latitude (b) of the group members. Column 5 lists the mean velocity width parameter, $\bar{\eta}$, of the members of the group. Column 6 is the rms scatter, in mag, of the group members about the TF relation. (The TF relation fitted to the group is the universal TF relation for the sample, not a fit just to the members of the group.) Column 7 lists the forward TF distance to the group, d_{TF} , in km s^{-1} . This distance is fully corrected for selection bias. Because the groups are formed using redshift-space criteria, it is selection rather than Malmquist bias which pertains (cf. Strauss & Willick 1995, § 6.4). Column 8 lists the inverse TF distance to the group, again corrected for selection bias (although in the inverse case the correction is extremely small; cf. the relevant discussions in Papers I and II). As noted above, the inverse TF zero points were chosen so that the forward and inverse TF group distances agree in the mean, although significant differences are occasionally seen in individual cases. Column 9 lists the distance modulus error $\delta\mu_{\text{TF}}$ (mag) associated with the TF distance; it is computed simply as $\sigma_{\text{TF}}/\sqrt{N_g}$, where σ_{TF} is the magnitude scatter of the TF relation for the sample in question (e.g., 0.43 mag MAT). Columns 10, 11, and 12 list, respectively, group heliocentric, LG, and CMB frame radial velocities in km s^{-1} . The heliocentric group radial velocities are computed as the mean heliocentric radial velocity of group members if $N_g = 2$, and as the median radial velocity for groups with three or more members; the LG and CMB frame group radial velocities are then obtained by transforming the heliocentric group radial velocity as described in § 6.1.

⁹The grouping algorithm initially sorted objects on heliocentric redshift, and the field sample singles files are thus listed precisely in this order. However, in the process of grouping there is some inevitable shuffling back and forth; as a result, the groups themselves are not listed *exactly* in order of their mean heliocentric redshifts.

6.4. The Electronic Catalog

The Mark III Catalog has been made available electronically at three separate sites. The first is NASA’s Astronomical Data Center, which may be accessed either using a Web browser or by anonymous FTP at `adc.gsfc.nasa.gov`. The second site is a Web page maintained by Willick, at the URL `http://astro.stanford.edu/MarkIII`. The third site is an anonymous FTP resource maintained by Burstein at `samuri.la.asu.edu`. The contents of these three archives are very similar, although slight differences of organization exist. At each site extensive documentation in the form of README files is available.

The files are given in ASCII format and are organized into five main directories: (i) individual spiral galaxy data, (ii) spiral group and cluster data, (iii) spiral “overlap galaxy” data, (iv) spiral ancillary data, and (v) elliptical galaxy data. The first directory contains data files named `mark3_mat_s`, `mark3_w91cl_s`, and so forth. These files correspond to Table 4 of this paper, and are described by a single README file called `RMk3_ind_dist`. The second directory contains data files called `mark3_mat_g`, `mark3_w91cl_g`, and so forth. They correspond to the information in Table 5 of this paper, and are described by a single README file called `RMk3_gp_dist`. The third directory contains just one data file, `mark3_match`, which is nearly identical in content to Table 2 of this paper (the electronic version does not contain Galactic coordinates) and is described by the README file `RMk3_match`. The fourth directory contains a set of data files not described in this paper. There are three separate data files for each Mark III spiral sample (there is no file of ancillary data for the elliptical galaxies), named `matfileX.lst`, where $X=1,2,3$, described by README files called `RMk3_mat`, and so forth. These files contain data that are not crucial to peculiar velocity analyses, but which might be useful for related studies, including apparent magnitudes and angular diameters from a variety of galaxy catalogs and cross-referencing information between catalogs. In addition, these files list the original photometric and velocity width data as reported by the original Mark III sample authors. Finally, in the fifth directory one may find the elliptical galaxy data. These data are presented in exactly the same manner as they were in the Mark II catalog distributed in 1989 by Burstein: there are two data files, `egalfile1.lst` and `egalfile2cor.lst`, and a single README file called `RMk3_egal`. These files differ from the Mark II distribution only by the small multiplicative correction to the D_n - σ distances, as described in § 7 below.

On the Web page maintained by Willick, two additional types of data are available. First, as mentioned in § 5.1, the (normalized) *IRAS* galaxy number densities $n(r)$, with values given at quadratically spaced positions along the line of sight toward each Mark III spiral, are provided. A short FORTRAN program to read the binary files containing this information is also made available. Second, twenty realizations of simulated Mark III catalogs, generated as described by Kolatt *et al.* (1996), may be found, along with documentation describing their use.

7. Matching the Elliptical and Spiral Distances

The sample of elliptical and S0 galaxies with D_n - σ distances is added almost as is from the Mark II data set compiled by D. Burstein (based on Lynden-Bell *et al.* 1988; Faber *et al.* 1989; Lucey & Carter 1988; Dressler & Faber 1990). It includes 544 galaxies in 249 objects (single galaxies, groups and clusters). However, we first rescaled the Mark II D_n - σ distances in order to match the elliptical and spiral distances, as we now describe.

The original D_n - σ zero point was determined independently, and is therefore not necessarily consistent with the global TF zero point determined in Paper I. We thus allow for a multiplicative degree of freedom in the D_n - σ distances, $d \rightarrow (1+\epsilon)d$, corresponding to a free Hubble-like monopole component in the peculiar velocities, $u \rightarrow u - \epsilon r$. The value of ϵ is determined subject to the assumption that both the ellipticals and the spirals are unbiased tracers of the same underlying velocity field (for a discussion of the validity of this assumption see Kolatt & Dekel 1994, hereafter KD). We found in three different ways that the best value is $\epsilon = -0.035 \pm 0.01$, and have corrected the D_n - σ distances accordingly before adding them to the catalog.

One method of matching is described in detail in KD. The same large-scale POTENT smoothing was applied separately to the TF and the D_n - σ data, yielding two independent radial peculiar velocity fields, $u_s(\mathbf{x})$ and $u_e(\mathbf{x})$, and their corresponding errors, $\sigma_s(\mathbf{x})$ and $\sigma_e(\mathbf{x})$, at common grid points \mathbf{x} . The POTENT smoothing mimics a spherical Gaussian window of radius 1200 km s^{-1} with minimum biases due to the sparse and nonuniform sampling of noisy radial velocities (Dekel, Bertschinger & Faber 1990; Dekel 1994; Dekel *et al.* 1996). The two velocity fields were then compared at grid points near which the sampling by both types of galaxies is “adequate”, which we define as having at least five neighboring galaxies of the same type within a sphere of radius 1500 km s^{-1} . The sampling by the ellipticals limits the comparison to a volume of an effective radius $\sim 4000 \text{ km s}^{-1}$. The two fields were matched by minimizing the statistic

$$D = \sum \left[\frac{(u_e - u_s)^2}{\sigma_e^2} + \frac{(u_e - u_s)^2}{\sigma_s^2} \right] / \sum \left[\frac{(u_e + u_s)^2}{\sigma_e^2} + \frac{(u_e + u_s)^2}{\sigma_s^2} \right], \quad (17)$$

where the sum is over the adequate grid points. The comparison at grid points together with the inverse weighting by the errors is a compromise between the desired equal-volume weighting and the optimal treatment of noise.

This analysis was applied in KD to a preliminary version of the Mark III data, and it was re-done recently using the final version of the catalog, with a very little change in the result. The best fit values range between $\epsilon = -0.05$ and -0.02 , depending on the exact volume of comparison. The correction is statistically significant despite the fact that it is small. Based on the distribution of D in Monte Carlo simulations, the probability that the elliptical and spiral velocity fields are both noisy versions of the same underlying field is more than 10% after an $\epsilon = -0.035$ correction, while it was less than 2% before the correction.

In an alternative analysis, the radial peculiar velocity of each elliptical galaxy (or group) was

compared with the average of the radial velocities of the neighboring spirals inside a top-hat sphere of radius 500 km s^{-1} . In this analysis the effective smoothing is on much smaller scales, thus reducing the biases within the effective window to a level where they can be practically ignored. However, this comparison is not volume weighted. The best fit is found again to be $\epsilon = -0.035$ with similar errors.

In a third analysis, the inferred distances of the “same” elliptical and spiral clusters were compared. It turns out that there are severe difficulties in trying to identify matching clusters. The spiral “clusters” in many cases extend over several Mpc and only a handful of them can be confidently identified with elliptical counterparts. Even when the identification is quite certain, the different types of galaxies may show different mean velocities because they tend to sample different components of the cluster. We ended up with 6 clusters in common, and with a best fit of $\epsilon \simeq -0.03$, fully consistent with the other tests.

8. Further Consideration of the TF Residuals

Several assumptions underlie most statistical analyses of TF-type data. The most frequently adopted are the following:

1. TF residuals are Gaussian;
2. TF residuals are independent of velocity width;
3. TF residuals are uncorrelated with morphological type.

In this section we subject these assumptions to simple but stringent tests using three samples: MAT, A82, and WCF. We will conclude that the first and third of the above assumptions are consistent with our data. The second assumption clearly fails for the MAT sample, but to a much lesser degree (if at all) for the other two; we discuss possible reasons for this and suggest how velocity analyses might account for this effect.

For each of the three samples, we use the TF residuals computed by the grouping algorithm (cf. Paper II, § 2.2.2) and tabulated in Table 3 (or the corresponding electronic file). These residuals are plotted versus η in the upper left panels of Figures 2, 3, and 4 for MAT, A82, and WCF respectively. The advantage of the grouping algorithm residuals (as compared with the HMCL and W91CL cluster fit residuals) is that the assignment of objects to groups was done objectively.¹⁰ Our test for Gaussianity utilizes the Kolmogorov-Smirnov (KS) statistic. The KS test measures the

¹⁰Recall from Paper II (§ 2.2.2) that the grouping algorithm used an “input” TF scatter to reject objects from group membership. Thus, extreme ($\gtrsim 3.3\sigma$) outliers are, in effect, already excluded from the present analysis. Were this not done, the TF residuals would not be strictly Gaussian. Our view is that Gaussianity of the residuals is sufficiently desirable as to warrant the exclusion of a small (~ 1 – 2%) number of sample objects.

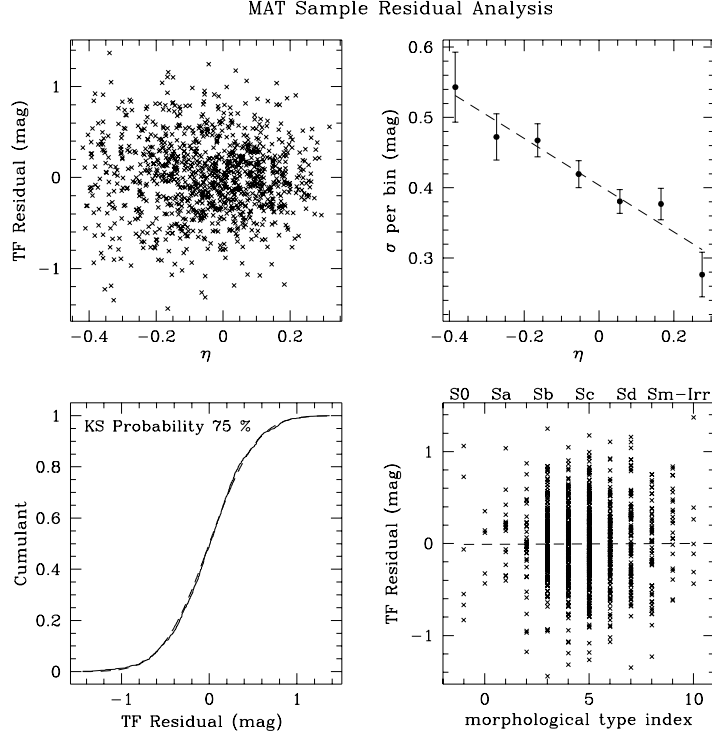


Fig. 2.— Upper left panel: MAT TF residuals are plotted versus the velocity width parameter η . Upper right panel: rms values of the TF residuals, computed within bins of width $\Delta\eta = 0.11$, are plotted against η . The dashed line shows the best-fit linear relation between the TF σ and η . Lower left panel: the cumulative distribution (normalized to unity) of the TF residuals (solid line) and the corresponding distribution for a Gaussian with the same rms dispersion (dashed line) are plotted. The Kolmogorov-Smirnov probability that the distributions are the same is indicated. Lower right panel: TF residuals are plotted versus RC3 morphological type index; the dashed line shows the best fit linear relation between the mean residual and the type index. See text for details.

probability that the cumulative distribution of the residuals is drawn from a Gaussian distribution with the same dispersion as the rms value of the residuals themselves. The results of the KS tests are plotted in the lower left panels of Figures 2–4. The cumulative distributions of the residuals are plotted as solid lines; the cumulative distributions of the corresponding Gaussians (with dispersions 0.43 mag for MAT, 0.47 mag for A82, and 0.38 mag for WCF) are plotted as dashed lines. It is visually apparent that the two curves are in good agreement in each case. The value of the KS probability is indicated in each panel as a percentage. For all three samples, the KS probability is large ($\gtrsim 60\%$), whereas a large deviation from Gaussianity would be signified by a small value ($\lesssim 10\%$). From these results we conclude that the assumption that TF residuals are Gaussian is justified.

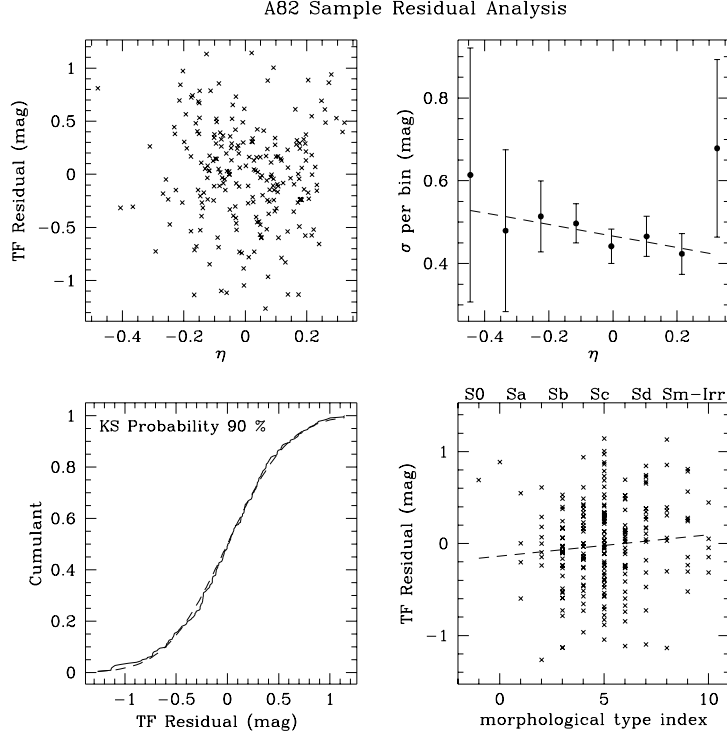


Fig. 3.— Same as Figure 2, except that the residual analysis is now done for the A82 sample.

Next, we consider whether the TF scatter is constant with velocity width (or, equivalently, with luminosity). For each of the three samples, we have computed the rms value of the TF residuals within bins of width $\Delta\eta = 0.11$. The results are plotted in the upper right panels of Figures 2–4. In the case of the MAT sample, a clear trend is seen: σ decreases with increasing η , i.e., the TF scatter is smaller for bright galaxies than it is for faint galaxies. The dashed line represents the best-fit straight line to the binned rms values. For the MAT sample, this straight line is given by $\sigma(\eta) = 0.404(.008) - 0.33(.05)\eta$, where 1σ errors are indicated in parentheses. The nonzero slope that characterizes the trend is highly significant. For the A82 and WCF samples, a qualitatively similar trend is seen. However, in each of these two cases, the fitted slopes differ from zero at only about the 1.5σ significance level. Specifically, for A82 the relation is $\sigma(\eta) = 0.466(.013) - 0.14(.09)\eta$. For WCF it is $\sigma(\eta) = 0.382(.010) - 0.09(.06)\eta$. Thus, the decrease in TF scatter with increasing velocity width is not unambiguously detected in the A82 and WCF samples.

Given the strong trend seen in the MAT sample, one must reinterpret the KS test for the Gaussianity of the MAT TF residuals. Because σ is not constant with η , the residuals cannot obey a strictly Gaussian distribution. However, their overall distribution irrespective of η can still be Gaussian if both the TF residuals at any given η , and the distribution of η -values, are Gaussian. It is difficult to test the latter assumption because of selection effects. We have, however, performed

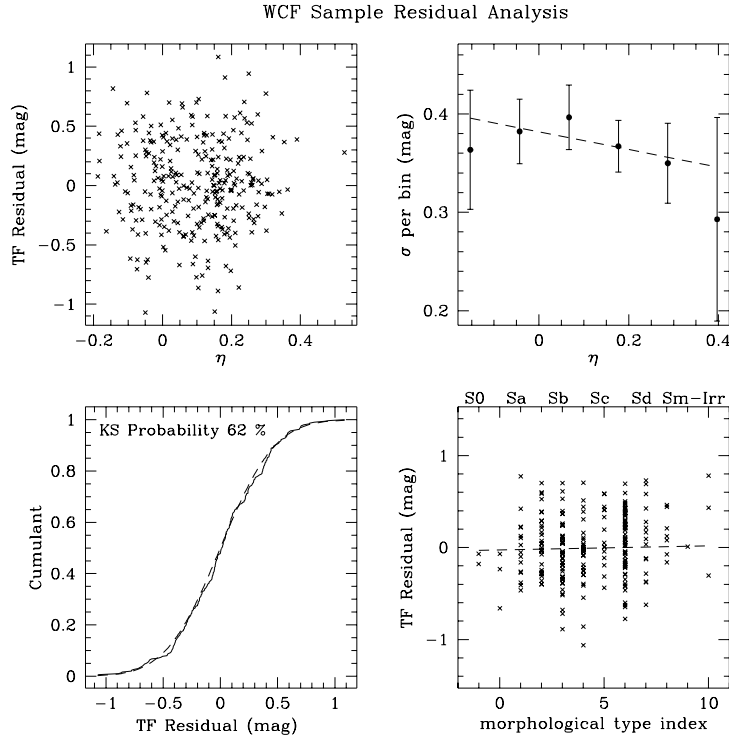


Fig. 4.— Same as Figure 2, except that the residual analysis is now done for the combined W91PP+CF sample.

KS tests on the residuals within each $\Delta\eta = 0.11$ bin shown in Figure 2. We find that within nearly all bins, the KS probability that the residuals obey a Gaussian distribution with scatter $\sigma(\eta)$ is $\gtrsim 50\%$. The one exception is the bin centered at $\eta = -0.16$, in which the KS probability is 2.6%. Inspection of the upper left panel of Figure 2 reveals the reason for this result—a scarcity of residuals in the range ~ -0.1 – 0 mag, and an excess of residuals of $\sim +0.2$ mag. The reason for this deviant bin is unknown.¹¹ Excepting this unaccounted-for behavior, our results indicate that it is valid to view the MAT TF scatter as Gaussian at any given η , but as a linear function $\sigma(\eta)$ as described above. This “local” Gaussianity ensures that the statistical techniques we have applied in this series of papers remain valid.

We have not explicitly carried out a test for Gaussianity using inverse TF residuals. However, such an exercise is unnecessary, because the forward and inverse residual distributions are in fact closely related. In Appendix C, we apply the laws of probability theory to derive the distribution of inverse TF residuals from those of the forward relation. We show that local Gaussianity of

¹¹It is worth noting, however, that if one analyzes a sequence of N Gaussian distributions for Gaussianity, the probability of finding one that appears *non-Gaussian* at a given significance level is proportional to N . It is thus not necessarily significant that one of the seven bins tested exhibits non-Gaussian behavior.

the forward residuals implies local Gaussianity of the inverse TF residuals as well—as long as the change in scatter with velocity width is gradual, and the luminosity function is wider than the TF scatter. These conditions are shown to hold quantitatively for actual TF samples. Statistical techniques that assume local Gaussianity are therefore valid for inverse, as for forward, TF analyses. We also discuss in Appendix C the factors which cause the inverse TF relation to differ from the mathematical inverse of the forward TF relation—i.e., which result in $D \neq A$, and $e \neq b^{-1}$ —properties of the observed TF relations that were previously unexplained.

The rather different scatter versus η behavior evidenced by MAT, as compared with A82 and WCF, represents an ambiguous result. If TF scatter were inherently a strongly decreasing function of η , we would expect to see the trend in all samples. But the $\sigma(\eta)$ versus η slopes for A82 and WCF differ from that of the MAT sample at the ~ 2 - and 3σ levels respectively. This raises the possibility that the trend seen in the MAT sample is an artifact of that data set. Alternatively, it could be that only the MAT sample is large enough, and in particular rich enough in low-linewidth objects, that an actual trend can be clearly detected. It is worth noting that, if velocity width errors $\delta(\Delta v)$ are roughly independent of the width itself, then η errors $\delta\eta \propto \delta(\Delta v)/\Delta v$ increase with decreasing velocity width. If so, the part of the TF scatter due to width errors ($\sim b\delta\eta$, where b is the forward TF slope), and thus the TF scatter itself, must similarly increase with decreasing η . Thus, at some level, the trend seen in the MAT data is bound to occur. Whether an additional effect of real physical significance (related, e.g., to galaxy formation physics) is present is difficult to say. For the present, the most prudent approach is to examine the effect of allowing the TF scatter to vary with velocity width, in any given peculiar velocity analysis. However, the allowed variation should be constrained by the results obtained above, e.g., the σ versus η relation should be taken as linear with the slopes calculated above. We will adopt this approach in future papers (Dekel *et al.* 1996; Willick *et al.* 1997). In the on-line catalog, however, we have assumed fixed TF scatter independent of velocity width in computing the Malmquist corrections (§ 6.2). The values of the TF scatter adopted are those given in Table 3.

Finally, in the lower right panels of Figures 2–4 we plot TF residuals versus RC3 morphological type index. This measure of morphology runs from $\lesssim 0$ for very early-type spirals (S0, S0a, Sa) to $\lesssim 10$ for the late-type spirals. Dwarf galaxies, multiple galaxies, and galaxies with highly uncertain morphology are not shown and are not considered in the analysis to follow. It is apparent in each case that the TF residuals do not correlate, or correlate at most very weakly, with galaxy morphology. To quantify this impression, we have carried out linear fits of the mean residual within each bin to the numerical index. The dashed lines show the results of these fits. For MAT, the slope of the fitted line is 0.001 ± 0.009 ; for A82, it is 0.023 ± 0.014 ; and for WCF, it is 0.005 ± 0.005 . Thus, for MAT and WCF we may confidently reject the presence of significant correlation between the TF residuals and morphological type. For A82, a weak trend may be present. It is possible that the trend is real for A82, which is based on aperture magnitudes, but is eliminated through the use of CCD total magnitudes. Given its marginal significance, a more conservative assumption is that the trend is negligible for A82, as it clearly is for MAT and WCF. Thus, the Mark III data

do not support the notion that galaxies of different morphological types obey distinct TF relations. This conclusion is unaffected if we restrict the analysis to the relatively large objects, $D \geq 2.5'$, whose morphologies are least uncertain.

9. Transforming the Samples to a Common System

An important principle underlying the calibration procedure of Papers I and II was that each individual sample had a distinct TF relation. This was understood as a consequence of the distinct character of each data set: I - versus r - versus H -band photometry, different measures of velocity width, etc. Indeed the TF parameters were found to differ markedly among the samples (Table 3). However, for some purposes it is inconvenient to have more than one TF relation involved in a velocity analysis. For example, the approach to velocity field reconstruction developed by Nusser & Davis (1995), and applied to the Mark III Catalog by Davis, Nusser, & Willick (1996), is greatly simplified if the entire sample obeys a single TF relation. In order for a catalog consisting of disparate samples to have this property, the TF observables (apparent magnitude and velocity width) for at least some of the spiral samples must be suitably transformed.¹² In this section we derive such transformations for the Mark III spiral samples.

As we did in finalizing TF distances (cf. Paper II, § 6), we take HMCL as a template. That is, all apparent magnitudes and velocity widths will be transformed to an “HMCL-equivalent” system, henceforth the *common system*. The basic idea is the following: we assume that for each sample (S , say) other than HMCL, the velocity widths η_S and apparent magnitudes m_S can be transformed to their HMCL-equivalent values according to relations of the form

$$\eta_{\text{common}} = a_{0,S} + a_{1,S}\eta_S + a_{2,S}\eta_S^2 \quad (18)$$

and

$$m_{\text{common}} = m_S + b_{0,S} + b_{1,S}(m_S - 5 \log r). \quad (19)$$

The possibility that the coefficient a_1 differs from unity arises because velocity width systems differ as to the precise quantity they measure. The quadratic term in equation (18) was found to differ from zero only in the case of the CF sample, as we discuss further below. A non-zero value of the coefficient b_1 allows for a luminosity dependence of galaxy color in the case that sample S is not based on I -band photometry. As we show below, b_1 differs significantly from zero only for the H -band A82 sample.

Proceeding in analogy with Paper II, § 6, we obtain the coefficients in equations (18) and (19) through a prioritized overlap comparison. The objects used in this comparison are those listed in Table 2. We first consider objects common to HMCL and W91CL, and determine the transformation coefficients for the latter sample by fitting the HMCL data (widths and magnitudes separately)

¹²We make no effort to incorporate the ellipticals into this scheme.

to the W91CL data by least squares. The fits are initially carried out assuming that all coefficients in equations 18 and 19 are potentially significant. However, when the initial fits fail to yield values of certain coefficients that differ significantly from zero, those coefficients are assumed to be identically zero and the fits are redone without them. That is, we assume that the data sets are as alike as they can possibly be, and only allow nonzero coefficients when these are forced upon us by the data.

Once the transformation is determined for W91CL, all W91CL magnitudes and velocity widths are transformed to their common system values. We then compare W91PP objects with their counterparts in both HMCL and W91CL, thus determining the transformation of W91PP to the common system. The CF sample is then compared with HMCL and the transformed W91CL and W91PP and its transformation determined; MAT is then compared with HMCL and the transformed W91CL, W91PP, and CF, and finally A82 is compared with HMCL and the transformed W91CL, W91PP, CF, and MAT. Each comparison yields the coefficients in equations (18) and (19) that allow a transformation to a common system. There is one exception to the hierarchy just described, however. Previous comparisons have shown full consistency between the W91CL, W91PP, and CF photometry (Willick 1991; Courteau 1992; Courteau 1996). Thus, in determining the magnitude transformation law, W91CL, W91PP, and CF are grouped together and compared with HMCL. For the velocity width transformation, however, these samples are treated separately for reasons discussed in Paper II.

Table 6 summarizes the results of these overlap comparisons. Note that the “transformation” coefficients for HMCL are trivial, as HMCL defines the common system. Several aspects of Table 6 warrant further comment.

1. The W91CL sample ought, by construction, to be on the HMCL η -system. The raw velocity widths used by W91CL and those used by Han & Mould (1992) for their northern clusters (which overlap completely with W91CL; see Paper I, Table 1) are the same, namely, those tabulated by Bothun *et al.* (1985). Any systematic difference between the HMCL and W91CL η ’s would therefore imply a systematic difference in the derived inclination corrections, and, thus, in the measured axial ratios. The fact that $a_0 = 0$ and $a_1 = 1$ for W91CL is thus indicative of a consistency between the W91CL and HMCL axial ratio assignments. W91PP and CF aimed at full consistency with the HMCL η -system. Their non-zero values of a_0 indicate a marginally significant discrepancy.
2. We present both a linear and a quadratic η -transformation for CF (fourth and fifth lines of Table 6). The quadratic fit results in a small reduction in scatter, and largely eliminates a trend seen in residuals from the linear fit. It is not surprising that the CF velocity widths, which are optically measured (Courteau 1992), are not as simply related to the H I 21 cm widths of HMCL and W91 as the latter are with one another. The quadratic transformation for the CF widths is used in the common-system analysis of Davis, Nusser, & Willick (1996). However, in the TF calibration of the CF sample presented in Paper II, and in the distributed

Mark III catalog, no transformation of the CF widths (nor those of any other sample) is made.

3. The coefficient a_1 for the MAT sample differs significantly from unity. This effect is a consequence of the very different definition of H I velocity width used by Mathewson *et al.* (1992) from that of the Aaronson group (see, e.g., Bothun *et al.* 1985). The nature of the transformation is such that the MAT η -value is markedly smaller for a faint galaxy than the common system η for the same object; however, for the brightest galaxies ($\eta \gtrsim 0.3$) the MAT η differs little from the common system value. This effect also explains why the MAT TF relation (cf. Table 12 of Paper II) is so much flatter than the HMCL TF relation; the ratio of the MAT to the HMCL TF slope is 0.86, very close to the value of a_1 for the MAT sample in Table 6.
4. The origin of the large photometric zero point offset between the MAT and common system (i.e., HMCL) apparent magnitudes (the coefficient b_0 in line 6 of Table 6) is not well understood. Both MAT and HMCL carried out Kron-Cousins I -band photometry. However, the offset is unmistakable; the coefficient b_0 differs from zero at the 6σ significance level. It is thus essential to transform the MAT magnitudes to bring them to the common system. We note that this magnitude transformation, in combination with the width transformation discussed above, fully accounts for the difference between the MAT and HMCL TF relations (Table 3).
5. The A82 magnitude transformation (row 7 of Table 6) has a coefficient b_1 that differs significantly from zero. This term is a consequence of a strong luminosity dependence of the $(I - H)$ colors of galaxies. Note that the size of this coefficient is very nearly what is expected from the difference between the I -band ($b_I = 7.87 \pm 0.16$) and H -band ($b_H = 10.29 \pm 0.22$) TF slopes (cf. Paper II, Table 12), i.e., $(1 - b_1)^{-1} \times b_I \simeq b_H$. In deriving the coefficient b_1 , it was necessary to estimate the distances r to A82 galaxies in carrying out the overlap fit (see equation 19). This was done by taking $r = cz_\odot$ for $cz_\odot > 100 \text{ km s}^{-1}$, and setting $r = 100 \text{ km s}^{-1}$ otherwise. This procedure, while imperfect, suffices for the purposes of the fit.
6. The A82 velocity widths are slightly offset, by 0.016 in η , from the common system widths. The origin of this offset is unknown, as both sets of widths stem from the work of the Aaronson group in the 1980s, and both measure width at 20% of the peak of the H I profile. Nonetheless, it is a clearly detected ($\sim 5\sigma$) effect. Because the widths of Ursa Major galaxies in W91CL were derived principally from the A82 sample, we have augmented W91CL Ursa Major galaxy width parameters by 0.016 in the Mark III singles catalog. This is necessary for W91CL Ursa Major galaxies to be mutually consistent with the remainder of the W91CL sample. The width increase has the effect of increasing W91CL Ursa Major distances by $7.73 \times 0.016 = 0.123 \text{ mag}$ over their original values. This distance increment largely accounts for the discrepancy originally seen in the A82 versus W91CL overlap comparison (cf. Paper II, § 6).

10. Summary and Further Discussion

We have presented a number of technical details concerning the construction of the Mark III Catalog of Galaxy Peculiar Velocities. Our procedures for converting raw apparent magnitudes and velocity widths into corrected values suitable for application of the TF relation were described. We presented the full list of overlap galaxies that allow us to bring together disparate spiral samples for peculiar velocity studies and reviewed the means by which elliptical galaxy D_n - σ data are zeropointed consistently with the spirals. We discussed our technique for computing inhomogeneous Malmquist bias corrections for spirals and indicated how such corrections can break down in the vicinity of redshift limits. Inverse TF zero points were rederived based on the requirement that forward and inverse TF group distances agree within each sample. The final TF relations for the Mark III spiral samples are given in Table 3. We presented abbreviated versions of the Mark III catalog, and provided potential users with a guide to accessing the electronic catalog in § 6.4.

A simple analysis of the properties of TF residuals was presented. We confirmed one of the widely-made assumptions about the TF relation, namely, that it exhibits Gaussian residuals. In the case of the MAT sample, however, we found that while the residuals are Gaussian at any given velocity width, their rms value $\sigma(\eta)$ is an approximately linearly decreasing function of η , i.e., the TF scatter decreases with increasing luminosity. This has been suggested elsewhere (e.g., Federspiel, Sandage, & Tammann 1994; Freudling *et al.* 1995) but never conclusively demonstrated. The WCF and A82 samples exhibited qualitatively similar but much weaker trends with marginal statistical significance. We found no evidence for a meaningful dependence of the TF relation on morphological type across the entire range (Sa–Sd) of spirals well represented in these samples.

Our chief concern in constructing the Mark III Catalog has been ensuring the uniformity of the data and the proper calibration of the individual sample TF relations. Toward this end, we have modified the observable data presented by the original authors, because we have applied our own, uniform set of corrections to the raw data. More importantly, we have substantially changed the derived TF distances as compared with the original authors because we have recalibrated the TF relations characterizing each data set. Thus, velocity analyses based on the Mark III catalog will differ significantly from, and should be considerably more reliable than, comparable analyses based on the original data.

We cannot be certain, however, that the final catalog is entirely free of systematic errors. A crucial link in our chain of reasoning is that the HMCL sample data are uniform between its Northern and Southern sky components. Any unaccounted for discrepancy between the photometric or HI properties of HMCL South as compared with HMCL North could vitiate that basic assumption. Another variable we cannot fully control is possible redshift-dependencies of the basic data in any given sample. For these reasons, it is essential that observational checks on the uniformity of the catalog be carried out in the future. Three of the present authors (JAW, SC, and MAS), along with D. Schlegel (Durham) and M. Postman (STScI), are carrying out a full-sky TF survey of galaxies in the redshift range 4500–7000 kms^{-1} , one of whose aims is to test for and correct

possible systematic errors in Mark III. Comparison with other TF surveys (e.g., Giovanelli *et al.* 1996) will also be important. We will attempt to disseminate results from these studies in a timely fashion.

The authors would like to thank Jeremy Mould and Ming-Sheng Han for their cooperation in our efforts to assemble and tabulate their cluster data set, and Don Mathewson for making his extensive TF sample available on computer tape. We also acknowledge the contributions of Amos Yahil in developing various methods of velocity and density field reconstruction from the *IRAS* redshift survey. The work presented here was supported in part by NSF Grant AST90-16930 to DB and by the US-Israel Binational Science Foundation. This research has made use of the NASA/IPAC Extragalactic Database (NED) which is operated by the Jet Propulsion Laboratory, California Institute of Technology, under contract with the National Aeronautics and Space Administration.

A. The Cosmological Correction for Tully-Fisher Magnitudes

As discussed in § 2.1.4, the standard K-correction is not appropriate for apparent magnitudes used in peculiar velocity studies.¹³ Whereas the standard correction is applied to apparent magnitudes so that they yield luminosity-distances, our correction must instead lead to an estimate of the “cosmological redshift” z_c and the associated distance in km s^{-1} units, $r = cz_c$. It is this distance that, when compared with the observed redshift (in velocity units) cz , yields a peculiar velocity estimate.

To obtain the desired correction, we begin with the monochromatic energy flux observed from a galaxy at redshift z (e.g., Peebles 1971):

$$f(\lambda) = \frac{L\left(\frac{\lambda}{1+z}\right)}{4\pi a_0^2 x^2 (1+z)^3} \quad (\text{A1})$$

Here $L(\lambda)$ is the spectral energy distribution of the galaxy in its rest frame, a_0 the present day scale factor of the universe, and x the comoving coordinate distance of the galaxy, which is related to its cosmological redshift z_c by the equation

$$a_0 x = \frac{c}{H_0} \left[\frac{q_0 z_c + (q_0 - 1)(-1 + \sqrt{2q_0 z_c + 1})}{q_0^2 (1 + z_c)} \right] \equiv \frac{c}{H_0} Z_q(z_c) \quad (\text{A2})$$

(e.g., Weinberg 1972). In equation (A2), q_0 is the deceleration parameter, and the convenient notation $Z_q(z)$ has been borrowed from Schneider, Gunn, & Hoessel (1983). It is important to note that while the cosmological redshift z_c determines the value of the coordinate distance x , the observed redshift z in equation (A1) incorporates not only the expansion of the universe but also the peculiar motions of the observer and the source; to sufficient accuracy it is simply the heliocentric redshift of the galaxy.

The magnitudes we are concerned with here are total magnitudes measured with a CCD, and hence depend not on the energy flux $f(\lambda)$, but instead on the photon number flux $n(\lambda)$. The energy of a single photon of wavelength λ is $e(\lambda) = hc/\lambda$, where h is Planck’s constant, and therefore $n(\lambda) = f(\lambda)/e(\lambda) \propto \lambda f(\lambda)$. Similarly, the photon luminosity in the galaxy rest frame is related to its energy luminosity by $N(\lambda) \propto \lambda L(\lambda)$. Combining these relations with equation (A1) one obtains the following proportionality:

$$n(\lambda) \propto \frac{N\left(\frac{\lambda}{1+z}\right)}{x^2 (1+z)^2}. \quad (\text{A3})$$

The CCD apparent magnitude is related to the number flux $n(\lambda)$, integrated over the transmission curve, $S(\lambda)$, of the bandpass in question:

$$m = C - 2.5 \log \int_0^\infty n(\lambda) S(\lambda) d\lambda$$

¹³The discussion to follow applies to the CCD samples (HMCL, W91, CF, MAT) only. The H -band A82 sample requires a different K-correction, as discussed in § 2.1.4).

$$= C' - 2.5 \log \int_0^\infty N\left(\frac{\lambda}{1+z}\right) S(\lambda) d\lambda + 5 \log(1+z) + 5 \log Z_q(z_c). \quad (\text{A4})$$

In our system of units (cf. Paper I, § 2.1), absolute magnitude is defined as the apparent magnitude at a distance of 1 km s^{-1} , corresponding to a redshift of $\sim 3 \times 10^{-6}$. For the time being, let us denote this minuscule redshift z_0 ; we will drop this quantity at the end, but it is convenient to maintain it in the derivation that follows. With this convention, it follows that the absolute magnitude of an object with photon luminosity $N(\lambda)$ is given by

$$M = C' - 2.5 \log \int_0^\infty N\left(\frac{\lambda}{1+z_0}\right) S(\lambda) d\lambda + 5 \log(1+z_0) + 5 \log Z_q(z_0). \quad (\text{A5})$$

Using equations A4 and A5 we see that the galaxy distance modulus, not yet corrected for cosmological effects, is given by

$$m - M = 2.5 \log \left[\frac{\int_0^\infty N\left(\frac{\lambda}{1+z_0}\right) S(\lambda) d\lambda}{\int_0^\infty N\left(\frac{\lambda}{1+z}\right) S(\lambda) d\lambda} \right] + 5 \log \left(\frac{1+z}{1+z_0} \right) + 5 \log \frac{Z_q(z_c)}{Z_q(z_0)}. \quad (\text{A6})$$

In order to obtain the desired cosmological correction, we must now “unpack” z_c from the complicated expression $Z_q(z_c)$ in equation (A6). Expanding equation (A2) through first order in z_c , we find

$$5 \log \frac{Z_q(z_c)}{Z_q(z_0)} \simeq 5 \log \frac{z_c}{z_0} - 1.086(1+q_0)(z_c - z_0). \quad (\text{A7})$$

Similarly, we expand the term containing the observed redshift in equation (A6):

$$5 \log \left(\frac{1+z}{1+z_0} \right) \simeq 2 \times 1.086(z - z_0). \quad (\text{A8})$$

An approximation for the term involving the photon luminosity may be derived by noting that, to first order in z , $N\left(\frac{\lambda}{1+z}\right) \simeq N(\lambda - \lambda z) \simeq N(\lambda) - \lambda z N'(\lambda)$. Using this expansion one then finds, after some algebra,

$$2.5 \log \left[\frac{\int_0^\infty N\left(\frac{\lambda}{1+z_0}\right) S(\lambda) d\lambda}{\int_0^\infty N\left(\frac{\lambda}{1+z}\right) S(\lambda) d\lambda} \right] \simeq 1.086 \frac{\int_0^\infty \lambda N'(\lambda) S(\lambda) d\lambda}{\int_0^\infty N(\lambda) S(\lambda) d\lambda} (z - z_0). \quad (\text{A9})$$

We may simplify further by noting that, as galaxy spectra are quite smooth in the red, it is reasonable to approximate $N(\lambda)$ as a power law for wavelengths within the R and I bandpasses. If we thus write $N(\lambda) \simeq N(\lambda_{\text{eff}}) \left(\frac{\lambda}{\lambda_{\text{eff}}} \right)^\epsilon$, then $\lambda N'(\lambda) = \epsilon N(\lambda)$. Substituting this into equation (A9) gives us the simplified approximation

$$2.5 \log \left[\frac{\int_0^\infty N\left(\frac{\lambda}{1+z_0}\right) S(\lambda) d\lambda}{\int_0^\infty N\left(\frac{\lambda}{1+z}\right) S(\lambda) d\lambda} \right] \simeq 1.086 \epsilon (z - z_0). \quad (\text{A10})$$

Using the approximations (A7), (A8), and (A10) in equation (A6), we may rewrite the distance modulus as

$$m - M = K_{\text{TF}}(z, z_c; z_0) + 5 \log \frac{z_c}{z_0}, \quad (\text{A11})$$

where

$$K_{\text{TF}}(z, z_c; z_0) = 1.086 [(\epsilon + 2)(z - z_0) - (1 + q_0)(z_c - z_0)]. \quad (\text{A12})$$

Equation A11 is correct to first order in z and z_c , and therefore adequate for work at redshifts $\lesssim 10,000 \text{ km s}^{-1}$. In the logarithmic term on the right hand side of equation (A11), we multiply z_c and z_0 by c . By definition, $cz_0 = 1$, while $cz_c = r$, the distance in units of km s^{-1} . In the remainder of the expression, the tiny quantity z_0 may be dropped, as it is several orders of magnitude smaller than either z or z_c . Finally, then, we have

$$[m - K_{\text{TF}}(z, z_c)] - M = 5 \log r, \quad (\text{A13})$$

where

$$K_{\text{TF}}(z, z_c) = 1.086 [(\epsilon + 2)z - (1 + q_0)z_c]. \quad (\text{A14})$$

Equation (A13) shows that $K(z, z_c)$ is the proper cosmological correction for peculiar velocity work involving the TF relation. The practical application of this correction is described in the main text (§ 3.1.4).

B. Burstein Numerical Morphological Types

The idea for developing a numerical code for the morphological types of galaxies originated in the Second Reference Catalog of Bright Galaxies (de Vaucouleurs, de Vaucouleurs & Corwin 1976). That first numerical system simply assigned a running number from -5 to 10 to Hubble types, with E galaxies being denoted as -5 and Irr galaxies denoted as 10.

However, once catalogs were transferred from paper to electronic means, a more detailed numerical classification system became desirable for several reasons. First, the whole reason to go to a numerical scheme is to permit easy indexing within computer programs. Hence, the fact that the absence of a morphological type in the catalog (a blank space) is numerically read as a zero meant that it was desirable to assign a unique morphological number to non-standard cases. Second, with the placing of the UGC into a computer data file, and later the ESO catalog, it further became desirable to extend the numerical classifications to include objects such as multiple galaxies, dwarf galaxies, etc., for easy computer analysis of these catalogs.

Third, and perhaps most importantly for the UGC and ESO computer versions, numerous differences exist in the alphanumeric characters assigned to a given galaxy class. For example, in the ESO catalog, the subclass E/S0 alone is written in 8 different ways, each way containing between 30 and 416 entries in the catalog (e.g., E - S0, e - S0, E- S0, E/S0, E-S0, E-S0:, S0 - E, E -S0). Each different alphanumeric rendition of the same type code is, of course, read as different entries by a computer. In all, the ESO catalog has 500 different alphanumeric sets of characters for the less than 40 actual morphological classifications. In the case of the UGC, the number is 181 separate alphanumeric sets. The easiest way to ensure uniform handling of morphological types was to assign a number to each type.

As such, when Burstein first began to work with computer galaxy files in 1977, it became desirable to define a numerical morphological code that could both uniquely identify the different subclasses of galaxies in the UGC, and could in principle be expanded for future catalogs if and when more detailed information is available on galaxies. Hence, what we call the Burstein Numerical Morphological Type was developed.

The principle behind this code is to define a three-digit number. The full three digits gives maximal information about the object (e.g., SBa, SBa/b, SABa, etc.). The first two significant digits gives more general information (e.g., E, S0, S0/a Sa, Sa/b, etc.), while the first significant digit (or absence of it) generally separates large classes (E+S0; Spirals; Irregulars; Dwarfs; Compacts; Multiples, etc.). Because accessing the first significant digit and the second two significant digits is produced by a simple integer division by 10 in standard programming, this code is hierarchical. Moreover, the existing computer catalogs of the UGC and ESO contain numerous typographical errors. Assigning a unique hierarchical morphological code to each galaxy is necessary if accurate assessments of galaxy types in each catalog are to be done.

The correspondence between the BNMT and the better-known RC3 morphological type indices is presented in Table 7.

C. A Note Concerning Forward versus Inverse TF Residuals

In § 8, we showed that forward TF residuals are well-approximated as “locally” Gaussian, i.e., Gaussian at a given value of η , with rms dispersion $\sigma(\eta)$. The function $\sigma(\eta)$ was found to be a linearly decreasing function of η , with a slope that was significantly nonzero only for the MAT sample.

We could carry out a similar study of inverse TF residuals. However, this is unnecessary because the forward and TF residuals are closely related. Given the distribution of forward residuals, that of inverse residuals follows from analytic considerations, as described below. While the general expressions are complicated, we will show that under a set of assumptions reasonably supported by the data, local Gaussianity of forward TF residuals implies local Gaussianity of inverse TF residuals as well.

The local Gaussianity of forward TF residuals may be expressed mathematically as

$$P(M|\eta) = \frac{1}{\sqrt{2\pi} \sigma(\eta)} \exp \left[-\frac{(M - M(\eta))^2}{2\sigma(\eta)^2} \right], \quad (\text{C1})$$

where $M(\eta) = A - b\eta$ is the TF relation. We may now ask, given equation C1, what is the distribution of velocity width parameters given M —i.e., of inverse TF residuals? Using the standard rules of probability distributions we obtain

$$P(\eta|M) = \frac{P(M, \eta)}{P(M)} = \frac{\phi(\eta)P(M|\eta)}{\int_{-\infty}^{\infty} \phi(\eta)P(M|\eta)}, \quad (\text{C2})$$

where $\phi(\eta)$ is the underlying distribution of velocity width parameters.

Let us write the linear scatter-width relation as

$$\sigma(\eta) = \sigma_0 - g\eta, \quad (\text{C3})$$

where g was found in § 8 to be 0.33 ± 0.05 for MAT, 0.14 ± 0.09 for A82, and 0.09 ± 0.06 for WCF. The exponent in equation C1 may be expressed in terms of

$$\frac{M - M(\eta)}{\sigma(\eta)} = \frac{\eta + b^{-1}(M - A)}{b^{-1}(\sigma_0 - g\eta)} = \frac{\eta - \eta_0(M)}{b^{-1}\sigma(\eta_0)[1 - \frac{g}{\sigma(\eta_0)}(\eta - \eta_0(M))]}, \quad (\text{C4})$$

where we have defined $\eta_0(M) \equiv -b^{-1}(M - A)$, and $\sigma(\eta_0) = \sigma_0 - g\eta_0(M)$. Note that $\eta_0(M)$ is the mathematical inverse of the forward TF relation; it is close to but not exactly equal to the inverse TF relation, as we show below.

If the term in square brackets in the denominator of equation C4 differed significantly from unity, it would induce a strong departure from Gaussianity when inserted into equation C2. However, the factor $g/\sigma(\eta_0)$ is $\lesssim 0.7$ for the MAT sample, and considerably smaller for the other TF samples (cf. § 8). Moreover, the quantity $\eta - \eta_0(M)$ is restricted to lie in the range $\sim \pm 0.05$, the inverse TF scatter. Thus, the correction represented by this term is typically only a few percent. Given the limited accuracy with which we can distinguish Gaussian from non-Gaussian residuals, the term is unimportant, and we drop it in what follows.

If we now substitute equation C4 into equation C2 we obtain

$$P(\eta|M) = \frac{\phi(\eta) \left[1 - \frac{g}{\sigma(\eta_0)}(\eta - \eta_0(M))\right]^{-1} \exp\left[-\frac{(\eta - \eta_0(M))^2}{2\sigma_\eta(M)^2}\right]}{\int_{-\infty}^{\infty} \phi(\eta) \left[1 - \frac{g}{\sigma(\eta_0)}(\eta - \eta_0(M))\right]^{-1} \exp\left[-\frac{(\eta - \eta_0(M))^2}{2\sigma_\eta(M)^2}\right]}, \quad (\text{C5})$$

where we have reexpressed as above the $\sigma(\eta)$'s that appear outside the exponential factors, and defined

$$\sigma_\eta(M) \equiv b^{-1}\sigma(\eta_0) = b^{-1} \left[\sigma_0 + gb^{-1}(M - A) \right]. \quad (\text{C6})$$

This last quantity is the inverse TF scatter. It has a luminosity dependence that corresponds to the velocity width dependence of the forward TF scatter. Now, in view of the small effective range of the exponential factor, $|\eta - \eta_0(M)| \lesssim \sigma_\eta(M) \simeq 0.05$, we can expand the factors that appear outside the exponential to first order:

$$\phi(\eta) \left[1 - \frac{g}{\sigma(\eta_0)}(\eta - \eta_0(M))\right]^{-1} \simeq \phi(\eta_0) \left[1 + \left(\frac{\phi'}{\phi} + \frac{g}{\sigma(\eta_0)}\right)(\eta - \eta_0(M))\right]. \quad (\text{C7})$$

In equation C7, both $\phi' = d\phi/d\eta$ and ϕ itself are understood to be evaluated at $\eta_0(M)$, and as such are functions of M . As noted above, the term representing the luminosity dependence of scatter is small, and higher order terms in its expansion can safely be neglected. The other term, ϕ'/ϕ , is the reciprocal of the effective range of η values, which is ~ 0.2 , while the inverse TF scatter is ~ 0.05 .

Thus, $\frac{\phi'}{\phi}(\eta - \eta_0(M))$ is relatively small (\lesssim a few tenths). Higher order terms in the expansion of $\phi(\eta)$ will be $\lesssim 10\%$ and may be neglected.

With these simplifications, we may substitute equation C7 into equation C5 to obtain an approximation to the distribution of η given M . This leads to an expression that contains a linear term multiplying a Gaussian. However, to the same order of approximation used in arriving at equation C7, the linear term may be reexpressed as an exponential one. Its exponent may then be combined with that of the Gaussian, and the square completed. When this is carried out, one arrives, finally, at the following result:

$$P(\eta|M) = \frac{1}{\sqrt{2\pi}\sigma_\eta(M)} \exp\left[-\frac{[\eta - (\eta_0(M) + \Delta\eta_0(M))]^2}{2\sigma_\eta(M)^2}\right], \quad (\text{C8})$$

where

$$\Delta\eta_0(M) \equiv \left[\frac{\phi'}{\phi} + \frac{g}{\sigma(\eta_0)}\right] \sigma_\eta(M)^2. \quad (\text{C9})$$

Equation C8 shows that, given our assumptions, inverse TF residuals possess a locally Gaussian distribution. The expectation value of η given M —i.e., the inverse TF relation—is given by

$$\eta^0(M) = \eta_0(M) + \Delta\eta_0(M) = -b^{-1}(M - A) + \left[\frac{\phi'}{\phi} + \frac{g}{\sigma(\eta_0)}\right] \sigma_\eta(M)^2. \quad (\text{C10})$$

Its scatter is $\sigma_\eta(M)$. Note that, because the η -distribution function, its derivative, and $\sigma(\eta_0)$ are all functions of absolute magnitude M , not only is the inverse TF zero point shifted from the “naive” expectation $b^{-1}A$, but the slope is shifted from b^{-1} as well. The size of the shift depends mainly on the logarithmic derivative of $\phi(\eta)$. For arbitrary $\phi(\eta)$, the shift is luminosity-dependent, and consequently produces a nonlinear inverse TF relation even if the forward relation is linear. Only in the case that $\phi(\eta)$ is Gaussian will the shift be luminosity-independent and thus preserve the linearity of the inverse TF relation. The fact that we cannot detect meaningful deviations from linearity in the inverse TF relation suggests that, for TF samples at least, $\phi(\eta)$ is well-approximated by a Gaussian distribution. The luminosity-dependent scatter factor g also will have a slight effect on the slope, although this will be quite small. Note that even if the forward scatter were independent of luminosity ($g = 0$), the inverse TF relation will not be the mathematical inverse of the forward. A more detailed discussion of these issues was given by Willick (1991, Appendix C).

In summary, we have considered the question of the distribution of inverse TF residuals given that forward TF residuals are locally Gaussian (§ 8). In this Appendix we have shown that, if we make the reasonable assumptions that (1) the change in TF scatter with velocity width is slow, in the sense $g\sigma_\eta/\sigma_0 \ll 1$, and (2) the η -distribution function ϕ is wide in comparison with σ_η , inverse TF residuals are locally Gaussian as well. The luminosity-dependence of the inverse TF scatter is straightforwardly related to the velocity-width dependence of the forward TF scatter (equation C6). Moreover, the inverse TF relation is shifted, relative to the mathematical inverse of the forward TF

relation, by an amount that depends on $\phi(\eta)$, g/σ_0 , and the TF scatter (equation C9). The larger the TF scatter, all other things being equal, the more the inverse TF relation will differ from the inverse of the forward.

REFERENCES

- Aaronson, M., Huchra, J., Mould, J., Sullivan, W., Schommer, R., & Bothun, G. 1980, ApJ, 239, 12
- Aaronson, M., Huchra, J., Mould, J., Schechter, P.L., & Tully, R.B. 1982, ApJ, 258, 64
- Bottinelli, L., Gouguenheim, L., Paturel, G., & Teerikorpi, P. 1995, A&A, 296, 64
- Burstein, D. 1989, *The Mark II Catalog of Galaxy Peculiar Velocities* (electronically distributed)
- Courteau, S. 1992, Ph.D. Thesis, University of California, Santa Cruz.
- Courteau, S. 1996, ApJS, 103, 363
- Courteau, S., Faber, S.M., Dressler, A., & Willick, J.A. 1993, ApJ, 412, L51
- da Costa, L.N., Freudling, W., Wegner, G., Giovanelli, R., Haynes, M.P., & Salzer, J.J. 1996, ApJ, 468, L5
- de Vaucouleurs, G. *et al.*, 1991, RC3 Catalog
- Davis, M., Nusser, A., & Willick, J.A. (1996), ApJ, in press
- Dekel, A. 1994, ARA&A, 32, 371
- Dekel, A. *et al.*, 1996 (in preparation, Paper V)
- Dressler, A., & Faber, S.M. 1990, ApJ, 354, 13
- Faber, S.M. *et al.*, 1996 (in preparation, Paper IV)
- Faber, S.M., Wegner, G., Burstein, D., Davies, R.L., Dressler, A., Lynden-Bell, D., & Terlevich, R. 1989, ApJS, 69, 763
- Federspiel, M., Sandage, A., & Tammann, G.A. 1994, ApJ, 430, 29
- Freudling, W., da Costa, L.N., Wegner, G., Giovanelli, R., Haynes, M.P., & Salzer, J.J. 1995, AJ, 110, 920
- Giovanelli, R., & Haynes, M.P. 1985, AJ, 90, 2445 (GH)
- Giovanelli, R., Haynes, M.P., Myers, S.T., & Roth, J. 1986, AJ, 92, 250 (GH)
- Giovanelli, R., & Haynes, M.P. 1989, AJ, 97, 633 (GH)
- Giovanelli, R., Haynes, M.P., Chamaraux, P., da Costa, L.N., Freudling, W., Salzer, J.J., & Wegner, G. 1995, IAU Symp. 168 preprint
- Han, M.-S. 1992, ApJ, 391, 617
- Han, M.-S., & Mould, J. R. 1992, ApJ, 396, 453
- Hudson, M.J. 1993, MNRAS, 265, 43
- Hudson, M.J. 1994, MNRAS, 266, 468
- Hudson, M.J., Dekel, A., Courteau, S., Faber, S.M., & Willick, J.A. 1995, MNRAS, 274, 305

- Kogut, A., *et al.* 1993, ApJ, 419, 1
- Kolatt, T., & Dekel, A. 1994, ApJ, 428, 35
- Kolatt, T., Dekel, A., Ganon, G., & Willick, J.A. 1996, ApJ, 458, 419
- Lucey, J.R., & Carter, D. 1988, MNRAS, 235, 1177
- Lynden-Bell, D., Faber, S.M., Burstein, D., Davies, R.L, Dressler, A., Terlevich, R., & Wegner, G. 1988, ApJ, 302, 536
- Mathewson, D.S., Ford, V.L, & Buchhorn, M. 1992, ApJS, 81, 413
- Mould, J.R., Stavely-Smith, L., Schommer, R.A., Bothun, G.D., Hall, P.J., Han, M-S., Huchra, J.P., Roth, J., Walsh, W., & Wright, A.E. 1991, ApJ, 383, 467
- Mould, J.R., Akeson, R.L., Bothun, G.D., Han, M-S., Huchra, J.P., Roth, J., & Schommer, R.A. 1993, ApJ, 409, 14
- Oke, J.B., & Sandage, A. 1968, ApJ, 154, 21
- Strauss, M.A., & Willick, J.A. 1995, Phys. Rep., 261, 271
- Tormen, B., & Burstein, D. 1995, ApJS, 96, 123
- Tully, R.B., & Fisher, J.R. 1977, A&A, 54, 661
- Willick, J.A. 1990, ApJ, 351, L5
- Willick, J.A. 1991, Ph.D. Thesis, University of California, Berkeley.
- Willick, J.A. 1994, ApJS, 92, 1 (W94)
- Willick, J.A., Courteau, S., Faber, S.M., Burstein, D., & Dekel, A. 1995a, ApJ, 446, 12 (Paper I)
- Willick, J.A., Courteau, S., Faber, S.M., Burstein, D., Dekel, A., & Kolatt, T. 1996, ApJ, 457, 460 (Paper II)
- Willick, J.A. 1997, ApJS, in preparation
- Willick, J.A., Strauss, M.A., Dekel, A., & Kolatt, T. 1997, ApJ, in preparation
- Yahil, A., Tammann, G.A., & Sandage, A. 1977, ApJ, 217, 903

Principal Characteristics of the Mark III Spiral Samples

Sample	Photometric Method	Spectroscopic Method	Number	Notes
HMCL	CCD <i>I</i> -Band	H I Profile Widths	428	a
W91CL	CCD <i>r</i> -Band	H I Profile Widths	156	b
W91PP	CCD <i>r</i> -Band	H I Profile Widths	326	c
CF	CCD <i>r</i> -band	Optical Rotation Curves	321	d
MAT	CCD <i>I</i> -band	H I + Optical	1355	e
A82	Photoelectric <i>H</i> -band	H I Profile Widths	359	f

Table 1: Notes: (a) The Han-Mould Cluster sample. The original papers describing these data are: Mould *et al.* (1991,1993); Han (1992); Han & Mould (1992). The electronic catalog includes the HMPP (Han-Mould Perseus-Pisces) subset of HMCL, which was not used in the global TF calibration; cf. Paper I. (b) Willick (1991) Cluster sample. (c) Willick (1991) Perseus-Pisces field sample (cf. also Willick 1990). (d) Courteau-Faber field sample; Courteau (1992, 1996; Courteau *et al.* 1993). (e) Mathewson, Ford, & Buchorn (1992) field sample. (f) Aaronson *et al.* (1982) field sample. A recalibration of the original A82 photometry was carried out by Tormen & Burstein (1995) and is adopted for the catalog.

Table 2: This table is contained in the file **table2.ps**.

Final TF Relations for Mark III Samples

Sample	forward			inverse		
	$A(\pm)$	$b(\pm)$	σ (mag)	$D(\pm)$	$e(\pm)$	σ_η
HM	−5.48 (0.03)	7.87 (0.16)	0.40	−5.58 (0.03)	0.1177 (0.0025)	0.048
W91CL	−4.18 (0.02)	7.73 (0.21)	0.38	−4.23 (0.02)	0.1190 (0.0032)	0.047
W91PP	−4.28 (0.02)	7.12 (0.18)	0.38	−4.32 (0.02)	0.1244 (0.0031)	0.049
CF	−4.22 (0.02)	7.73 (0.21)	0.38	−4.27 (0.02)	0.1190 (0.0032)	0.047
MAT	−5.79 (0.03)	6.80 (0.08)	0.43	−5.96 (0.03)	0.1328 (0.0016)	0.059
A82	−5.95 (0.04)	10.29 (0.22)	0.47	−5.98 (0.04)	0.0893 (0.0018)	0.043

Table 3: Parameters of the fully calibrated TF relations for the Mark III spiral samples.

Table 4: This table is contained in the file **table4.ps**.

Table 5: This table is contained in the file **table5.ps**.

Common-System Transformations for Mark III Samples

Sample	a_0	a_1	a_2	σ_η	N_η	b_0	b_1	σ_m	N_m
HMCL	0.000	1.000	0.000	–	–	0.00	0.000	–	–
W91CL	0.000	1.000	0.000	0.013	112	−1.31	0.000	0.135	184 ^(a)
W91PP	0.004	1.000	0.000	0.016	74	−1.31	0.000	0.135	184 ^(a)
CF ^(b)	0.004	1.000	0.000	0.028	135	−1.31	0.000	0.135	184 ^(a)
	0.011	1.069	−0.663	0.027	135				
MAT	0.065	0.831	0.000	0.034	113	−0.19	0.000	0.130	114
A82	0.016	1.000	0.000	0.039	130	−0.92	−0.212	0.246	130

Table 6: Coefficients for transforming the Mark III magnitude and velocity width data to a common system. The meaning of the coefficients a_0 , a_1 , a_2 , b_0 , b_1 , and b_2 is defined by equations 18 and 19. The quantities σ_η and σ_m are the rms dispersions resulting from, and N_η and N_m the number of objects involved in, the least-squares fits used to determine the transformation coefficients. Notes: (a) W91CL, W91PP, and CF were combined to obtain a common transformation for the r -band magnitudes. (b) Two width transformations, one linear and one quadratic, are given for CF; see text for further details.

Table 7: This table is contained in the file **table7.ps**.

Table 2: TF Data for Objects Common to Two or More Samples

PGC	l	b	cz_{\odot}	HMCL			W91CL			W91PP			CF			MAT			A82		
				η	m	d_{TF}	η	m	d_{TF}	η	m	d_{TF}	η	m	d_{TF}	η	m	d_{TF}	η	m	d_{TF}
73049	4.53	-77.17	228	0.000	0.00	0	0.000	0.00	0	0.000	0.00	0	0.000	0.00	0	-0.214	8.11	308	-0.086	7.87	386
55165	100.56	44.97	456	0.000	0.00	0	0.000	0.00	0	0.000	0.00	0	-0.062	11.91	1349	0.000	0.00	0	-0.135	10.37	969
701	43.69	-80.43	552	0.000	0.00	0	0.000	0.00	0	0.000	0.00	0	0.000	0.00	0	-0.270	9.65	526	-0.142	9.63	666
38361	143.57	67.79	576	0.000	0.00	0	0.063	10.43	1045	0.000	0.00	0	0.000	0.00	0	0.000	0.00	0	0.045	8.76	1083
36136	154.45	65.96	740	0.000	0.00	0	-0.245	12.88	1079	0.000	0.00	0	0.000	0.00	0	0.000	0.00	0	-0.251	11.71	1036
16517	227.00	-35.02	741	0.000	0.00	0	0.000	0.00	0	0.000	0.00	0	0.000	0.00	0	-0.209	10.22	827	-0.088	9.66	873
38302	140.33	65.00	758	0.000	0.00	0	0.116	10.21	1141	0.000	0.00	0	0.000	0.00	0	0.000	0.00	0	0.107	8.44	1254
35164	163.66	66.18	769	0.000	0.00	0	0.222	9.80	1377	0.000	0.00	0	0.000	0.00	0	0.000	0.00	0	0.197	7.70	1366
38795	138.46	65.40	771	0.000	0.00	0	0.144	10.59	1501	0.000	0.00	0	0.000	0.00	0	0.000	0.00	0	0.139	8.28	1355
44086	305.76	67.15	791	0.000	0.00	0	0.000	0.00	0	0.000	0.00	0	0.004	11.74	1578	0.000	0.00	0	-0.008	9.89	1418
37038	151.76	67.78	803	0.000	0.00	0	-0.235	13.84	1740	0.000	0.00	0	0.000	0.00	0	0.000	0.00	0	-0.230	12.84	1926
37290	147.64	66.40	804	0.000	0.00	0	0.086	11.03	1496	0.000	0.00	0	0.000	0.00	0	0.000	0.00	0	0.037	9.42	1413
54117	93.24	51.40	805	0.000	0.00	0	0.000	0.00	0	0.000	0.00	0	0.043	11.30	1481	0.000	0.00	0	-0.029	9.25	956
37691	151.86	70.10	835	0.000	0.00	0	0.119	10.74	1472	0.000	0.00	0	0.000	0.00	0	0.000	0.00	0	0.104	8.49	1265
37466	138.86	60.06	848	0.000	0.00	0	-0.042	11.97	1462	0.000	0.00	0	0.000	0.00	0	0.000	0.00	0	-0.062	10.46	1427
26259	251.42	18.51	885	0.000	0.00	0	0.000	0.00	0	0.000	0.00	0	0.000	0.00	0	-0.151	9.17	612	-0.034	8.97	820
38392	138.09	63.06	889	0.000	0.00	0	0.110	10.87	1513	0.000	0.00	0	0.182	10.87	1992	0.000	0.00	0	0.000	0.00	0
36699	150.72	65.96	894	0.000	0.00	0	0.083	10.55	1186	0.000	0.00	0	0.000	0.00	0	0.000	0.00	0	0.048	8.62	1030
37697	146.69	67.36	905	0.000	0.00	0	-0.039	12.02	1512	0.000	0.00	0	0.000	0.00	0	0.000	0.00	0	-0.052	10.20	1327
17819	239.45	-27.43	921	0.000	0.00	0	0.000	0.00	0	0.000	0.00	0	0.000	0.00	0	0.000	9.39	1086	0.029	8.55	911
38988	145.42	71.73	933	0.000	0.00	0	-0.084	11.90	1219	0.000	0.00	0	0.000	0.00	0	0.000	0.00	0	-0.087	10.54	1315
11812	248.06	-58.46	954	0.000	0.00	0	0.000	0.00	0	0.000	0.00	0	0.000	0.00	0	-0.425	11.25	676	-0.246	11.61	1013
37036	143.65	62.78	969	0.000	0.00	0	-0.033	11.41	1166	0.000	0.00	0	0.000	0.00	0	0.000	0.00	0	-0.031	9.95	1307
21375	260.29	-12.70	970	0.000	0.00	0	0.000	0.00	0	0.000	0.00	0	0.000	0.00	0	-0.088	9.64	925	-0.033	8.99	832
36875	148.16	65.23	972	0.000	0.00	0	0.117	10.52	1320	0.000	0.00	0	0.000	0.00	0	0.000	0.00	0	0.096	8.71	1348
36343	146.27	62.28	974	0.000	0.00	0	-0.188	13.04	1423	0.000	0.00	0	0.000	0.00	0	0.000	0.00	0	-0.180	12.11	1744
13854	241.73	-51.68	991	0.000	0.00	0	0.000	0.00	0	0.000	0.00	0	0.000	0.00	0	-0.382	12.67	1488	-0.280	13.16	1761
39241	139.93	68.85	1030	0.000	0.00	0	0.151	10.50	1477	0.000	0.00	0	0.000	0.00	0	0.000	0.00	0	0.123	8.68	1511
13090	263.65	-51.19	1058	0.000	0.00	0	0.000	0.00	0	0.000	0.00	0	0.000	0.00	0	-0.115	10.27	1137	-0.090	9.76	905
13458	229.79	-53.34	1066	0.000	0.00	0	0.000	0.00	0	0.000	0.00	0	0.000	0.00	0	-0.015	10.09	1431	0.039	9.35	1381
11836	268.22	-53.41	1076	0.000	0.00	0	0.000	0.00	0	0.000	0.00	0	0.000	0.00	0	-0.113	10.70	1394	-0.082	10.22	1162
38370	141.11	65.92	1076	0.000	0.00	0	0.162	10.67	1661	0.000	0.00	0	0.000	0.00	0	0.000	0.00	0	0.138	8.81	1722
37553	140.51	62.06	1083	0.000	0.00	0	-0.226	13.10	1278	0.000	0.00	0	0.000	0.00	0	0.000	0.00	0	-0.226	12.02	1346
14169	257.17	-48.24	1131	0.000	0.00	0	0.000	0.00	0	0.000	0.00	0	0.000	0.00	0	-0.251	10.96	1020	-0.101	10.71	1331
11984	273.28	-50.83	1152	0.000	0.00	0	0.000	0.00	0	0.000	0.00	0	0.000	0.00	0	-0.079	10.68	1537	-0.122	10.68	1188
38645	136.79	62.87	1163	0.000	0.00	0	-0.133	13.47	2110	0.000	0.00	0	0.000	0.00	0	0.000	0.00	0	-0.151	12.15	2038
13727	251.52	-51.39	1169	0.000	0.00	0	0.000	0.00	0	0.000	0.00	0	0.000	0.00	0	0.088	9.09	1246	0.116	8.30	1227
70304	357.18	-64.15	1205	0.000	0.00	0	0.000	0.00	0	0.000	0.00	0	0.000	0.00	0	-0.146	10.59	1195	-0.097	10.25	1097
16709	241.70	-36.46	1210	0.000	0.00	0	0.000	0.00	0	0.000	0.00	0	0.000	0.00	0	0.036	8.75	906	0.059	8.01	819
12916	193.54	-48.52	1236	0.000	0.00	0	0.000	0.00	0	0.000	0.00	0	0.000	0.00	0	-0.165	10.33	999	-0.059	9.99	1166
69539	19.31	-61.60	1251	0.000	0.00	0	0.000	0.00	0	0.000	0.00	0	0.000	0.00	0	-0.184	10.88	1213	-0.117	10.87	1328
35931	144.59	59.58	1294	0.000	0.00	0	0.058	11.31	1540	0.000	0.00	0	0.000	0.00	0	0.000	0.00	0	0.039	9.74	1653
70184	1.64	-64.24	1296	0.000	0.00	0	0.000	0.00	0	0.000	0.00	0	0.000	0.00	0	-0.098	10.29	1210	-0.043	10.00	1263
14814	274.52	-41.19	1298	0.000	0.00	0	0.000	0.00	0	0.000	0.00	0	0.000	0.00	0	-0.027	9.45	1026	0.052	8.90	1194
11851	212.14	-58.22	1326	0.000	0.00	0	0.000	0.00	0	0.000	0.00	0	0.000	0.00	0	-0.129	11.05	1558	-0.078	10.75	1512

Table 2 (continued)

PGC	l	b	cz_{\odot}	HMCL			W91CL			W91PP			CF			MAT			A82		
				η	m	d_{TF}	η	m	d_{TF}	η	m	d_{TF}	η	m	d_{TF}	η	m	d_{TF}	η	m	d_{TF}
69364	87.47	-29.72	1340	0.000	0.00	0	0.000	0.00	0	0.050	11.58	1751	0.050	11.62	1759	0.026	10.41	1885	0.000	0.00	0
17042	274.92	-34.32	1350	0.000	0.00	0	0.000	0.00	0	0.000	0.00	0	0.000	0.00	0	-0.184	10.98	1270	-0.123	10.66	1172
12285	222.42	-57.52	1366	0.000	0.00	0	0.000	0.00	0	0.000	0.00	0	0.000	0.00	0	-0.076	10.94	1748	-0.044	10.42	1526
53578	359.09	50.19	1369	0.000	0.00	0	0.000	0.00	0	0.000	0.00	0	0.142	11.23	2040	0.000	0.00	0	0.105	9.27	1820
14824	265.74	-43.41	1372	0.000	0.00	0	0.000	0.00	0	0.000	0.00	0	0.000	0.00	0	-0.240	11.71	1491	-0.172	11.79	1563
44992	304.71	12.50	1374	0.000	0.00	0	0.000	0.00	0	0.000	0.00	0	0.000	0.00	0	-0.143	10.44	1126	-0.084	9.39	785
69253	27.13	-59.74	1427	0.000	0.00	0	0.000	0.00	0	0.000	0.00	0	0.000	0.00	0	0.024	9.73	1370	0.049	9.15	1321
13931	286.34	-39.23	1437	0.000	0.00	0	0.000	0.00	0	0.000	0.00	0	0.000	0.00	0	-0.143	10.74	1293	-0.118	10.67	1205
25169	284.54	-15.05	1442	0.000	0.00	0	0.000	0.00	0	0.000	0.00	0	0.000	0.00	0	-0.193	11.25	1398	-0.095	10.61	1308
16983	233.30	-32.95	1474	0.000	0.00	0	0.000	0.00	0	0.000	0.00	0	0.000	0.00	0	-0.152	11.35	1664	-0.100	11.14	1630
57799	21.02	37.17	1486	0.000	0.00	0	0.000	0.00	0	0.000	0.00	0	0.014	12.06	1895	0.000	0.00	0	-0.020	10.23	1566
13368	218.46	-52.71	1498	0.000	0.00	0	0.000	0.00	0	0.000	0.00	0	0.000	0.00	0	-0.118	9.92	958	-0.061	9.35	860
9057	202.14	-68.32	1504	0.000	0.00	0	0.000	0.00	0	0.000	0.00	0	0.000	0.00	0	0.083	8.94	1145	0.130	8.22	1263
13602	227.52	-52.60	1507	0.000	0.00	0	0.000	0.00	0	0.000	0.00	0	0.000	0.00	0	0.069	9.51	1425	0.106	8.82	1486
59635	328.46	-12.68	1508	0.000	0.00	0	0.000	0.00	0	0.000	0.00	0	0.000	0.00	0	-0.176	13.19	3603	-0.123	10.78	1238
9236	152.17	-38.96	1516	0.000	0.00	0	0.000	0.00	0	0.000	0.00	0	-0.063	11.74	1243	0.000	0.00	0	-0.003	9.80	1393
13926	223.31	-50.53	1525	0.000	0.00	0	0.000	0.00	0	0.000	0.00	0	0.000	0.00	0	-0.235	11.68	1494	-0.113	11.49	1801
50676	340.47	55.76	1542	0.000	0.00	0	0.000	0.00	0	0.000	0.00	0	0.000	0.00	0	-0.135	11.21	1646	-0.078	10.90	1620
12181	237.30	-58.02	1569	0.000	0.00	0	0.000	0.00	0	0.000	0.00	0	0.000	0.00	0	-0.279	12.47	1873	-0.211	12.57	1861
57924	11.46	31.47	1574	0.000	0.00	0	0.000	0.00	0	0.000	0.00	0	0.000	0.00	0	0.039	9.82	1496	0.084	9.32	1686
12412	208.17	-55.22	1580	0.000	0.00	0	0.000	0.00	0	0.000	0.00	0	0.000	0.00	0	0.110	9.04	1305	0.079	8.80	1296
1851	338.27	-82.38	1583	0.000	0.00	0	0.000	0.00	0	0.000	0.00	0	0.000	0.00	0	0.167	8.63	1292	0.205	7.47	1276
2052	21.88	-86.13	1585	0.000	0.00	0	0.000	0.00	0	0.000	0.00	0	0.000	0.00	0	0.066	10.04	1802	0.068	9.12	1425
12737	212.31	-54.84	1589	0.000	0.00	0	0.000	0.00	0	0.000	0.00	0	0.000	0.00	0	0.043	9.97	1624	0.060	9.52	1650
70800	346.42	-64.49	1595	0.000	0.00	0	0.000	0.00	0	0.000	0.00	0	0.000	0.00	0	0.084	10.10	1960	0.070	8.84	1265
52641	354.51	52.85	1609	0.000	0.00	0	0.000	0.00	0	0.000	0.00	0	0.116	11.75	2362	0.000	0.00	0	0.100	9.55	2022
31428	184.62	59.83	1612	0.000	0.00	0	0.000	0.00	0	0.000	0.00	0	0.150	11.11	1986	0.000	0.00	0	0.168	9.31	2499
5619	188.31	-80.09	1628	0.000	0.00	0	0.000	0.00	0	0.000	0.00	0	0.000	0.00	0	-0.054	10.09	1266	0.097	9.51	1957
70565	17.35	-67.33	1634	0.000	0.00	0	0.000	0.00	0	0.000	0.00	0	0.000	0.00	0	-0.189	12.26	2254	-0.106	11.61	1967
13179	237.96	-54.60	1637	0.000	0.00	0	0.000	0.00	0	0.000	0.00	0	0.000	0.00	0	0.192	8.21	1151	0.173	6.91	847
7262	166.33	-66.31	1639	0.000	0.00	0	0.000	0.00	0	0.000	0.00	0	0.000	0.00	0	-0.192	11.29	1428	-0.071	10.63	1479
37325	285.21	40.32	1657	0.000	0.00	0	0.000	0.00	0	0.000	0.00	0	0.000	0.00	0	-0.087	11.03	1761	0.021	10.69	2351
17436	225.27	-26.50	1659	0.000	0.00	0	0.000	0.00	0	0.000	0.00	0	0.000	0.00	0	0.144	9.39	1705	0.158	8.03	1322
70070	5.19	-64.05	1668	0.000	0.00	0	0.000	0.00	0	0.000	0.00	0	0.000	0.00	0	-0.150	11.28	1622	-0.093	11.25	1773
68128	334.85	-48.36	1685	0.000	0.00	0	0.000	0.00	0	0.000	0.00	0	0.000	0.00	0	0.057	9.73	1519	0.074	8.91	1331
12007	218.61	-58.26	1696	0.000	0.00	0	0.000	0.00	0	0.000	0.00	0	0.000	0.00	0	0.029	10.11	1657	0.024	9.82	1597
12041	183.67	-48.12	1709	0.000	0.00	0	0.000	0.00	0	0.000	0.00	0	0.000	0.00	0	-0.013	10.33	1608	0.059	9.84	1903
12011	217.62	-58.12	1733	0.000	0.00	0	0.000	0.00	0	0.000	0.00	0	0.000	0.00	0	-0.321	12.16	1424	-0.231	12.31	1502
66784	334.70	-42.43	1736	0.000	0.00	0	0.000	0.00	0	0.000	0.00	0	0.000	0.00	0	-0.055	12.18	3305	0.092	10.31	2763
46452	309.39	27.42	1738	-0.217	13.14	2412	0.000	0.00	0	0.000	0.00	0	0.000	0.00	0	-0.360	13.30	2130	0.000	0.00	0
68389	323.00	-43.68	1747	0.000	0.00	0	0.000	0.00	0	0.000	0.00	0	0.000	0.00	0	0.044	10.55	2127	0.092	9.45	1859
52395	350.46	51.86	1763	0.000	0.00	0	0.000	0.00	0	0.000	0.00	0	0.000	0.00	0	-0.190	11.83	1843	-0.041	11.40	2430
12309	219.20	-57.17	1803	0.000	0.00	0	0.000	0.00	0	0.000	0.00	0	0.000	0.00	0	-0.190	11.59	1650	-0.154	11.27	1340
6826	164.66	-67.61	1827	0.000	0.00	0	0.000	0.00	0	0.000	0.00	0	0.000	0.00	0	-0.040	10.83	1860	0.002	10.01	1571
38550	126.12	40.06	1848	0.000	0.00	0	0.000	0.00	0	0.000	0.00	0	0.068	12.62	2973	0.000	0.00	0	0.001	10.58	2033

Table 2 (continued)

PGC	l	b	cz_{\odot}	HMCL			W91CL			W91PP			CF			MAT			A82		
				η	m	d_{TF}	η	m	d_{TF}	η	m	d_{TF}	η	m	d_{TF}	η	m	d_{TF}	η	m	d_{TF}
54097	348.54	39.04	1859	0.000	0.00	0	0.000	0.00	0	0.000	0.00	0	0.000	0.00	0	0.073	10.24	2020	0.124	9.68	2405
19531	237.31	-13.55	1895	0.000	0.00	0	0.000	0.00	0	0.000	0.00	0	0.000	0.00	0	0.156	9.57	1924	0.155	8.32	1489
70117	5.96	-64.40	1921	0.000	0.00	0	0.000	0.00	0	0.000	0.00	0	0.000	0.00	0	-0.082	10.92	1700	-0.087	10.29	1172
13809	235.86	-52.04	1922	0.000	0.00	0	0.000	0.00	0	0.000	0.00	0	0.000	0.00	0	-0.076	10.16	1221	-0.028	9.71	1187
72001	79.71	-63.12	2015	0.000	0.00	0	0.000	0.00	0	0.000	0.00	0	0.000	0.00	0	-0.014	10.28	1567	0.046	9.62	1617
57345	12.47	35.59	2022	0.000	0.00	0	0.000	0.00	0	0.000	0.00	0	0.138	11.22	2001	0.000	0.00	0	0.171	9.32	2546
37178	286.99	34.13	2024	0.000	0.00	0	0.000	0.00	0	0.000	0.00	0	0.000	0.00	0	-0.046	10.24	1391	0.029	9.90	1697
21164	134.30	28.38	2058	0.000	0.00	0	0.000	0.00	0	0.000	0.00	0	-0.020	12.43	1991	0.000	0.00	0	0.033	10.74	2546
13620	202.82	-47.88	2072	0.000	0.00	0	0.000	0.00	0	0.000	0.00	0	0.000	0.00	0	0.059	9.97	1707	0.089	9.54	1911
23852	207.51	29.32	2078	-0.166	11.92	1655	0.000	0.00	0	0.000	0.00	0	0.000	0.00	0	0.000	0.00	0	-0.116	10.68	1223
69161	357.92	-58.60	2081	0.000	0.00	0	0.000	0.00	0	0.000	0.00	0	0.000	0.00	0	-0.144	11.25	1630	-0.041	11.29	2310
46574	311.85	40.31	2094	-0.233	12.40	1619	0.000	0.00	0	0.000	0.00	0	0.000	0.00	0	-0.312	12.04	1386	-0.235	12.05	1307
7849	147.17	-43.41	2097	0.000	0.00	0	0.000	0.00	0	0.000	0.00	0	0.029	12.12	2055	0.000	0.00	0	-0.068	10.39	1343
45701	308.02	34.71	2129	-0.324	13.42	1862	0.000	0.00	0	0.000	0.00	0	0.000	0.00	0	0.000	0.00	0	-0.331	13.56	1663
30569	152.12	49.85	2141	0.000	0.00	0	0.000	0.00	0	0.000	0.00	0	0.021	13.06	3079	0.000	0.00	0	-0.023	11.57	2862
39979	296.75	22.74	2149	0.000	0.00	0	0.000	0.00	0	0.000	0.00	0	0.000	0.00	0	-0.009	10.93	2147	0.073	10.81	3179
46551	311.04	36.33	2162	-0.310	12.82	1486	0.000	0.00	0	0.000	0.00	0	0.000	0.00	0	-0.288	13.08	2412	-0.265	12.97	1732
26295	139.01	35.93	2287	0.000	0.00	0	0.000	0.00	0	0.000	0.00	0	0.067	11.86	2087	0.000	0.00	0	0.054	10.53	2553
31708	165.86	57.26	2331	0.000	0.00	0	0.000	0.00	0	0.000	0.00	0	-0.002	12.52	2213	0.000	0.00	0	0.026	10.80	2532
69661	359.82	-61.17	2357	0.000	0.00	0	0.000	0.00	0	0.000	0.00	0	0.000	0.00	0	0.053	10.91	2583	0.102	9.90	2398
58470	37.17	39.22	2377	0.000	0.00	0	0.000	0.00	0	0.000	0.00	0	0.174	11.45	2529	0.000	0.00	0	0.122	9.23	1937
47321	311.97	29.03	2389	0.078	9.76	1482	0.000	0.00	0	0.000	0.00	0	0.000	0.00	0	0.031	10.06	1630	0.081	9.10	1502
34005	281.54	21.81	2416	0.244	10.30	3468	0.000	0.00	0	0.000	0.00	0	0.000	0.00	0	0.000	0.00	0	0.205	9.26	2910
47002	311.41	30.17	2429	-0.207	12.94	2281	0.000	0.00	0	0.000	0.00	0	0.000	0.00	0	-0.343	13.13	2077	0.000	0.00	0
33952	281.70	21.24	2433	-0.007	10.44	1489	0.000	0.00	0	0.000	0.00	0	0.000	0.00	0	-0.001	10.75	2026	-0.004	10.00	1520
28909	263.92	19.98	2480	0.225	10.00	2819	0.000	0.00	0	0.000	0.00	0	0.000	0.00	0	0.104	10.17	2155	0.225	9.12	3000
29727	269.50	17.64	2514	-0.058	12.00	2539	0.000	0.00	0	0.000	0.00	0	0.000	0.00	0	-0.116	12.38	2994	0.000	0.00	0
34445	281.89	24.03	2597	-0.120	11.65	1726	0.000	0.00	0	0.000	0.00	0	0.000	0.00	0	0.000	0.00	0	-0.109	11.72	2040
42510	300.79	21.85	2600	0.213	9.69	2340	0.000	0.00	0	0.000	0.00	0	0.000	0.00	0	0.146	9.88	2151	0.000	0.00	0
45487	307.83	39.86	2608	-0.082	11.75	2075	0.000	0.00	0	0.000	0.00	0	0.000	0.00	0	-0.127	11.86	2277	0.000	0.00	0
67904	32.90	-51.11	2626	0.000	0.00	0	0.000	0.00	0	0.000	0.00	0	0.000	0.00	0	0.226	9.32	2135	0.233	8.63	2486
49112	86.38	71.32	2627	0.000	0.00	0	0.000	0.00	0	0.000	0.00	0	0.085	12.24	2651	0.000	0.00	0	0.049	10.28	2223
49676	319.92	31.36	2661	0.258	9.46	2478	0.000	0.00	0	0.000	0.00	0	0.000	0.00	0	0.000	0.00	0	0.219	8.48	2171
46878	313.19	41.07	2675	0.121	10.89	2914	0.000	0.00	0	0.000	0.00	0	0.000	0.00	0	0.105	10.92	3054	0.000	0.00	0
70795	82.85	-50.66	2689	0.000	0.00	0	0.000	0.00	0	0.000	0.00	0	0.181	11.22	2333	0.000	0.00	0	0.191	9.14	2577
66669	354.14	-45.11	2693	0.090	10.67	2353	0.000	0.00	0	0.000	0.00	0	0.000	0.00	0	0.040	10.76	2314	0.000	0.00	0
65299	354.26	-38.40	2716	-0.054	11.81	2361	0.000	0.00	0	0.000	0.00	0	0.000	0.00	0	-0.111	11.96	2506	0.000	0.00	0
31565	277.64	14.74	2757	-0.080	11.99	2334	0.000	0.00	0	0.000	0.00	0	0.000	0.00	0	-0.248	12.29	1900	0.000	0.00	0
10507	173.51	-51.44	2763	0.000	0.00	0	0.000	0.00	0	0.000	0.00	0	0.000	0.00	0	0.052	10.84	2493	0.067	9.82	1958
45911	309.85	42.60	2764	0.016	11.37	2484	0.000	0.00	0	0.000	0.00	0	0.000	0.00	0	-0.044	11.46	2456	0.000	0.00	0
65338	354.43	-38.63	2767	-0.043	14.33	7840	0.000	0.00	0	0.000	0.00	0	0.000	0.00	0	-0.294	14.43	4407	0.000	0.00	0
33962	281.08	22.59	2771	0.047	11.68	3206	0.000	0.00	0	0.000	0.00	0	0.000	0.00	0	-0.081	11.76	2511	0.000	0.00	0
31533	277.67	14.57	2774	0.183	10.44	2965	0.000	0.00	0	0.000	0.00	0	0.000	0.00	0	0.104	10.64	2676	0.000	0.00	0
31761	275.43	19.36	2788	0.068	11.02	2553	0.000	0.00	0	0.000	0.00	0	0.000	0.00	0	0.004	11.07	2385	0.000	0.00	0
64980	11.27	-34.69	2794	0.000	0.00	0	0.000	0.00	0	0.000	0.00	0	0.000	0.00	0	0.214	8.97	1750	0.222	8.62	2349

Table 2 (continued)

PGC	l	b	cz_{\odot}	HMCL			W91CL			W91PP			CF			MAT			A82		
				η	m	d_{TF}	η	m	d_{TF}	η	m	d_{TF}	η	m	d_{TF}	η	m	d_{TF}	η	m	d_{TF}
35405	217.71	71.29	2827	0.037	11.97	3534	0.000	0.00	0	0.000	0.00	0	0.002	13.00	2800	0.000	0.00	0	0.029	11.47	3497
29747	226.26	50.24	2827	0.000	0.00	0	0.000	0.00	0	0.000	0.00	0	-0.002	12.92	2660	0.000	0.00	0	-0.067	11.56	2313
71948	332.95	-64.88	2852	0.000	0.00	0	0.000	0.00	0	0.000	0.00	0	0.000	0.00	0	0.183	10.27	2890	0.244	9.41	3751
31493	272.51	22.46	2871	0.101	10.65	2426	0.000	0.00	0	0.000	0.00	0	0.000	0.00	0	0.085	10.91	2855	0.000	0.00	0
33964	151.35	57.83	2877	0.000	0.00	0	0.000	0.00	0	0.000	0.00	0	0.107	11.84	2385	0.000	0.00	0	0.139	10.10	3134
35521	221.02	71.45	2905	-0.190	13.20	2735	0.000	0.00	0	0.000	0.00	0	0.000	0.00	0	0.000	0.00	0	-0.190	13.84	3690
30308	270.79	19.10	2908	0.280	9.17	2348	0.000	0.00	0	0.000	0.00	0	0.000	0.00	0	0.254	9.27	2277	0.000	0.00	0
29993	269.42	19.03	2920	0.145	9.96	2071	0.000	0.00	0	0.000	0.00	0	0.000	0.00	0	0.124	10.45	2610	0.000	0.00	0
31995	277.05	18.11	2941	0.087	10.67	2328	0.000	0.00	0	0.000	0.00	0	0.000	0.00	0	0.085	10.78	2689	0.000	0.00	0
45666	308.29	38.44	2949	-0.042	12.07	2779	0.000	0.00	0	0.000	0.00	0	0.000	0.00	0	-0.147	12.32	2643	0.000	0.00	0
32039	273.90	23.40	2953	0.020	11.74	2989	0.000	0.00	0	0.000	0.00	0	0.000	0.00	0	0.002	11.83	3363	0.000	0.00	0
6275	141.77	-48.42	2986	0.000	0.00	0	0.000	0.00	0	0.000	0.00	0	0.092	12.33	2833	0.000	0.00	0	0.083	10.08	2381
29898	269.46	18.44	2992	-0.017	11.82	2712	0.000	0.00	0	0.000	0.00	0	0.000	0.00	0	-0.046	11.96	3072	0.000	0.00	0
45953	310.05	43.02	3007	0.087	10.90	2588	0.000	0.00	0	0.000	0.00	0	0.000	0.00	0	0.034	11.00	2537	0.000	0.00	0
34362	281.24	24.85	3026	0.059	11.68	3349	0.000	0.00	0	0.000	0.00	0	0.000	0.00	0	-0.003	11.77	3220	0.000	0.00	0
35288	284.79	23.38	3033	-0.009	11.64	2569	0.000	0.00	0	0.000	0.00	0	0.000	0.00	0	-0.054	11.71	2670	0.000	0.00	0
44930	305.77	35.69	3060	-0.064	11.73	2194	0.000	0.00	0	0.000	0.00	0	0.000	0.00	0	-0.082	11.95	2732	0.000	0.00	0
31683	269.72	27.38	3090	0.059	11.75	3458	0.000	0.00	0	0.000	0.00	0	0.000	0.00	0	0.004	11.93	3544	0.000	0.00	0
6848	140.68	-38.44	3112	0.000	0.00	0	0.000	0.00	0	0.195	11.30	2476	0.000	0.00	0	0.125	10.26	2399	0.000	0.00	0
67023	329.35	-41.82	3114	0.000	0.00	0	0.000	0.00	0	0.000	0.00	0	0.000	0.00	0	0.146	10.06	2336	0.119	9.03	1741
34519	284.36	18.88	3115	0.118	10.43	2332	0.000	0.00	0	0.000	0.00	0	0.000	0.00	0	0.028	11.61	3297	0.000	0.00	0
33647	280.86	21.19	3129	0.127	10.81	2870	0.000	0.00	0	0.000	0.00	0	0.000	0.00	0	0.082	10.72	2591	0.000	0.00	0
64240	353.60	-32.75	3161	0.036	11.26	2539	0.000	0.00	0	0.000	0.00	0	0.000	0.00	0	-0.103	11.31	1905	0.000	0.00	0
43809	303.54	37.44	3187	-0.140	12.67	2568	0.000	0.00	0	0.000	0.00	0	0.000	0.00	0	0.000	0.00	0	-0.210	12.60	1896
31875	276.02	19.08	3199	0.059	11.24	2734	0.000	0.00	0	0.000	0.00	0	0.000	0.00	0	0.033	11.34	2957	0.000	0.00	0
45573	306.25	19.05	3202	-0.118	13.57	4210	0.000	0.00	0	0.000	0.00	0	0.000	0.00	0	-0.292	13.83	3364	-0.120	13.48	4356
64219	351.06	-32.84	3203	-0.318	13.05	1605	0.000	0.00	0	0.000	0.00	0	0.000	0.00	0	-0.390	13.17	1826	0.000	0.00	0
43812	303.54	36.58	3229	0.005	12.16	3435	0.000	0.00	0	0.000	0.00	0	0.000	0.00	0	0.000	0.00	0	0.011	11.35	3038
35776	286.40	23.18	3246	0.013	12.62	4370	0.000	0.00	0	0.000	0.00	0	0.000	0.00	0	-0.117	12.55	3228	0.012	12.13	4372
44695	304.59	19.54	3285	-0.080	13.03	3768	0.000	0.00	0	0.000	0.00	0	0.000	0.00	0	-0.126	13.30	4432	0.000	0.00	0
32666	275.98	23.67	3291	0.264	10.17	3512	0.000	0.00	0	0.000	0.00	0	0.000	0.00	0	0.206	10.16	2952	0.000	0.00	0
42880	301.30	26.34	3319	-0.113	12.92	3178	0.000	0.00	0	0.000	0.00	0	0.000	0.00	0	-0.170	13.11	3538	0.000	0.00	0
31590	271.42	23.94	3402	0.047	12.56	4808	0.000	0.00	0	0.000	0.00	0	0.000	0.00	0	-0.070	12.79	4176	0.000	0.00	0
71450	99.69	-33.94	3477	0.000	0.00	0	0.000	0.00	0	0.131	12.34	3240	0.185	12.30	3891	0.000	0.00	0	0.000	0.00	0
31981	271.84	26.14	3479	-0.032	12.97	4361	0.000	0.00	0	0.000	0.00	0	0.000	0.00	0	-0.047	13.04	5036	0.000	0.00	0
70702	83.37	-49.35	3480	-0.016	13.52	5954	0.003	13.54	3537	0.000	0.00	0	0.031	13.54	3980	-0.046	12.41	3780	0.000	0.00	0
70265	79.69	-47.74	3484	0.000	0.00	0	-0.001	13.14	2900	0.000	0.00	0	-0.064	13.22	2449	0.000	0.00	0	0.000	0.00	0
43282	302.42	17.86	3494	0.022	12.07	3505	0.000	0.00	0	0.000	0.00	0	0.000	0.00	0	-0.051	12.30	3537	0.000	0.00	0
70881	85.10	-49.10	3501	-0.104	12.71	2981	-0.099	14.38	3622	0.000	0.00	0	0.000	0.00	0	-0.178	13.08	3403	0.000	0.00	0
23309	201.26	28.60	3504	-0.214	13.74	3215	-0.207	15.26	3698	0.000	0.00	0	0.000	0.00	0	0.000	0.00	0	0.000	0.00	0
70541	81.24	-49.15	3517	-0.020	13.63	6173	-0.019	14.80	5843	0.000	0.00	0	0.000	0.00	0	-0.147	13.70	4990	0.000	0.00	0
15638	196.14	-29.67	3530	0.000	0.00	0	0.000	0.00	0	0.000	0.00	0	0.199	11.64	3018	0.127	10.40	2575	0.000	0.00	0
71517	99.32	-35.50	3549	0.000	0.00	0	0.000	0.00	0	0.039	13.18	3528	0.000	0.00	0	0.041	11.90	3924	0.000	0.00	0
70803	83.67	-49.94	3630	-0.180	13.12	2733	-0.174	14.54	2985	0.000	0.00	0	0.000	0.00	0	0.000	0.00	0	0.000	0.00	0
42369	300.52	22.08	3726	-0.003	11.46	2417	0.000	0.00	0	0.000	0.00	0	0.000	0.00	0	-0.069	11.57	2389	0.000	0.00	0

Table 2 (continued)

PGC	l	b	cz_{\odot}	HMCL			W91CL			W91PP			CF			MAT			A82		
				η	m	d_{TF}	η	m	d_{TF}	η	m	d_{TF}	η	m	d_{TF}	η	m	d_{TF}	η	m	d_{TF}
39479	279.69	68.54	3733	0.000	0.00	0	0.000	0.00	0	0.000	0.00	0	0.108	12.69	3540	0.000	0.00	0	0.130	11.31	5243
37156	246.77	72.81	3738	0.098	11.98	4428	0.000	0.00	0	0.000	0.00	0	0.000	0.00	0	0.000	0.00	0	0.110	11.49	5181
31987	269.15	30.00	3738	0.118	11.61	4015	0.000	0.00	0	0.000	0.00	0	0.000	0.00	0	0.017	11.86	3574	0.000	0.00	0
2035	108.85	-72.10	3740	0.000	0.00	0	0.000	0.00	0	0.000	0.00	0	0.000	0.00	0	0.187	10.22	2860	0.205	9.25	2897
23465	200.96	29.44	3742	-0.166	13.41	3286	-0.157	14.71	3430	0.000	0.00	0	0.000	0.00	0	0.000	0.00	0	0.000	0.00	0
71181	88.07	-48.47	3756	0.111	11.34	3457	0.124	12.76	3799	0.000	0.00	0	0.116	12.68	3625	0.070	11.52	3607	0.000	0.00	0
71262	89.10	-48.01	3758	-0.135	13.30	3496	-0.129	14.77	3896	0.000	0.00	0	-0.088	14.76	4570	-0.195	13.90	4708	0.000	0.00	0
51143	322.62	24.65	3763	-0.122	12.97	3148	0.000	0.00	0	0.000	0.00	0	0.000	0.00	0	-0.072	12.90	4366	0.000	0.00	0
31677	271.78	24.46	3774	0.138	10.83	3014	0.000	0.00	0	0.000	0.00	0	0.000	0.00	0	0.116	10.90	3132	0.000	0.00	0
48125	313.94	28.88	3776	-0.047	12.13	2806	0.000	0.00	0	0.000	0.00	0	0.000	0.00	0	-0.082	12.41	3377	0.000	0.00	0
71753	103.56	-29.86	3809	0.000	0.00	0	0.000	0.00	0	0.028	13.09	3265	0.017	13.02	2980	0.000	0.00	0	0.000	0.00	0
30915	265.93	28.39	3822	-0.029	12.15	3022	0.000	0.00	0	0.000	0.00	0	0.000	0.00	0	-0.145	12.80	3317	0.000	0.00	0
71260	91.11	-45.56	3859	0.000	0.00	0	-0.200	15.11	3538	0.000	0.00	0	-0.151	15.04	4155	-0.308	14.15	3708	0.000	0.00	0
43717	303.22	22.42	3862	0.127	11.06	3220	0.000	0.00	0	0.000	0.00	0	0.000	0.00	0	0.119	11.26	3731	0.000	0.00	0
71288	92.26	-44.25	3909	0.060	12.63	5205	0.000	0.00	0	0.000	0.00	0	0.000	0.00	0	0.015	12.71	5253	0.000	0.00	0
42271	300.41	20.59	3941	-0.033	11.75	2478	0.000	0.00	0	0.000	0.00	0	0.000	0.00	0	-0.128	12.11	2546	0.000	0.00	0
35952	242.93	69.22	3965	0.102	12.44	5553	0.000	0.00	0	0.000	0.00	0	0.000	0.00	0	0.000	0.00	0	0.035	11.90	4386
32813	272.77	29.82	3967	0.164	11.41	4326	0.000	0.00	0	0.000	0.00	0	0.000	0.00	0	0.131	11.61	4552	0.000	0.00	0
43214	302.23	22.27	3981	-0.162	12.94	2685	0.000	0.00	0	0.000	0.00	0	0.000	0.00	0	-0.200	13.00	3062	0.000	0.00	0
34922	283.76	22.81	4033	-0.125	14.21	5511	0.000	0.00	0	0.000	0.00	0	0.000	0.00	0	0.000	0.00	0	-0.108	14.37	6946
5440	131.89	-30.69	4037	0.048	11.97	3677	0.000	0.00	0	0.061	13.21	3845	0.000	0.00	0	0.000	0.00	0	0.000	0.00	0
69367	88.38	-28.58	4074	0.000	0.00	0	0.000	0.00	0	-0.131	14.90	4461	0.000	0.00	0	-0.228	14.01	4466	0.000	0.00	0
23319	202.27	28.32	4090	-0.020	13.37	5477	0.084	13.19	4017	0.000	0.00	0	0.134	13.38	5335	0.000	0.00	0	0.000	0.00	0
70981	89.34	-45.34	4101	0.054	12.39	4560	0.000	0.00	0	0.000	0.00	0	0.000	0.00	0	-0.073	12.47	3570	0.000	0.00	0
50420	321.29	28.08	4138	0.089	10.98	2704	0.000	0.00	0	0.000	0.00	0	0.000	0.00	0	0.011	11.17	2552	0.000	0.00	0
23420	200.84	29.20	4142	0.004	12.66	4308	-0.037	13.89	3604	0.000	0.00	0	0.000	0.00	0	0.000	0.00	0	0.000	0.00	0
71051	87.28	-48.27	4186	0.056	11.95	3751	0.052	13.44	4022	0.000	0.00	0	0.015	13.42	3558	0.000	0.00	0	0.000	0.00	0
71034	86.20	-49.30	4201	-0.085	13.09	3804	-0.086	14.36	3759	0.000	0.00	0	-0.109	14.34	3495	0.000	0.00	0	0.000	0.00	0
4563 ^a	128.71	-28.78	4210	0.047	12.77	5296	0.000	0.00	0	0.028	14.10	5198	0.000	0.00	0	0.000	0.00	0	0.000	0.00	0
62346	333.20	-23.09	4232	0.109	11.57	3816	0.000	0.00	0	0.000	0.00	0	0.000	0.00	0	-0.094	11.67	2313	0.000	0.00	0
43701	303.19	23.84	4247	0.183	11.26	4326	0.000	0.00	0	0.000	0.00	0	0.000	0.00	0	0.112	11.33	3770	0.000	0.00	0
46786	311.13	32.25	4261	-0.085	12.97	3599	0.000	0.00	0	0.000	0.00	0	0.000	0.00	0	-0.162	13.37	4090	0.000	0.00	0
23169	199.85	28.32	4281	0.114	11.67	4069	0.115	13.08	4264	0.000	0.00	0	0.100	13.14	4233	0.000	0.00	0	0.000	0.00	0
42460	300.71	21.76	4298	-0.035	12.61	3655	0.000	0.00	0	0.000	0.00	0	0.000	0.00	0	-0.167	12.61	2837	0.000	0.00	0
5702	132.55	-28.63	4349	0.167	11.22	4007	0.170	12.67	4294	0.173	12.68	4349	0.182	12.71	4649	0.000	0.00	0	0.000	0.00	0
62922	335.59	-26.08	4370	0.268	10.20	3613	0.000	0.00	0	0.000	0.00	0	0.000	0.00	0	0.255	10.35	3757	0.000	0.00	0
48533	315.57	30.58	4378	0.179	11.87	5646	0.000	0.00	0	0.000	0.00	0	0.000	0.00	0	0.110	12.01	5124	0.000	0.00	0
47255	312.03	30.36	4385	0.011	12.69	4480	0.000	0.00	0	0.000	0.00	0	0.000	0.00	0	-0.132	12.82	3487	0.000	0.00	0
23661	202.38	30.03	4393	-0.102	13.78	4914	-0.102	15.20	5228	0.000	0.00	0	0.000	0.00	0	0.000	0.00	0	0.000	0.00	0
23748	204.10	29.99	4440	-0.106	13.83	4956	-0.105	15.31	5441	0.000	0.00	0	0.000	0.00	0	0.000	0.00	0	0.000	0.00	0
1231	113.38	-38.79	4451	0.000	0.00	0	0.000	0.00	0	-0.050	14.66	5210	-0.024	14.65	5456	0.000	0.00	0	0.000	0.00	0
1413	114.30	-38.63	4472	0.000	0.00	0	0.000	0.00	0	-0.026	14.59	5457	-0.035	14.59	5104	-0.177	13.61	4358	0.000	0.00	0
23662	202.62	29.95	4497	-0.075	13.12	3999	-0.074	14.43	4051	0.000	0.00	0	-0.072	14.46	4214	0.000	0.00	0	0.000	0.00	0
3222	123.78	-31.51	4500	-0.030	13.12	4707	-0.032	14.32	4472	-0.013	14.32	5029	0.000	0.00	0	0.000	0.00	0	0.000	0.00	0
57110	36.66	45.61	4522	0.195	10.91	3845	0.000	0.00	0	0.000	0.00	0	0.203	12.20	3961	0.000	0.00	0	0.000	0.00	0

Table 2 (continued)

PGC	l	b	cz_{\odot}	HMCL			W91CL			W91PP			CF			MAT			A82		
				η	m	d_{TF}	η	m	d_{TF}	η	m	d_{TF}	η	m	d_{TF}	η	m	d_{TF}	η	m	d_{TF}
8954	147.30	-33.17	4555	0.000	0.00	0	0.000	0.00	0	-0.064	13.93	3555	-0.029	13.96	3901	0.000	0.00	0	0.000	0.00	0
41924	178.06	85.74	4573	0.012	13.20	5687	0.000	0.00	0	0.000	0.00	0	0.000	0.00	0	0.000	0.00	0	0.001	12.75	5522
61762	331.33	-20.77	4574	-0.026	12.54	3657	0.000	0.00	0	0.000	0.00	0	0.000	0.00	0	-0.086	12.75	3900	0.000	0.00	0
10029	150.21	-29.28	4587	0.000	0.00	0	0.000	0.00	0	0.090	12.90	3666	0.074	12.86	3392	0.000	0.00	0	0.000	0.00	0
3235	123.81	-33.61	4621	0.167	12.57	7462	0.179	13.82	7529	0.181	13.82	7546	0.179	13.82	7669	0.000	0.00	0	0.000	0.00	0
57353	30.83	43.04	4638	0.074	12.05	4193	0.000	0.00	0	0.000	0.00	0	0.088	13.33	4426	0.000	0.00	0	0.000	0.00	0
23567	202.88	29.35	4649	0.197	11.01	4056	0.208	12.57	4694	0.000	0.00	0	0.212	12.71	5173	0.000	0.00	0	0.000	0.00	0
1913	117.62	-33.67	4660	0.000	0.00	0	0.000	0.00	0	-0.091	14.52	4270	-0.125	14.53	3604	0.000	0.00	0	0.000	0.00	0
6607 ^a	135.49	-25.03	4661	0.083	12.73	5924	0.000	0.00	0	0.098	14.03	6332	0.000	0.00	0	0.000	0.00	0	0.000	0.00	0
1971	117.33	-39.26	4666	0.000	0.00	0	0.000	0.00	0	-0.101	14.73	4552	0.000	0.00	0	-0.225	13.87	4227	0.000	0.00	0
43170	302.11	23.29	4667	0.172	10.90	3522	0.000	0.00	0	0.000	0.00	0	0.000	0.00	0	0.133	10.99	3443	0.000	0.00	0
3336	124.14	-31.77	4668	-0.002	12.96	4840	-0.001	14.33	5017	0.000	0.00	0	0.000	0.00	0	0.000	0.00	0	0.000	0.00	0
5284 ^a	131.27	-30.18	4671	0.147	11.51	4260	0.150	12.83	4304	0.122	12.83	3942	0.118	12.79	3841	0.000	0.00	0	0.000	0.00	0
61750	329.90	-21.16	4672	0.143	10.69	2878	0.000	0.00	0	0.000	0.00	0	0.000	0.00	0	0.168	10.95	3771	0.000	0.00	0
6560 ^a	135.53	-25.94	4676	0.434	10.38	7163	0.000	0.00	0	0.390	11.71	5667	0.000	0.00	0	0.000	0.00	0	0.000	0.00	0
70765	89.70	-43.08	4713	0.082	11.78	3811	0.077	13.06	3690	0.000	0.00	0	0.076	13.11	3833	0.044	12.00	4148	0.000	0.00	0
67339	58.35	-37.09	4730	0.000	0.00	0	0.000	0.00	0	0.000	0.00	0	0.098	13.40	4737	0.000	0.00	0	0.091	11.54	4845
3611	125.27	-32.16	4802	0.000	0.00	0	0.260	12.17	4699	0.264	12.17	4634	0.283	12.26	5414	0.000	0.00	0	0.000	0.00	0
8520	145.16	-33.45	4805	0.000	0.00	0	0.000	0.00	0	0.005	13.82	4238	0.008	13.86	4250	0.000	0.00	0	0.000	0.00	0
1154	114.30	-32.09	4834	0.000	0.00	0	0.000	0.00	0	-0.001	14.01	4535	0.048	14.06	5373	0.000	0.00	0	0.000	0.00	0
4561 ^a	129.07	-31.50	4838	-0.032	12.64	3747	-0.030	13.81	3561	-0.043	13.82	3620	-0.054	13.82	3346	0.000	0.00	0	0.000	0.00	0
70708	83.99	-48.89	4847	0.221	11.55	5674	0.221	12.83	5542	0.000	0.00	0	0.000	0.00	0	0.149	11.82	5304	0.000	0.00	0
23347	202.42	28.34	4850	-0.004	13.54	6276	-0.043	14.80	5364	0.000	0.00	0	0.000	0.00	0	0.000	0.00	0	0.000	0.00	0
42968	301.72	18.85	4902	0.079	12.08	4329	0.000	0.00	0	0.000	0.00	0	0.000	0.00	0	0.060	12.18	4738	0.000	0.00	0
71244	85.93	-51.25	4907	-0.092	13.77	5072	-0.091	15.08	5144	0.000	0.00	0	0.000	0.00	0	-0.195	14.10	5162	0.000	0.00	0
70507	85.07	-45.12	4907	0.000	0.00	0	-0.045	14.37	4369	0.000	0.00	0	-0.049	14.40	4449	-0.105	13.32	4777	0.000	0.00	0
7387	137.71	-25.05	4924	0.000	0.00	0	0.000	0.00	0	0.151	12.06	3041	0.225	11.98	3871	0.000	0.00	0	0.000	0.00	0
3020	122.97	-33.15	4934	-0.042	13.01	4284	-0.057	14.17	3818	-0.094	14.17	3599	0.000	0.00	0	0.000	0.00	0	0.000	0.00	0
66414	352.33	-43.58	4936	0.296	10.37	4324	0.000	0.00	0	0.000	0.00	0	0.000	0.00	0	0.263	10.58	4282	0.000	0.00	0
4596 ^a	129.17	-31.54	4960	0.224	11.13	4727	0.221	12.37	4484	0.211	12.37	4270	0.000	0.00	0	0.000	0.00	0	0.000	0.00	0
70996	85.77	-49.45	4962	0.190	11.41	4754	0.195	12.66	4672	0.000	0.00	0	0.238	12.63	5470	0.158	11.53	4774	0.000	0.00	0
45151	305.65	24.61	4964	0.090	12.36	5125	0.000	0.00	0	0.000	0.00	0	0.000	0.00	0	0.062	12.33	5109	0.000	0.00	0
65785	353.42	-40.64	4965	0.062	11.99	3905	0.000	0.00	0	0.000	0.00	0	0.000	0.00	0	0.055	12.13	4558	0.000	0.00	0
10421	147.77	-22.13	4984	0.000	0.00	0	0.000	0.00	0	-0.033	14.08	4217	0.009	13.95	4445	0.000	0.00	0	0.000	0.00	0
71750	104.43	-27.69	4999	0.000	0.00	0	0.000	0.00	0	0.037	13.55	4156	0.049	13.55	4263	0.000	0.00	0	0.000	0.00	0
3108	123.32	-33.85	5002	0.017	12.54	4273	0.033	13.66	4159	0.033	13.63	4256	0.002	13.54	3590	0.000	0.00	0	0.000	0.00	0
23338	202.74	28.22	5030	0.005	13.69	6948	0.007	14.96	6900	0.000	0.00	0	0.000	0.00	0	0.000	0.00	0	0.000	0.00	0
71354	98.61	-34.76	5054	0.000	0.00	0	0.000	0.00	0	-0.024	14.89	6307	0.000	0.00	0	-0.097	14.03	6793	0.000	0.00	0
5563 ^a	132.22	-30.12	5076	-0.228	14.52	4377	0.000	0.00	0	0.000	0.00	0	0.000	0.00	0	0.000	0.00	0	0.000	0.00	0
2865	122.28	-34.65	5091	0.111	12.21	5161	0.111	13.64	5440	0.101	13.64	5343	0.000	0.00	0	0.000	0.00	0	0.000	0.00	0
9035	146.27	-30.44	5095	0.000	0.00	0	0.000	0.00	0	0.210	12.73	5024	0.232	12.76	5684	0.000	0.00	0	0.000	0.00	0
36604	234.62	73.21	5096	0.284	11.18	6012	0.256	12.66	5805	0.000	0.00	0	0.000	0.00	0	0.000	0.00	0	0.000	0.00	0
3950	126.75	-30.37	5105	-0.190	14.16	4255	-0.184	15.42	4321	-0.183	15.47	4891	-0.110	15.46	5834	0.000	0.00	0	0.000	0.00	0
71204	85.58	-51.27	5106	-0.092	13.02	3591	-0.097	14.26	3452	0.000	0.00	0	0.000	0.00	0	0.000	0.00	0	0.000	0.00	0
5344 ^a	131.04	-27.62	5185	0.240	10.49	3730	0.273	11.95	4447	0.259	11.87	3970	0.000	0.00	0	0.000	0.00	0	0.000	0.00	0

Table 2 (continued)

PGC	l	b	cz_{\odot}	HMCL			W91CL			W91PP			CF			MAT			A82		
				η	m	d_{TF}	η	m	d_{TF}	η	m	d_{TF}	η	m	d_{TF}	η	m	d_{TF}	η	m	d_{TF}
50784	37.26	71.81	5306	0.145	12.11	5575	0.000	0.00	0	0.000	0.00	0	0.171	13.43	6228	0.000	0.00	0	0.000	0.00	0
47093	68.47	80.78	5319	0.000	0.00	0	0.000	0.00	0	0.000	0.00	0	0.152	13.50	6012	0.000	0.00	0	0.139	11.72	6608
72788	99.24	-52.23	5388	0.000	0.00	0	0.000	0.00	0	0.000	0.00	0	0.352	11.94	5973	0.000	0.00	0	0.332	9.89	7100
10913	168.63	-45.24	5430	0.082	12.99	6654	0.000	0.00	0	0.000	0.00	0	0.000	0.00	0	0.000	0.00	0	0.068	12.03	5444
4210	127.53	-29.13	5442	0.066	12.41	4807	0.065	13.66	4661	0.054	13.66	4623	0.049	13.63	4423	0.000	0.00	0	0.000	0.00	0
6045 ^a	134.21	-29.36	5447	0.015	12.88	4961	0.000	0.00	0	0.022	14.35	5719	0.000	0.00	0	0.000	0.00	0	0.000	0.00	0
5035 ^a	130.48	-29.24	5462	0.231	10.80	4165	0.000	0.00	0	0.235	12.34	4557	0.000	0.00	0	0.000	0.00	0	0.000	0.00	0
3260	123.85	-31.33	5463	0.197	10.83	3733	0.191	11.99	3383	0.198	11.99	3435	0.184	12.10	3536	0.000	0.00	0	0.000	0.00	0
6189 ^a	134.26	-27.17	5501	0.097	12.06	4578	0.000	0.00	0	0.095	13.17	4220	0.000	0.00	0	0.000	0.00	0	0.000	0.00	0
46293	69.33	83.06	5534	0.102	12.36	5352	0.000	0.00	0	0.000	0.00	0	0.000	0.00	0	0.000	0.00	0	0.079	12.02	5709
9707	151.23	-33.90	5558	0.000	0.00	0	0.000	0.00	0	-0.040	14.77	5663	0.000	0.00	0	-0.166	13.73	4767	0.000	0.00	0
4735 ^a	129.60	-29.47	5571	-0.017	12.83	4318	-0.013	14.15	4425	-0.001	14.15	4837	0.000	0.00	0	0.000	0.00	0	0.000	0.00	0
3664	125.40	-31.31	5583	0.121	12.24	5426	0.122	13.54	5403	0.118	13.54	5396	0.092	13.55	4969	0.000	0.00	0	0.000	0.00	0
50087	350.24	65.49	5633	0.089	12.80	6253	0.088	13.54	4787	0.000	0.00	0	0.000	0.00	0	0.000	0.00	0	0.000	0.00	0
6473 ^a	135.33	-26.44	5653	0.037	13.28	6460	0.000	0.00	0	0.010	14.48	5838	0.000	0.00	0	0.000	0.00	0	0.000	0.00	0
23685	200.76	30.62	5656	0.222	11.92	6752	0.224	13.25	6797	0.000	0.00	0	0.000	0.00	0	0.000	0.00	0	0.000	0.00	0
3274	123.90	-31.19	5657	-0.056	13.10	4245	-0.054	14.23	3967	-0.077	14.23	3912	-0.055	14.28	4121	0.000	0.00	0	0.000	0.00	0
1412 ^a	114.05	-39.95	5687	0.316	11.31	7168	0.000	0.00	0	0.278	12.73	6279	0.000	0.00	0	0.000	0.00	0	0.000	0.00	0
50021	349.42	65.39	5866	-0.160	14.42	5348	-0.160	15.67	5280	0.000	0.00	0	0.000	0.00	0	0.000	0.00	0	0.000	0.00	0
50030	348.88	65.07	5881	-0.009	13.79	6916	-0.004	15.17	7308	0.000	0.00	0	0.000	0.00	0	0.000	0.00	0	0.000	0.00	0
2094	118.86	-30.80	5905	0.000	0.00	0	0.000	0.00	0	0.070	14.25	6393	0.038	14.24	5633	0.000	0.00	0	0.000	0.00	0
70323	92.04	-34.38	5925	0.000	0.00	0	0.000	0.00	0	0.121	13.85	6285	0.150	13.84	6981	0.069	12.66	6079	0.000	0.00	0
23714	207.21	28.76	5941	0.170	11.74	5147	0.172	13.17	5444	0.000	0.00	0	0.206	13.18	6287	0.000	0.00	0	0.000	0.00	0
36349	233.17	72.73	5961	0.121	12.70	6706	0.103	13.93	6043	0.000	0.00	0	0.000	0.00	0	0.000	0.00	0	0.000	0.00	0
23589	203.46	29.24	5972	0.111	13.28	8447	0.103	14.77	8897	0.000	0.00	0	0.000	0.00	0	0.000	0.00	0	0.000	0.00	0
45580	49.19	85.99	5973	0.125	12.25	5530	0.000	0.00	0	0.000	0.00	0	0.000	0.00	0	0.000	0.00	0	0.226	11.44	8772
37143	241.90	73.83	5974	0.066	13.80	9118	0.066	15.21	9551	0.000	0.00	0	0.000	0.00	0	0.000	0.00	0	0.000	0.00	0
71184	99.39	-31.61	5978	0.000	0.00	0	0.000	0.00	0	-0.073	14.69	4898	-0.004	14.74	6107	0.000	0.00	0	0.000	0.00	0
50006	349.22	65.34	5992	0.083	12.71	5870	0.103	13.75	5562	0.000	0.00	0	0.148	13.74	6619	0.000	0.00	0	0.000	0.00	0
23878	203.96	30.67	6000	0.042	13.24	6458	0.044	14.67	6887	0.000	0.00	0	0.000	0.00	0	0.000	0.00	0	0.000	0.00	0
11504	173.20	-45.11	6003	0.069	12.50	5065	0.000	0.00	0	0.000	0.00	0	0.073	13.89	5431	0.000	0.00	0	0.075	11.95	5424
71149	97.61	-34.57	6005	0.000	0.00	0	0.000	0.00	0	0.192	13.95	8306	0.000	0.00	0	0.156	12.57	7659	0.000	0.00	0
5061	130.49	-28.86	6007	0.000	0.00	0	0.078	13.49	4514	0.086	13.49	4747	0.033	13.46	3864	0.000	0.00	0	0.000	0.00	0
1158 ^a	113.24	-37.57	6047	0.037	13.03	5758	0.000	0.00	0	0.048	14.24	5920	0.000	0.00	0	0.000	0.00	0	0.000	0.00	0
35622	230.24	70.65	6120	0.035	13.56	7296	0.008	14.81	6462	0.000	0.00	0	0.000	0.00	0	0.000	0.00	0	0.000	0.00	0
36779	236.10	74.04	6189	0.167	12.79	8258	0.169	14.22	8735	0.000	0.00	0	0.000	0.00	0	0.000	0.00	0	0.000	0.00	0
49991	349.61	65.68	6246	0.225	11.85	6609	0.180	13.13	5499	0.000	0.00	0	0.161	13.14	5259	0.000	0.00	0	0.000	0.00	0
3903	126.61	-31.37	6253	0.024	13.30	6220	0.000	0.00	0	0.002	14.71	6322	0.023	14.77	6816	0.000	0.00	0	0.000	0.00	0
35347	227.03	70.10	6261	0.000	0.00	0	0.248	12.75	5880	0.000	0.00	0	0.249	12.78	6095	0.000	0.00	0	0.000	0.00	0
1736 ^a	117.08	-31.81	6276	0.171	12.00	5823	0.000	0.00	0	0.174	13.27	5725	0.000	0.00	0	0.000	0.00	0	0.000	0.00	0
1654 ^a	116.83	-30.88	6281	0.119	12.42	5852	0.000	0.00	0	0.119	13.67	5747	0.000	0.00	0	0.000	0.00	0	0.000	0.00	0
49952	349.51	65.78	6287	0.147	11.91	5121	0.157	13.21	5257	0.000	0.00	0	0.139	13.29	5211	0.000	0.00	0	0.000	0.00	0
1828 ^a	117.54	-31.25	6302	0.117	13.04	7730	0.000	0.00	0	0.130	14.31	8001	0.156	14.31	8855	0.000	0.00	0	0.000	0.00	0
1724 ^a	117.01	-31.84	6331	0.179	12.80	8665	0.000	0.00	0	0.183	14.05	8445	0.000	0.00	0	0.000	0.00	0	0.000	0.00	0
69934	96.54	-23.07	6333	0.000	0.00	0	0.000	0.00	0	0.221	12.40	4474	0.250	12.40	5135	0.000	0.00	0	0.000	0.00	0

Table 2 (continued)

PGC	l	b	cz_{\odot}	HMCL			W91CL			W91PP			CF			MAT			A82		
				η	m	d_{TF}	η	m	d_{TF}	η	m	d_{TF}	η	m	d_{TF}	η	m	d_{TF}	η	m	d_{TF}
1957 ^a	118.15	-31.01	6343	0.024	12.98	5368	0.000	0.00	0	0.028	14.27	5622	0.000	0.00	0	0.000	0.00	0	0.000	0.00	0
37463	245.79	74.18	6345	0.056	13.32	7049	0.061	14.59	7052	0.000	0.00	0	0.000	0.00	0	0.000	0.00	0	0.000	0.00	0
9398	150.13	-34.49	6389	0.000	0.00	0	0.000	0.00	0	0.138	13.86	6676	0.000	0.00	0	0.084	12.69	6460	0.000	0.00	0
5473 ^a	131.90	-30.19	6419	0.042	12.89	5497	0.000	0.00	0	0.049	14.14	5673	0.000	0.00	0	0.000	0.00	0	0.000	0.00	0
69922	95.64	-24.40	6437	0.000	0.00	0	0.000	0.00	0	0.231	12.93	5901	0.235	12.90	6128	0.000	0.00	0	0.000	0.00	0
37288	225.74	76.43	6469	0.174	12.12	6221	0.182	13.46	6447	0.000	0.00	0	0.000	0.00	0	0.000	0.00	0	0.000	0.00	0
36431	243.47	70.99	6538	0.122	11.97	4809	0.122	13.48	5255	0.000	0.00	0	0.000	0.00	0	0.000	0.00	0	0.000	0.00	0
23443	202.76	28.74	6541	0.079	13.03	6704	0.075	14.42	6854	0.000	0.00	0	0.000	0.00	0	0.000	0.00	0	0.000	0.00	0
5986	134.06	-29.90	6625	0.000	0.00	0	0.000	0.00	0	0.104	14.39	7622	0.069	14.34	6587	0.000	0.00	0	0.000	0.00	0
37153	233.68	75.18	6662	0.050	12.65	5066	0.047	13.94	4973	0.000	0.00	0	0.000	0.00	0	0.000	0.00	0	0.000	0.00	0
46427	47.19	83.72	6664	0.261	11.45	6263	0.272	12.99	7153	0.000	0.00	0	0.000	0.00	0	0.000	0.00	0	0.000	0.00	0
45097	21.40	87.26	6688	0.133	12.87	7574	0.117	14.05	6712	0.000	0.00	0	0.064	14.07	5714	0.000	0.00	0	0.000	0.00	0
36283	241.46	70.93	6732	-0.017	13.49	5851	-0.016	14.69	5614	0.000	0.00	0	0.000	0.00	0	0.000	0.00	0	0.000	0.00	0
37409	246.65	73.85	6778	0.101	12.62	6011	0.107	14.10	6629	0.000	0.00	0	0.000	0.00	0	0.000	0.00	0	0.000	0.00	0
1572 ^a	116.35	-31.18	6785	0.128	12.02	5029	0.000	0.00	0	0.132	13.30	5058	0.000	0.00	0	0.000	0.00	0	0.000	0.00	0
36856	232.12	74.45	6839	0.134	12.91	7743	0.142	14.32	8309	0.000	0.00	0	0.000	0.00	0	0.000	0.00	0	0.000	0.00	0
35978	224.62	72.57	6868	0.022	13.44	6586	0.024	14.71	6533	0.000	0.00	0	0.000	0.00	0	0.000	0.00	0	0.000	0.00	0
39519	225.50	82.33	6955	0.086	12.45	5265	0.000	0.00	0	0.000	0.00	0	0.120	13.62	5669	0.000	0.00	0	0.000	0.00	0
742 ^a	112.26	-33.02	7033	0.202	11.88	6165	0.000	0.00	0	0.200	13.32	6380	0.000	0.00	0	0.000	0.00	0	0.000	0.00	0
1387 ^a	115.20	-32.76	7041	0.022	13.29	6147	0.000	0.00	0	0.026	14.57	6412	0.000	0.00	0	0.000	0.00	0	0.000	0.00	0
45358	64.39	86.19	7044	0.211	11.87	6340	0.219	13.32	6896	0.000	0.00	0	0.000	0.00	0	0.000	0.00	0	0.000	0.00	0
45366	71.54	85.85	7049	-0.085	13.76	5179	-0.085	15.02	5112	0.000	0.00	0	0.000	0.00	0	0.000	0.00	0	0.000	0.00	0
43726	108.85	88.71	7055	0.251	12.09	8111	0.275	13.46	8977	0.000	0.00	0	0.000	0.00	0	0.000	0.00	0	0.000	0.00	0
36683	232.86	73.68	7064	0.015	13.03	5316	0.012	14.45	5553	0.000	0.00	0	0.000	0.00	0	0.000	0.00	0	0.000	0.00	0
47855	334.84	69.49	7068	0.202	11.86	6109	0.000	0.00	0	0.000	0.00	0	0.000	0.00	0	0.000	0.00	0	0.177	11.40	6828
44921	73.65	87.02	7086	0.198	12.32	7441	0.201	13.62	7426	0.000	0.00	0	0.000	0.00	0	0.000	0.00	0	0.000	0.00	0
45668	51.06	85.72	7110	0.008	13.60	6739	0.011	15.00	7129	0.000	0.00	0	0.000	0.00	0	0.000	0.00	0	0.000	0.00	0
1516 ^a	115.61	-34.15	7214	0.026	13.82	7960	0.000	0.00	0	0.019	15.01	7675	0.007	15.01	7192	0.000	0.00	0	0.000	0.00	0
50341	351.48	64.82	7239	-0.038	14.00	6858	0.000	0.00	0	0.000	0.00	0	-0.080	15.24	5866	0.000	0.00	0	0.000	0.00	0
51423	354.00	59.93	7244	0.128	11.97	4914	0.000	0.00	0	0.000	0.00	0	0.163	13.35	5834	0.000	0.00	0	0.000	0.00	0
250	108.87	-38.35	7257	0.000	0.00	0	0.000	0.00	0	0.132	13.24	4920	0.151	13.24	5314	0.080	12.30	5331	0.000	0.00	0
70192	93.02	-31.45	7277	0.000	0.00	0	0.000	0.00	0	0.167	14.04	7976	0.000	0.00	0	0.061	12.88	6561	0.000	0.00	0
3120	123.46	-40.95	7288	0.000	0.00	0	0.000	0.00	0	-0.015	15.06	7025	0.000	0.00	0	-0.174	14.06	5412	0.000	0.00	0
69530	92.58	-24.43	7291	0.000	0.00	0	0.000	0.00	0	0.256	13.33	7701	0.319	13.32	10027	0.000	0.00	0	0.000	0.00	0
44795	76.45	87.23	7296	0.148	12.48	6683	0.152	13.70	6471	0.000	0.00	0	0.166	13.78	7188	0.000	0.00	0	0.000	0.00	0
36477	233.86	73.02	7370	0.193	12.21	6947	0.136	13.76	6284	0.000	0.00	0	0.000	0.00	0	0.000	0.00	0	0.000	0.00	0
69429	79.18	-39.64	7373	0.000	0.00	0	0.000	0.00	0	0.000	0.00	0	0.151	13.60	6273	0.000	0.00	0	0.163	11.74	7472
10927	168.96	-45.40	7388	0.295	11.36	6797	0.297	12.90	7502	0.000	0.00	0	0.000	0.00	0	0.000	0.00	0	0.000	0.00	0
41225	210.17	85.18	7418	0.000	0.00	0	0.000	0.00	0	0.000	0.00	0	0.224	13.55	7949	0.000	0.00	0	0.160	11.69	7199
72188	104.69	-33.13	7440	0.187	12.30	7085	0.193	13.69	7454	0.164	13.69	6723	0.133	13.63	5965	0.000	0.00	0	0.000	0.00	0
70299	94.80	-29.77	7523	0.000	0.00	0	0.000	0.00	0	0.161	13.32	5614	0.155	13.35	5671	0.000	0.00	0	0.000	0.00	0
567 ^a	111.10	-34.18	7550	0.138	12.54	6625	0.000	0.00	0	0.144	13.87	6840	0.000	0.00	0	0.000	0.00	0	0.000	0.00	0
72024	103.71	-33.05	7608	0.174	12.55	7584	0.154	13.74	6639	0.152	13.74	6614	0.150	13.57	6165	0.000	0.00	0	0.000	0.00	0
10943	169.08	-45.35	7609	0.167	12.25	6440	0.176	13.93	7836	0.000	0.00	0	0.000	0.00	0	0.000	0.00	0	0.000	0.00	0
11306	169.54	-43.70	7629	0.087	12.97	6713	0.091	14.37	7091	0.000	0.00	0	0.093	14.40	7375	0.000	0.00	0	0.000	0.00	0

Table 2 (continued)

PGC	l	b	cz_{\odot}	HMCL			W91CL			W91PP			CF			MAT			A82		
				η	m	d_{TF}	η	m	d_{TF}	η	m	d_{TF}	η	m	d_{TF}	η	m	d_{TF}	η	m	d_{TF}
44416	80.29	87.83	7647	0.080	12.96	6515	0.093	14.29	6883	0.000	0.00	0	0.000	0.00	0	0.000	0.00	0	0.000	0.00	0
72328	105.40	-33.25	7693	0.291	11.79	8166	0.297	13.10	8225	0.263	13.10	7088	0.299	13.13	8556	0.000	0.00	0	0.000	0.00	0
11074	169.38	-44.87	7720	0.179	12.31	6914	0.182	13.70	7201	0.000	0.00	0	0.157	13.73	6803	0.000	0.00	0	0.000	0.00	0
35973	231.35	71.71	7736	0.147	13.17	9149	0.150	14.45	9076	0.000	0.00	0	0.000	0.00	0	0.000	0.00	0	0.000	0.00	0
11102	169.79	-45.06	7772	0.077	13.22	7264	0.084	14.62	7760	0.000	0.00	0	0.000	0.00	0	0.000	0.00	0	0.000	0.00	0
36330	233.54	72.62	7780	0.001	13.84	7338	-0.011	15.00	6592	0.000	0.00	0	0.000	0.00	0	0.000	0.00	0	0.000	0.00	0
72972	108.17	-34.19	7874	0.263	12.25	9119	0.258	13.56	8848	0.250	13.56	8395	0.000	0.00	0	0.000	0.00	0	0.000	0.00	0
43686	335.60	89.54	7880	0.098	13.18	7696	0.099	14.44	7534	0.000	0.00	0	0.000	0.00	0	0.000	0.00	0	0.000	0.00	0
17031	195.57	-17.59	7978	0.253	12.35	9209	0.256	13.88	10181	0.000	0.00	0	0.000	0.00	0	0.000	0.00	0	0.000	0.00	0
71124	102.79	-23.77	8043	0.000	0.00	0	0.000	0.00	0	0.132	14.24	7798	0.100	14.31	7254	0.000	0.00	0	0.000	0.00	0
41895	175.81	85.54	8052	0.000	0.00	0	0.200	13.88	8341	0.000	0.00	0	0.186	13.80	7790	0.000	0.00	0	0.000	0.00	0
43359	129.23	86.26	8089	0.137	12.81	7475	0.133	14.07	7172	0.000	0.00	0	0.129	14.06	7169	0.000	0.00	0	0.000	0.00	0
72618	93.27	-58.31	8118	0.000	0.00	0	0.000	0.00	0	0.000	0.00	0	0.183	13.32	6179	0.000	0.00	0	0.173	11.38	6638
72665	107.03	-33.68	8132	0.061	13.27	7015	0.089	14.59	7791	0.000	0.00	0	0.000	0.00	0	0.000	0.00	0	0.000	0.00	0
11099	171.31	-46.28	8265	0.131	13.12	8437	0.136	14.33	8171	0.000	0.00	0	0.000	0.00	0	0.000	0.00	0	0.000	0.00	0
10631	167.34	-46.00	8350	0.021	13.17	5795	0.021	14.33	5426	0.000	0.00	0	0.022	14.33	5546	0.000	0.00	0	0.000	0.00	0
70892	96.84	-33.52	8397	0.000	0.00	0	0.000	0.00	0	0.189	13.85	7855	0.000	0.00	0	0.141	12.80	8124	0.000	0.00	0
16469	192.75	-21.19	8486	0.042	13.36	6825	0.020	14.56	6011	0.000	0.00	0	0.025	14.41	5816	0.000	0.00	0	0.000	0.00	0
16650	193.71	-20.38	8511	0.172	12.88	8765	0.162	14.12	8137	0.000	0.00	0	0.166	14.14	8485	0.000	0.00	0	0.000	0.00	0
16468	192.63	-21.12	8512	0.065	13.69	8636	-0.007	14.93	6474	0.000	0.00	0	0.004	14.86	6640	0.000	0.00	0	0.000	0.00	0
71257	97.79	-35.29	8517	0.000	0.00	0	0.000	0.00	0	0.107	14.40	7733	0.000	0.00	0	0.039	13.31	7465	0.000	0.00	0
17126	196.74	-17.28	8567	0.211	12.90	10189	0.204	14.20	9804	0.000	0.00	0	0.000	0.00	0	0.000	0.00	0	0.000	0.00	0
16984	195.52	-17.97	8660	0.120	13.29	8768	0.115	14.42	7903	0.000	0.00	0	0.095	14.42	7497	0.000	0.00	0	0.000	0.00	0
72233	105.33	-32.21	8788	0.275	12.08	8807	0.282	13.40	8953	0.287	13.40	8804	0.276	13.29	8486	0.000	0.00	0	0.000	0.00	0
71880	103.34	-32.03	8864	0.074	13.60	8560	0.085	14.87	8738	0.096	14.88	9305	0.047	14.94	8029	0.000	0.00	0	0.000	0.00	0
16989	194.89	-17.56	8917	0.131	12.92	7695	0.133	14.14	7407	0.000	0.00	0	0.000	0.00	0	0.000	0.00	0	0.000	0.00	0
16764	196.65	-21.01	8947	0.181	12.09	6294	0.182	13.35	6129	0.000	0.00	0	0.190	13.23	6078	0.000	0.00	0	0.000	0.00	0
16951	195.31	-18.20	8958	0.147	12.66	7234	0.142	13.81	6569	0.000	0.00	0	0.171	13.78	7318	0.000	0.00	0	0.000	0.00	0
71795	102.28	-33.47	8964	0.236	12.56	9538	0.239	13.98	10034	0.215	13.98	9082	0.231	13.98	9934	0.000	0.00	0	0.000	0.00	0
72411	106.24	-32.39	9042	0.135	12.73	7153	0.138	14.02	7134	0.000	0.00	0	0.000	0.00	0	0.000	0.00	0	0.000	0.00	0
9533	144.74	-23.31	9135	0.000	0.00	0	0.000	0.00	0	0.222	13.73	8282	0.192	13.67	7496	0.000	0.00	0	0.000	0.00	0
71597	101.42	-32.35	9192	0.189	12.52	7897	0.193	13.76	7698	0.214	13.76	8180	0.219	13.79	8721	0.000	0.00	0	0.000	0.00	0
56345	31.33	47.20	9723	0.122	12.88	7312	0.146	14.16	7829	0.000	0.00	0	0.000	0.00	0	0.000	0.00	0	0.000	0.00	0
3076	123.24	-38.52	10153	0.000	0.00	0	0.000	0.00	0	0.339	13.11	9136	0.000	0.00	0	0.244	11.92	7479	0.000	0.00	0
70537	93.74	-34.22	10412	0.000	0.00	0	0.000	0.00	0	0.266	13.66	9264	0.000	0.00	0	0.236	12.58	9885	0.000	0.00	0
57037	31.15	44.42	10431	0.189	13.05	10081	0.207	14.43	11016	0.000	0.00	0	0.000	0.00	0	0.000	0.00	0	0.000	0.00	0
57278	30.72	43.38	10594	0.214	12.85	10066	0.231	14.18	10694	0.000	0.00	0	0.000	0.00	0	0.000	0.00	0	0.000	0.00	0
56987	31.13	44.52	10630	0.079	13.71	9170	0.069	14.90	8369	0.000	0.00	0	0.000	0.00	0	0.000	0.00	0	0.000	0.00	0
57111	32.28	44.56	10727	0.254	12.83	11529	0.259	14.10	11387	0.000	0.00	0	0.000	0.00	0	0.000	0.00	0	0.000	0.00	0
9102	146.91	-31.04	10731	0.000	0.00	0	0.000	0.00	0	0.188	14.27	9500	0.156	14.32	8896	0.000	0.00	0	0.000	0.00	0
57061	31.57	44.47	11070	0.002	14.43	9664	0.008	15.84	10384	0.000	0.00	0	0.000	0.00	0	0.000	0.00	0	0.000	0.00	0
57122	32.89	44.67	11602	0.249	12.64	10374	0.240	14.65	13710	0.000	0.00	0	0.000	0.00	0	0.000	0.00	0	0.000	0.00	0
71263	97.65	-35.56	12373	0.000	0.00	0	0.000	0.00	0	0.221	14.23	10392	0.225	14.25	11012	0.000	0.00	0	0.000	0.00	0

Table 2: Table of overlap objects for the Mark III catalog. Notes: (a) galaxy part of the HMPP subset of HMCL, was not used in the overlap comparison described in Paper II.

Table 4: Mark III Catalog Data for Individual Galaxies – MAT Sample

INT	PGC	Name	grp	l	b	η	m	D_{ESO}	Δm	A_B	\mathcal{R}	T_B	d_{TF}	$d_{\text{TF}}^{\text{mc}}$	$d_{\text{TF}}^{\text{inv}}$	cz_{\odot}	cz_{LG}	cz_{CMB}	d_{IRAS}	δ_{IRAS}	δm_{TF}
1322	73049	E349-012	0	4.52	-77.17	-0.214	8.11	14.0	0.26	0.00	0.217	180	308	349	305	226	250	-51	307	0.061	-9.999
1313	72228	E471-006	-1	10.69	-74.53	-0.606	12.20	5.0	0.55	0.00	0.584	196	594	690	514	266	296	-16	338	-0.096	-9.999
6	701	E472-016	0	43.70	-80.43	-0.270	9.65	9.0	0.59	0.06	0.592	160	526	602	510	543	604	242	541	-0.107	-9.999
199	12460	E200-007	-1	265.30	-52.66	-0.646	11.36	3.5	0.50	0.00	0.524	196	356	409	304	571	426	502	489	0.218	-9.999
218	13163	E200-039	-1	261.28	-51.54	-0.460	11.57	3.8	0.55	0.00	0.581	196	702	830	639	640	495	577	565	0.775	-9.999
1303	71866	E347-028	0	353.80	-70.87	-0.219	10.14	6.0	0.29	0.00	0.304	181	773	925	762	692	691	434	650	0.150	-9.999
318	16517	E486-005	0	227.00	-35.02	-0.209	10.22	16.0	0.31	0.00	0.327	181	827	962	819	740	629	742	773	0.592	-9.999
1064	64181	E143-010	-1	334.89	-32.84	-0.517	11.52	3.5	0.68	0.06	0.685	191	574	647	512	803	658	724	716	-0.049	-9.999
477	26484	E565-001	-1	252.10	19.03	-0.487	12.98	4.6	0.77	0.26	0.722	200	1235	1448	1113	846	591	1162	861	-0.128	-9.999
1160	66836	E188-009	1	344.17	-44.82	-0.336	11.22	4.2	0.67	0.00	0.744	161	881	1034	836	855	770	693	792	-0.136	0.125
474	26259	E564-035	0	251.41	18.51	-0.151	9.17	9.0	0.43	0.41	0.183	161	612	690	617	879	626	1192	902	0.452	-9.999
265	14391	E250-004	3	248.67	-48.16	0.018	8.93	18.0	0.26	0.00	0.173	121	930	1080	993	893	757	846	901	1.330	0.236
361	17819	E363-023	3	239.46	-27.43	0.000	9.39	9.0	0.33	0.00	0.343	160	1086	1220	1153	906	733	977	968	0.469	0.650
268	14475	E550-007	3	216.33	-45.30	-0.358	10.57	4.2	0.41	0.03	0.411	191	610	719	574	914	862	834	907	0.357	-0.888
1238	68618	E289-018	1	350.32	-54.84	-0.287	10.71	11.0	0.27	0.00	0.286	171	812	970	783	916	873	703	858	0.039	-0.125
520	29166	E499-037	4	262.82	22.49	-0.254	11.76	5.0	0.60	0.16	0.558	182	1461	1751	1424	955	679	1286	899	-0.181	0.569
178	11812	E300-014	-1	248.06	-58.46	-0.425	11.25	6.0	0.40	0.00	0.418	197	676	802	622	957	861	846	948	0.654	-9.999
211	13106	E418-009	-1	229.62	-54.93	-0.356	12.46	1.5	0.26	0.00	0.089	200	1465	1597	1380	962	893	853	931	1.831	-9.999
550	31178	E317-046	-1	275.54	16.42	-0.465	12.87	3.0	0.68	0.25	0.607	181	1258	1458	1142	964	664	1273	809	-0.014	-9.999
310	16172	E119-016	2	271.58	-37.77	-0.339	13.54	3.2	0.26	0.02	0.268	200	2541	2834	2407	969	757	993	975	-0.820	1.371
426	21375	E208-027	5	260.29	-12.70	-0.088	9.64	6.5	0.64	0.73	0.348	192	925	1039	954	970	707	1148	944	0.611	0.385
249	13912	E201-003	2	257.65	-49.61	-0.106	10.46	5.0	0.67	0.00	0.714	171	1276	1396	1307	980	833	929	1016	1.106	-0.252
284	15388	E157-038	2	263.11	-41.91	-0.364	11.66	2.4	0.52	0.00	0.550	100	988	1129	929	982	796	981	1022	1.268	-0.832
275	14818	E202-004	2	257.93	-44.78	-0.316	12.05	1.7	0.31	0.00	0.320	130	1375	1476	1312	982	815	962	1028	0.969	-0.068
243	13854	E302-009	2	241.73	-51.68	-0.382	12.67	3.2	0.56	0.00	0.589	191	1488	1595	1389	988	879	913	1005	1.228	0.120
491	27966	E434-034	-1	261.96	17.37	-0.443	12.42	3.5	0.86	0.47	0.720	200	1095	1217	1002	997	717	1313	943	0.097	-9.999
399	19349	E206-017	-1	260.99	-22.98	-0.428	13.13	2.2	0.72	0.12	0.730	170	1592	1709	1464	1028	786	1146	1041	-0.250	-9.999
257	14212	E249-035	-1	252.61	-48.67	-0.548	14.49	2.0	0.66	0.00	0.699	171	2045	1985	1806	1031	889	983	1083	-0.009	-9.999
196	12390	E200-003	2	261.49	-53.90	-0.198	11.41	5.5	0.31	0.00	0.323	182	1482	1564	1472	1031	896	954	1067	0.577	0.089
573	31919	E501-080	-1	268.62	30.22	-0.433	12.09	3.0	0.60	0.22	0.538	160	971	1078	891	1035	763	1385	957	0.589	-9.999
252	14071	E359-006	2	239.09	-50.42	-0.262	11.71	2.8	0.53	0.00	0.555	141	1392	1521	1353	1049	942	978	1085	1.413	-0.051
305	16120	E422-001	11	233.56	-38.55	-0.260	10.61	4.0	0.26	0.00	0.154	196	844	984	821	1054	928	1047	1119	0.868	-0.619
213	13090	E200-036	2	263.64	-51.20	-0.115	10.27	3.5	0.26	0.00	0.274	141	1137	1266	1161	1060	911	1000	1107	1.114	-0.516
202	12807	E155-025	2	265.53	-51.63	-0.196	11.50	2.5	0.26	0.00	0.259	182	1554	1617	1545	1062	913	999	1106	0.376	0.199
223	13458	E418-015	2	229.79	-53.34	-0.015	10.09	4.3	0.51	0.00	0.536	151	1431	1569	1512	1070	996	970	1077	1.785	0.008
180	11836	E155-006	2	268.21	-53.41	-0.113	10.70	7.0	0.26	0.00	0.262	171	1394	1481	1425	1071	927	997	1108	0.572	-0.050
524	29216	E435-035	4	263.93	21.51	-0.224	11.17	4.7	0.58	0.22	0.516	182	1223	1377	1204	1083	804	1412	1022	-0.121	0.137
415	20531	E162-017	5	268.25	-19.43	-0.386	11.12	2.5	0.66	0.47	0.488	140	720	835	671	1094	830	1234	1065	0.751	-0.387
535	29892	E436-003	4	266.12	22.58	-0.024	9.37	7.0	0.59	0.24	0.511	122	999	1099	1052	1098	817	1430	1022	0.361	-0.355
527	29530	E435-047	4	265.21	21.67	-0.105	10.16	9.0	0.54	0.21	0.471	170	1115	1232	1143	1105	824	1434	1035	0.117	-0.087
595	33385	E502-013	4	272.90	33.41	-0.028	9.48	9.0	0.50	0.20	0.435	160	1037	1161	1091	1109	839	1463	1020	0.735	-0.262
255	14169	E201-012	6	257.16	-48.23	-0.251	10.96	4.0	0.26	0.00	0.223	182	1020	1164	995	1129	977	1086	1201	1.379	-0.651
274	14773	E118-016	-1	271.36	-42.27	-0.016	10.62	2.0	0.26	0.00	0.048	152	1821	1816	1923	1133	938	1129	1182	-0.044	-9.999
266	14397	E156-036	6	264.10	-45.85	0.108	9.18	6.3	0.55	0.00	0.570	152	1383	1480	1523	1134	962	1108	1201	0.844	0.072
496	28044	E037-005	0	291.42	-16.03	-0.241	12.25	3.5	0.65	0.80	0.329	142	1907	2104	1867	1153	871	1288	981	-0.069	-9.999

Table 4: First 45 single galaxies in the MAT sample. The full singles catalog is available electronically, as described in the main text (§ 6.4).

Table 5: Mark III Catalog Data for Groups – MAT Sample

Group #	N_g	l	b	$\bar{\eta}$	σ_g	d_{TF}	$d_{\text{TF}}^{\text{inv}}$	$\delta\mu$	cz_{\odot}	cz_{LG}	cz_{CMB}
1	2	347.24	-49.83	-0.312	0.13	846	801	0.30	886	823	697
2	11	261.49	-51.20	-0.219	0.52	1410	1368	0.13	1031	885	971
3	3	239.46	-45.30	-0.113	0.65	890	947	0.25	906	782	867
4	5	265.21	22.49	-0.127	0.33	1135	1179	0.19	1098	818	1430
5	2	264.27	-16.07	-0.237	0.39	817	801	0.30	1032	768	1192
6	6	254.34	-49.92	-0.064	0.40	1327	1443	0.18	1162	1021	1107
7	3	1.64	-64.16	-0.143	0.02	1208	1238	0.25	1245	1248	985
8	6	274.72	-39.56	-0.204	0.27	1087	1085	0.18	1301	1093	1312
9	3	212.14	-58.22	-0.011	0.48	1267	1430	0.25	1261	1245	1106
10	6	236.86	-57.55	-0.200	0.20	1670	1647	0.18	1393	1315	1278
11	5	235.18	-38.35	-0.115	0.45	1152	1145	0.19	1186	1055	1183
12	4	268.40	-36.06	-0.145	0.64	1886	1937	0.22	1337	1122	1373
13	5	234.87	-32.95	-0.195	0.84	2307	1956	0.19	1389	1245	1418
14	3	309.43	24.15	-0.254	0.34	1107	1036	0.25	1440	1171	1711
15	2	175.54	-56.56	-0.085	0.54	1547	1594	0.30	1390	1477	1163
16	2	15.29	-61.81	0.005	0.07	1340	1451	0.30	1435	1469	1152
17	3	286.34	-41.37	-0.199	0.19	1411	1381	0.25	1443	1238	1433
18	2	282.42	-18.82	-0.068	0.33	1562	1647	0.30	1401	1124	1534
19	8	4.22	-66.21	-0.130	0.63	1637	1698	0.15	1681	1692	1414
20	8	212.17	-53.89	0.009	0.59	2119	2240	0.15	1570	1547	1436
21	2	288.45	60.81	0.115	0.29	1390	1563	0.30	1489	1307	1838
22	7	346.42	-66.90	-0.135	0.24	1941	1954	0.16	1508	1485	1270
23	6	214.43	-56.09	-0.272	0.45	1419	1271	0.18	1687	1661	1547
24	6	286.43	36.47	-0.215	0.20	1801	1723	0.18	1648	1380	1994
25	7	197.50	-68.32	-0.183	0.38	1387	1332	0.16	1615	1645	1395
26	5	227.52	-52.71	-0.074	0.57	1387	1447	0.19	1524	1454	1424
27	3	308.20	40.12	-0.258	0.72	1955	1685	0.25	1622	1383	1935
28	3	11.64	26.67	-0.101	0.45	1962	1979	0.25	1572	1539	1631
29	5	353.99	-82.38	-0.138	0.35	1739	1650	0.19	1552	1575	1280
30	4	286.54	-17.10	-0.137	0.71	2003	2060	0.22	1686	1405	1823
31	11	227.60	-22.28	-0.124	0.31	1853	1869	0.13	1755	1617	1832
32	2	38.46	-51.76	-0.204	0.06	1970	1900	0.30	1692	1797	1372
33	2	296.29	-32.75	-0.148	0.30	1727	1680	0.30	1685	1453	1712
34	2	318.04	16.39	-0.090	0.25	1419	1487	0.30	1722	1466	1940
35	2	123.30	-66.98	-0.038	0.01	1415	1507	0.30	1707	1855	1380
36	6	238.52	-14.69	-0.143	0.42	2359	2325	0.18	1911	1717	2054
37	2	307.60	-52.90	-0.297	0.04	1940	1804	0.30	1776	1636	1666
38	5	334.70	-43.68	-0.077	0.67	2184	2331	0.19	1747	1630	1618
39	7	287.15	36.24	-0.277	0.30	1632	1418	0.16	1891	1622	2236
40	2	309.05	26.36	-0.342	0.50	1865	1575	0.30	1801	1534	2080
41	3	235.86	-57.03	-0.157	0.33	1401	1417	0.25	1805	1728	1692
42	3	152.54	-67.61	-0.030	0.20	1885	2012	0.25	1840	1953	1551
43	3	316.34	-49.87	-0.123	0.47	2269	2296	0.25	2008	1868	1896
44	5	213.26	-44.36	-0.226	0.27	1816	1707	0.19	1861	1819	1779
45	2	338.36	-26.76	-0.188	0.35	1868	1886	0.30	1885	1739	1823

Table 5: First 45 groups in the MAT sample. The full catalog of groups is available electronically, as described in the main text.

Burstein and RC3 Numerical Morphological Type Indices

Galaxy Type	BNMT	RC3 Code	Galaxy Type	BNMT	RC3 Code
E - normal	10	-5	Sd	180	7
cD or '+' in RC3	11	-4	SBd	181	7
Compact E's in RC3	12	-6	Sd/SBd	182	7
E? in RC3	14	-	Sd-Irr	190	8
E-S0 (UGC,ESO)	15	-	SBd-Irr	191	8
S0	100	-3, -2, -1	Sd/SBd-Irr	192	8
SB0	101	-3, -2, -1	Sm	195	9
S0/SB0	102	-3, -2, -1	SBm	196	9
S0-a	110	0	Sm/IBm	197	9
SB0-a	111	0	Irr, Im	200	10,11
S0-a/SB0-a	112	0	Dwarf Irr	201	-
Sa	120	1	Pec Irr	210	99
SBa	121	1	'S'	300	-
Sa/SBa	122	1	'SB'	305	-
Sa-b	130	2	'I?', 'IB'	310	-
SBa-b	131	2	Dwarf spirals	320	-
Sa-b/SBa-b	132	2	Dwarf spirals	330	-
Sb	140	3	'S0?'	350	-
SBb	141	3	Dwarf	400	-
Sb/SBb	142	3	Compact	500	-
Sb-c	150	4	N galaxies	510	-
SBb-c	151	4	multiple galaxy	600	-
Sb-c/SBb-c	152	4	compact group	610	-
Sc	160	5	galaxy cluster	620	-
SBc	161	5	double galaxy	650	-
Sc/SBc	162	5	E+E; E+S0; S0+S0	651	-
Sc-d	170	6	E+S, S0+S	652	-
SBc-d	171	6	Peculiar	700	99
Sc-d/SBc-d	172	6	no classification	900	-

Table 1: The standard Hubble morphological types (Sa, etc.) along with the corresponding Burstein and RC3 numerical morphological type indices (BNMT and RC3 Code, respectively).